Development of an anisotropic hyperelastic model with damage for the mechanical behaviour of arterial wall tissue

Zhenheng Kong

Development of an anisotropic hyperelastic model with damage for the mechanical behaviour of arterial wall tissue

by

Zhenheng Kong

to obtain the degree of Master of Science
at the Delft University of Technology,
to be defended publicly on Friday May 29, 2020 at 15:00 PM.

Student number:	4738047	
Project duration:	March 1,2019 – May 29, 2020	
Thesis committee:	Dr. ir. F. P. van der Meer,	TU Delft, Chair
	Dr. ir. A. C. Akyildiz,	Erasmus MC
	Prof. dr. ir. L. J. Sluys,	TU Delft
	Ir. C. Kasbergen,	TU Delft

TU Delft

Abstract

Cardiovascular disease has caused 3.9 million deaths in Europe and over 1.8 million deaths in the European Union, which accounts for 45% of all deaths in Europe and 37% of all death in the European Union in 2017. Cardiovascular disease is mainly caused by atherosclerosis. Atherosclerosis is a kind of disease where the inside of the artery gets narrow due to the build-up of plaque. Plaque is an abnormal accumulation of material in the inner layer of the arterial wall. A swelling can be formed by the accumulated material. The swelling may intrude into the channel of the artery wall, which will make the channel get narrower and restrict blood flow. Based on current medical technology, images of the plaques can be taken. However, there are no efficient simulation tools for plaque rupture. In order to set up sufficient simulation tools, a good representation of the material behaviour and the progression of the failure is needed. There are material models for the arterial wall accounting for large deformations (hyperelasticity) and anisotropy in the material response. And, there are also failure models. However, the material models and the failure models have not been combined. In this thesis, three material models and one failure model are included. The three material models are Neo-Hookean material model and two anisotropic models developed for arterial wall tissue developed by Holzapfel and Gasser. They are combined with anisotropic damage model to obtain three new constitutive models for failure of hyperelastic material. After the three constitutive models are set up, a parameter study is performed to explore the material properties of the new constitutive models. Verification of the material models is also included. Finally, the performance of the model is demonstrated with failure analyses on different geometries: a simple plane, a bar, a plane with an imperfection and a plane with a rectangular hole in the middle.

Zhenheng Kong
Delft, March 2020

Contents

1 Introduction

1.1. Background

In recent years, cardiovascular disease has become the leading cause of death in all areas of the world except Africa. Cardiovascular disease has resulted in 17.9 million deaths (32.1%) in 2015, up from 12.3 million (25.8%) in 1990. In 2017, cardiovascular disease has caused 3.9 million deaths in Europe and over 1.8 million deaths in the European Union(EU), which accounts for 45% of all deaths in Europe and 37% of all deaths in the EU [10]. Cardiovascular disease is mainly caused by atherosclerosis.

Atherosclerosis is a disease where the inside of the artery gets narrow due to the build-up of plaque. Plaque is an abnormal accumulation of material in the intima which is the inner layer of the artery wall. A swelling can be formed by the accumulated material. The swelling may intrude into the channel of the artery wall, which will make the channel get narrower and restrict blood flow. When atherosclerosis gets severe, it can lead to different kinds of diseases which are coronary artery disease, peripheral artery disease, stroke, or kidney problems. This depends on which arteries are affected. According to some experiment results, the artery wall has a highly organized structural arrangement which makes the artery wall to be anisotropic. Healthy artery wall can be regarded as a highly deformable composite structure which also has nonlinear stress-strain response and a typical stiffening around the physiological level.

Most of the current research focuses on developing robust and accurate constitutive frameworks for artery wall which can be implemented in finite element environments by applying stress-strain relationships. The artery wall is modelled as a fibre-reinforced composite material. There are several material models which can be applied to model the mechanical behaviour of the arterial wall. In order to obtain a predictive tool for the plaque rupture, failure model needs to be added to the material model. In this thesis, only one failure model is included. By combing the material model and the failure model, the failure behaviour of the atherosclerosis can be analyzed.

1.2. Motivation

Cardiovascular disease has become a serious society issue since it leads to lots of death every year. In order to reduce the death which is caused by cardiovascular disease, research works are performed. Based on current technology, images of the artery wall can be taken. However, the actual state of the artery wall cannot be judged based on the images. As a result, it would be really helpful, if sufficient simulation tools can be set up. With the help of the simulation tool, the actual state of the artery wall can be judged based on the geometry of the artery wall and doctors can figure out where the plaque rupture is going to happen.

Good representations of the material model, geometry and load scenario are needed to set up sufficient simulation tools for the plaque rupture. This thesis will only focus on the material model. There are material models for the arterial wall accounting for large deformations (hyperelasticity) and anisotropy in the material response. And, there are also failure models. However, the material models and the failure models have not been combined. In order to analysis the plaque rupture, the material model needs to be combined with the damage model which has never been done before.

1.3. Aim of the research

The objective of the research is to extend the hyperelastic anisotropic constitutive model with a damage formulation to allow for progressive failure simulations of arterial wall rupture.

1.4. Methodology

First, three different material models are chosen to represent the mechanical behaviour of the artery wall. Then one failure model is chosen to represent the failure behaviour after the artery wall reaches the ultimate strength. By combining the material model and failure model, the failure models can be obtained. Since three material models are included, three different failure models can be obtained. Then failure models are tested by changing different material parameters. As a result, the material properties of these three failure models can be observed. Since material properties have been obtained, FEM models are set up for further analyses. In this thesis, four different models have been build up. Based on the above-mentioned analyses, a predictive tool can be set up for the plaque rupture. All of the above analyses are implemented and programmed by using an advanced numerical simulations toolkit, called *Jive*, which is written in C++.

2

Literature Review

2.1. Arterial histology

This thesis focuses on arteries which are composed by three distinct layers. The three layers are the *intima* (*tunica intima*), the *media* (tunica media) and the *adventitia* (*tunica externa*). For each layer, it has a distinct biological structure and mechanical behaviour[7]. Figure 2.1 shows a model of a healthy artery.

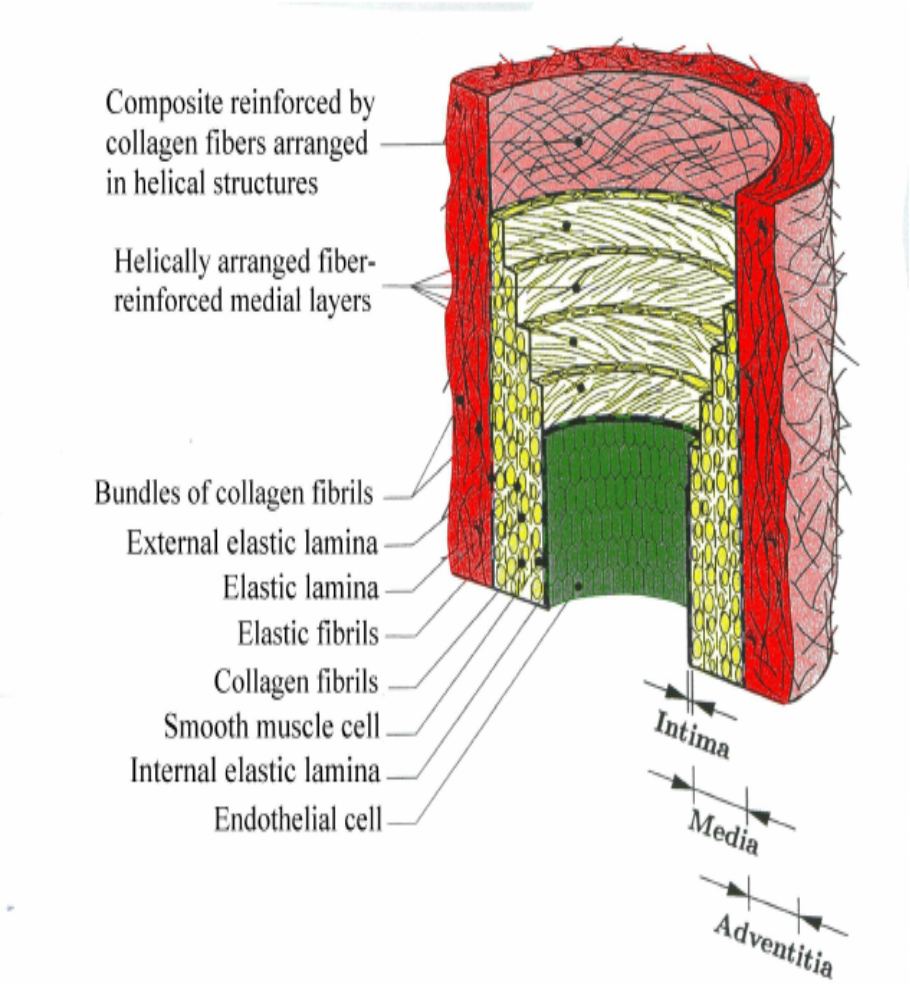

Figure 2.1: Diagrammatic model of a healthy artery[7]

The intima is located in the inner layer of the artery wall. It is formed by a single layer of endothelial cells lining the arterial wall and lying on a thin basal membrane and a subendothelial layer.[6] The subendothelial layer's thickness varies with disease, age and topography. For a healthy young person, the intima will be quite thin, so that its contribution to solid mechanical behaviour of the artery wall can be neglected. However, since the thickness of the intima will increase with age, the contribution will then become significant.

It is known that atherosclerosis, which is the most common disease of the artery walls, may be associated with the pathological changes of the intimal components. Atherosclerosis involves deposition of many kinds of material. They are fatty substances, cellular waste products, collagen fibres, calcium and fibrin. Due to deposition, atherosclerosis plaque will be built up. It has been observed that the atherosclerosis plaque would be very complex in geometry and biochemical components. These pathological changes will have a significant influence on the mechanical behaviour of the artery walls. As a result, the mechanical behaviour of arteries with atherosclerosis plaques is quite different from that of healthy arteries.

The media is located in the middle layer of the artery wall. It consists of a complex three-dimensional network of smooth muscle cells and elastin and collagen fibrils. The media can be separated from the intima and adventitia by the internal elastic lamina and the external elastic lamina.[7] There is a so-called continuous fibrous helix which is formed by the elastic and collagen fibrils, elastic laminae and smooth muscle cells. Since the helix has a small pitch, the fibrils in the media are almost circumferentially oriented. Due to this structure arrangement, the media obtains high strength and the ability to resit loads from both the longitudinal and circumferential directions. As a result, the media becomes the significant layer in a healthy artery.

The adventitia is located in the outer layer of the artery wall. It contains fibroblasts, fibrocytes, histological ground substance and thick bundles of collagen fibrils. It is surrounded continuously by loose connective tissue[7]. The adventita has wavy collagen fibres which are arranged in helical structures. Due to this arrangement, the adventitia contributes significantly to the stability and strength of the artery wall. Not like the media, which shows a high stiffness at low pressure and in the load-free configuration, the adventitia shows a lower stiffness under these situations. However, the adventitia changes to a stiff 'jacket-like' tube at a higher level of pressure which make the artery avoid overstretch and rupture.

2.2. Mechanical properties of the arterial wall

It is known that healthy arterial walls are highly deformed composite structures and have a non-linear stress-strain response with a typical stiffening effect at higher pressure[7]. For all biological tissues, this stiffening effect is quite common. This stiffening effect is based on the recruitment of the embedded (load carrying) wavy collagen fibres, which will lead to the characteristic anisotropic mechanical behaviour of arterial walls. For some early works, the arterial walls are considered to be cylindrically orthotropic, which is also generally accepted[4].

The mechanical behaviours of the arterial wall can be influenced by a lot of external factors which can be divided into physical factors and chemical environmental factors. The factors can be temperature, osmotic pressure, pH, partial pressure of carbon dioxide and oxygen, ionic concentrations and monosaccharide concentration[8]. As a result, the arteries need to be tested in an appropriate environment with appropriate oxygen concentration and appropriate temperature, and they need to be tested as fresh as possible.

In order to obtain the mechanical properties of the arterial wall, lots of different kinds of experiments are performed. Although the mechanical properties of the arterial wall can be influenced by a lot of factors, the general mechanical characteristics of the arterial wall remain the same. One of the experimental results is shown in the following figure(Figure 2.2) to represent the general mechanical properties of the arterial wall. To obtain this result, a circumferential strip of the media is subjected to uniaxial cyclic loading and unloading.

It can be observed from the figure that, during the first several load cycles, the arterial wall has a significant stress softening. With the increase of the load cycles, this softening phenomenon diminishes and a nearly repeatable cyclic behaviour can be obtained. As a result, the biological material is regarded to be 'pre-conditioned'.

There are three points which are indicated in the figure. These three points represent three different loading stages. Loading beyond the (visco)elastic domain (indicated by point I) which is far outside

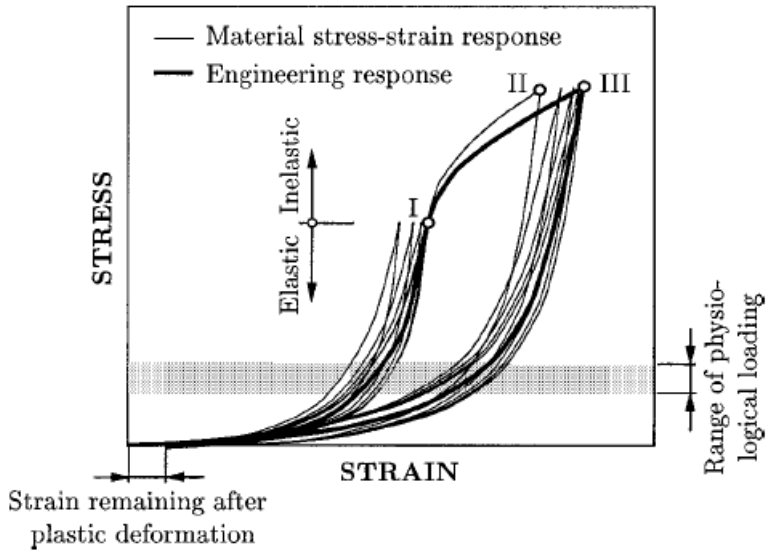

Figure 2.2: Schematic diagram of typical uniaxial stress-strain curves for circumferential arterial strips in passive condition[7]

the physiological range of deformation, always happens during performing mechanical treatments, for example: percutaneous transluminal angioplasty. This procedure involves dilation of an artery by using a balloon catheter. In the strain range up to point II, the deformation process in an arterial wall is associated with inelastic effects(elastoplastic and/or damage mechanisms). This inelastic effects will have significant influence in the mechanical behaviour. This overstretching involves dissipation, which can be represented by the area between the loading and unloading curves. As a result, starting from point II, additional cyclic loading and unloading again display stress softening, which diminishes with the number of loading cycles. The material shows a perfectly elastic or viscoelastic behaviour at point III. However, unloading initiated from point III makes the arterial strip return to an unstressed state with non-vanishing strains remaining. These are responsible for the change of the shape. So, the thick solid line can represent the engineering response associated with the actual physical behaviour by neglecting the preconditioning effects.

The following material models are intended to capture only the elastic portion of the curves in Figure 2.2, which is up to point I.

2.3. Atherosclerosis

Atherosclerosis is a kind of disease where the inside of the artery gets narrow due to the build up of plaque. Plaque is an abnormal accumulation of material in the intima which is the inner layer of the artery of the artery wall. The material which forms the plaque consists of macrophage cells, or debris, containing lipids, calcium and a variable amount of fibrous connective tissue. A swelling can be formed by the accumulated material. The swelling may intrude into the channel of the artery wall, which will make the channel get narrower and restrict blood flow. When atherosclerosis get severe, it can lead to different kinds of diseases which are coronary artery disease, peripheral artery disease,stroke, or kidney problems. This depends on which arteries are affected. This progress is shown in Figure 2.3.

The formation of the artery can be divided into six stages in detail. These stages are initial lesion, fatty streak, intermediate lesion, atheroma, fibroatheroma and complicated lesion. For the initial lesion stage, the artery is regarded as normal artery from histological point of view. After the initial lesion, it comes to the fatty streak stage. In this stage, mainly the intracellular lipid is accumulated in the intima. When small extracellular lipid pools appear, it comes to the third stage which is called intermediate lesion. Due to the accumulation of the extracellular lipid pools, a core of extracellular lipid will be formed. Then it comes to the fourth stage called atheroma. As time goes by, more cores will appear in the intima and fibrotic or calcific layers will also appear. As a result, fibroatheroma is formed which is the fifth stage. As the fibroatheroma gets bigger, the inner surface of the artery may rupture, and hematoma and haemorrhage will happen. The lipid will also intrude into the channel of the artery which will lead

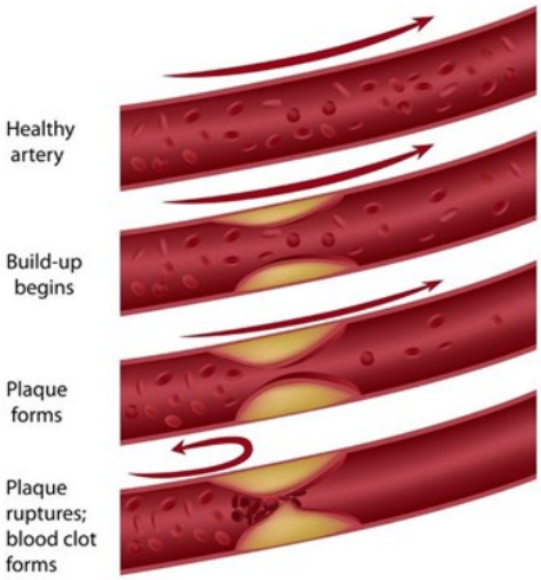

Figure 2.3: Plaque formation of the artery

to the formation of thrombosis which is the final stage called complicated lesion. The thrombosis will become a big threaten to human's life.

Based on a lot of observation results, these six stages normally start from different time of human's life. The first two stages start from the first decade of human's life. Intermediate lesion and atheroma start from the third decade. The last two stages: fibroatheroma and complicated lesion starts from the fourth decade. In the first four stages, the plaque is mainly grown by the lipid addition. In the fibroatheroma stage, smooth muscle and collagen increase in the intima. This will make the plaque come the to final stage where hematoma, haemorrhage and thrombosis are going to happen. From a clinical point of the view, when the plaque reaches to the last three stages, the doctor needs to decide to inform the patients or not based on the actual situation. The doctor also needs to decide to perform operations or not. The whole progression is shown in Figure 2.4.

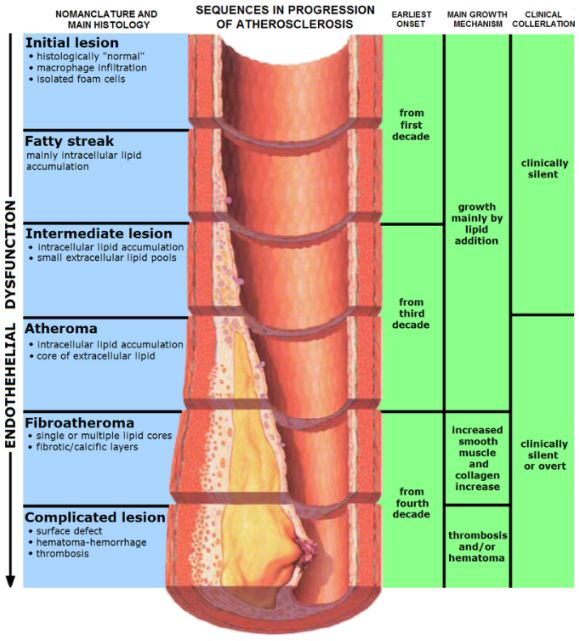

Figure 2.4: Progression of atherosclerosis

There are some pictures which are shown in Figure 2.5. These pictures are taken from really coronary arteries with plaques. The upper panel contains histological cross-sections and the lower panel contains the corresponding colour-coded, manually drawn contours. In the lower panel, brown represents adventitia, red represents media, yellow represents intima and orange represents necrotic core[1].

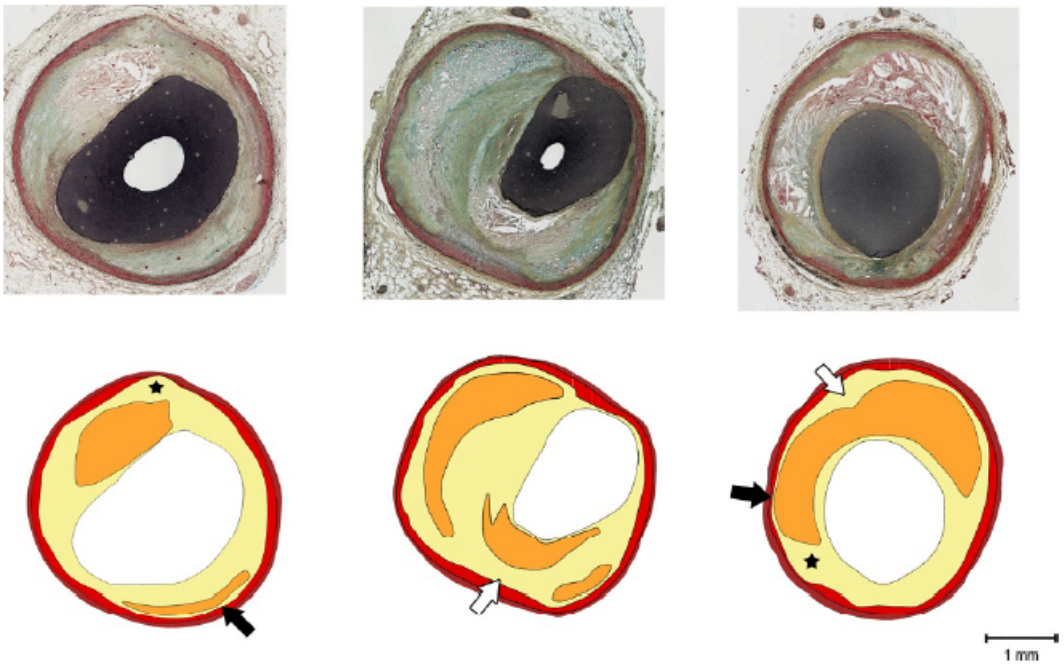

Figure 2.5: Examples of coronary artery plaque with different geometric features: histological cross-sections(upper panel),and corresponding color-coded,manually drawn contours (lower panel). [1]

2.4. Continuum mechanical framework for hyperelasticity

Hyperelastic material is a constitutive model which is set up for ideally elastic material whose strain-stress relation can be derived from a strain energy density function. It can provide a means of modelling some material which has a non-linear mechanical behaviour. It is known from section 2.2 that the healthy arterial walls have a non-linear strain-stress relation. So, the mechanical behaviour of the arterial wall can be modelled by the hyperelastic material model. Before applying the hyperelastic material model, some basic knowledge needs to be introduced

Deformation gradient:

In non-linear continuum mechanics, the description of deformation is quite important. The deformation gradient is an important variable in the description of deformation. It is defined as:

$$F_{ij} = \frac{\partial x_i}{\partial X_j} \qquad or \qquad \mathbf{F} = \frac{\partial \mathbf{x}}{\partial \mathbf{X}} \tag{2.1}$$

The $\partial\mathbf{X}$ is the infinitesimal line segment in the reference configuration, and the $\partial\mathbf{x}$ is the corresponding line segment in the current configuration.

The deformation gradient can also be written in the matrix form. In three dimensions, the matrix form is written as:

$$F_{ij} = \frac{\partial x_i}{\partial X_j} = \begin{bmatrix} \frac{\partial x_1}{\partial X_1} & \frac{\partial x_1}{\partial X_2} & \frac{\partial x_1}{\partial X_3} \\ \frac{\partial x_2}{\partial X_1} & \frac{\partial x_2}{\partial X_2} & \frac{\partial x_2}{\partial X_3} \\ \frac{\partial x_3}{\partial X_1} & \frac{\partial x_3}{\partial X_2} & \frac{\partial x_3}{\partial X_3} \end{bmatrix} \tag{2.2}$$

The determinant of the deformation gradient **F** is denoted as *J* which is called *Jacobian determinant*.

$$J = det(\mathbf{F}) \tag{2.3}$$

The deformation gradient can be divided into dilatational and distortional parts by multiplicative decomposition which is:

$$\mathbf{F} = (J^{1/3}\mathbf{I})\overline{\mathbf{F}} \tag{2.4}$$

The **I** is the second-order unit tensor.

The right and left Cauchy-Green tensors which are **C** and **b**. They are associated with the deformation gradient **F**. And their modified counterparts are also associated with the counterparts of the deformation gradient $\overline{\mathbf{F}}$.

$$\mathbf{C} = \mathbf{F}^T\mathbf{F} = J^{2/3}\overline{\mathbf{C}}, \qquad \overline{\mathbf{C}} = \overline{\mathbf{F}}^T\overline{\mathbf{F}} \tag{2.5}$$

$$\mathbf{b} = \mathbf{F}\mathbf{F}^T = J^{2/3}\overline{\mathbf{b}}, \qquad \overline{\mathbf{b}} = \overline{\mathbf{F}}\overline{\mathbf{F}}^T \tag{2.6}$$

Strain:

There are many different measures of the strain which can be applied in the non-linear continuum mechanics. The Green strain is the most widely used in the finite element methods. The Green strain can be expressed by the deformation gradient. According to the relation between the deformation gradient and the Cauchy-Green tensors, the Green strain can also be expressed by the Cauchy-Green tensors.

$$\mathbf{E} = \frac{1}{2}(\mathbf{F}^T \cdot \mathbf{F} - \mathbf{I}) = \frac{1}{2}(\mathbf{C} - \mathbf{I}) \tag{2.7}$$

The modified counterpart of the Cauchy-Green strain can be expressed as:

$$\overline{\mathbf{E}} = \frac{1}{2}(\overline{\mathbf{C}} - \mathbf{I}) \tag{2.8}$$

Stress:

There are lots of stress measures in non-linear continuum mechanics, and three measures are considered in this thesis. They are the Cauchy stress σ, the second Piola-Kirchhoff (PK2) stress tensor **S** and the Kirchhoff stress. The Cauchy stress can be expressed by the second Piola-Kirchhoff stress tensor as:

$$\sigma = J^{-1}\mathbf{F} \cdot \mathbf{S} \cdot \mathbf{F}^T \qquad or \qquad \sigma_{ij} = J^{-1}F_{ik}S_{kl}F_{lj}^T \tag{2.9}$$

This relation can also be inverted to express the Piola-Kirchhoff stress tensor by the Cauchy stress.

$$\mathbf{S} = J\mathbf{F}^{-1} \cdot \sigma \cdot \mathbf{F}^{-T} \qquad or \qquad S_{ij} = JF_{ik}^{-1}\sigma_{kl}F_{lj}^{-T} \tag{2.10}$$

The Kirchhoff stress is defined as:

$$\tau = J\sigma \qquad or \qquad \tau = \mathbf{F} \cdot \mathbf{S} \cdot \mathbf{F}^T \tag{2.11}$$

It can be observed from (2.11) that the Kirchhoff stress is almost identical to the Cauchy stress. The only difference is that the Kirchhoff stress is scaled by the Jacobian determinant. So, it is also called as the weighted Cauchy stress. It is identical to the Cauchy stress in isochoric motion. It can arise in hyperelastic constitutive relations. Since it can lead to symmetric tangent moduli, it is really useful in hyperelastic-plastic models.

As for the hyperelastic material, the Piola-Kirchhoff stress can be derived from a stored energy function (ψ) which is a potential for the stress. The Piola-kirchhoff stress can be expressed as:

$$\mathbf{S} = 2\frac{\partial\psi(\mathbf{C})}{\partial\mathbf{C}} = \frac{\partial w(\mathbf{E})}{\partial\mathbf{E}} \tag{2.12}$$

where ψ is the stored energy potential. When the potential is written as a function of the Green strain **E**, the notation w is used where the relation between the two scalar functions is given by w(**E**) = ψ (2 **E** + **I**). Hyperelastic material model can also provide a framework for frame-invariant formulation of

anisotropic material. This can be achieved by embodying the anisotropy in the potential w. Expressions for Kirchhoff stress can be obtained by appropriate transformations:

$$\tau = J\sigma = \mathbf{F}\cdot\mathbf{S}\cdot\mathbf{F}^T = 2\mathbf{F}\cdot\frac{\partial\psi(\mathbf{C})}{\partial\mathbf{C}}\cdot\mathbf{F}^T = \mathbf{F}\cdot\frac{\partial w(\mathbf{E})}{\partial\mathbf{E}}\cdot\mathbf{F}^T \tag{2.13}$$

Elasticity tensor:

As for the hyperelastic material, the rate forms of the constitutive equations are required in the linearization of the weak form. It can be obtained through taking the time derivative of (2.12).

$$\dot{\mathbf{S}} = 4\frac{\partial^2\psi(\mathbf{C})}{\partial\mathbf{C}\partial\mathbf{C}} : \frac{\dot{\mathbf{C}}}{2} = \frac{\partial^2 w(\mathbf{E})}{\partial\mathbf{E}\partial\mathbf{E}} : \dot{\mathbf{E}} = \mathbf{C}^{SE} : \frac{\dot{\mathbf{C}}}{2} = \mathbf{C}^{SE} : \dot{\mathbf{E}} \tag{2.14}$$

where

$$\mathbf{C}^{SE} = 4\frac{\partial^2\psi(\mathbf{C})}{\partial\mathbf{C}\partial\mathbf{C}} = \frac{\partial^2 w(\mathbf{E})}{\partial\mathbf{E}\partial\mathbf{E}} \tag{2.15}$$

is the second modulus which is also called as *second elasticity tensor*. It is known that the tangent modulus of the hyperelastic material has the major symmetry which is $C^{SE}_{ijkl} = C^{SE}_{klij}$. The second elasticity tensor also relates to symmetric measures of stress rate and strain rate. As a result, it also has the minor symmetries.

Isotropic hyperelastic materials:

As for isotropic hyperelastic materials, the stored strain energy function can be written as a function of the principal invariants (I_1, I_2, I_3) of the right Cauchy-Green deformation, such as $\psi = \psi(I_1, I_2, I_3)$. The principle invariants of a second-order tensor and their derivatives play important roles in elastic and elastic-plastic constitutive relations.

The derivatives of the principal invariants of a second-order tensor with respect to the tensor itself are required in constitutive equations. For reference:

$$\frac{\partial I_1}{\partial\mathbf{A}} = \mathbf{I}; \qquad \frac{\partial I_1}{\partial A_{ij}} = \delta_{ij} \tag{2.16}$$

$$\frac{\partial I_2}{\partial\mathbf{A}} = I_1\mathbf{I} - \mathbf{A}^T; \qquad \frac{\partial I_2}{\partial A_{ij}} = A_{kk}\delta_{ij} - A_{ji} \tag{2.17}$$

$$\frac{\partial I_3}{\partial\mathbf{A}} = I_3\mathbf{A}^{-T}; \qquad \frac{\partial I_3}{\partial A_{ij}} = I_3 A^{-1}_{ji} \tag{2.18}$$

The second Piola-Kirchhoff stress tensor for a hyperelastic material is given by (2.12). Thus, for an isotropic hyperelastic material:

$$\mathbf{S} = 2\frac{\partial\psi}{\partial\mathbf{C}} = 2\left(\frac{\partial\psi}{\partial I_1}\frac{\partial I_1}{\partial\mathbf{C}} + \frac{\partial\psi}{\partial I_2}\frac{\partial I_2}{\partial\mathbf{C}} + \frac{\partial\psi}{\partial I_3}\frac{\partial I_3}{\partial\mathbf{C}}\right) = 2\left(\frac{\partial\psi}{\partial I_1} + I_1\frac{\partial\psi}{\partial I_2}\right)\mathbf{I} - 2\frac{\partial\psi}{\partial I_2}\mathbf{C} + 2I_3\frac{\partial\psi}{\partial I_3}\mathbf{C}^1 \tag{2.19}$$

The Kirchhoff stress tensor is expressed as:

$$\tau = \mathbf{F}\cdot\mathbf{S}\cdot\mathbf{F}^T = 2\left(\frac{\partial\psi}{\partial I_1} + I_1\frac{\partial\psi}{\partial I_2}\right)\mathbf{B} - 2\frac{\partial\psi}{\partial I_2}\mathbf{B}^2 + 2I_3\frac{\partial\psi}{\partial I_3}\mathbf{I} \tag{2.20}$$

2.5. Hyperelastic material models for arterial wall tissue

There are three material models which are included in this thesis. They are Neo-Hookean material model, Holzapfel material model and Gasser material model. The Neo-Hookean material model is an extension of the Hooke's law to large deformations. The Neo-Hookean material model can be applied to represent the material behaviour of the matrix in the arterial wall. In order to include the influence of the collagen fibre in the material model, an anisotropic term is added to the formualtion, accounting for the direction of the collagen fibres following Holzapfel material model. Since the mechanical behaviour of the anisotropic part can be influenced by the arrangement of the collagen fibres, the influence of the collagen fibre dispersion is added to the Holzapfel material model which makes it become Gasser material model.

2.5.1. Neo-Hookean material model

The Neo-Hookean material a hyperelastic material model which can be regarded as an extension of the isotropic linear Hooke's law. The strain-stress curve of the Neo-Hookean material model is linear initially. However, when it reaches a certain point, the strain-stress curve will plateau. It can be applied to model the non-linear mechanical behaviour of materials under larger deformations. Based on the mechanical properties of the Neo-Hookean material model, it can be applied to model the non-linear behaviour of the matrix in the arterial wall.

The stored energy function for the Neo-Hookean material(isotropic with respect to the initial unstressed configuration) is:

$$\Psi(\mathbf{C}) = \frac{1}{2}\lambda_0(lnJ)^2 - \mu_0 lnJ + \frac{1}{2}\mu_0(trace\mathbf{C} - 3) \tag{2.21}$$

where λ_0 and μ_0 are the Lamé constants which are also associated with the Young's modulus E and Poisson's ratio ν as:

$$\lambda_0 = \frac{\nu E}{1 - \nu - 2\nu^2} \tag{2.22}$$

$$\mu_0 = \frac{E}{2(1+\nu)} \tag{2.23}$$

According to (2.19), the second Piola-Kirchhoff stress can be expressed as:

$$\mathbf{S} = \lambda_0 lnJ\mathbf{C}^{-1} + \mu_0(\mathbf{I} - \mathbf{C}^{-1}) \tag{2.24}$$

According to (2.20), the Kirchhoff stress can be expressed as:

$$\tau = \lambda_0 lnJ\mathbf{C}^{-1} + \mu_0(\mathbf{B} - \mathbf{I}) \tag{2.25}$$

According to (2.15), the elasticity tensor can be expressed as:

$$C^{SE}_{ijkl} = \lambda C^{-1}_{ij} C^{-1}_{kl} + \mu(C^{-1}_{ik} C^{-1}_{jl} + C^{-1}_{il} C^{-1}_{kj}) \tag{2.26}$$

$$C^{\tau}_{ijkl} = \lambda\delta_{ij}\delta_{kl} + \mu(\delta_{ik}\delta_{jl} + \delta_{il}\delta_{kj}) \tag{2.27}$$

where $\lambda = \lambda_0, \quad \mu = \mu_0 - \lambda lnJ$.

2.5.2. Holzapfel material model

In this thesis, the Holzapfel material model is chosen from the available constitutive models for arterial walls. The Holzapfel model was developed in 2000 by Gerhard A. Holzapfel and Thomas C.Gasser. It assumes that the arterial wall has a two-layer cylindrical geometry(Figure 2.6). Each layer can be regarded as a composite which is reinforced by two families of collagen fibres. The two collagen fibre families are arranged in symmetrical spirals.

It is assumed that each layer has similar mechanical properties. So, the same form of strain-energy function can be applied to different layers with different material parameters. The strain-energy function can be split into two parts, since there are two main components which contribute to the mechanical behaviour of the arterial wall. As a result, the strain-energy function $\overline{\Psi}$ is split a part $\overline{\Psi}_{iso}$ which is associated with the isotropic part of the response, related to the collagen fibres and a part $\overline{\Psi}_{aniso}$ which is associated with the anisotropic part of the response, related to the matrix. The non-collagenous matrix material which is assumed to be isotropic is associated with $\overline{\Psi}_{iso}$. As for the collagen fibres, they hardly contribute stiffness to the arterial wall in low pressure. However, when the arterial walls are under high pressure, the collagen fibres contribute almost entirely resistance and the mechanical behaviour of arterial wall is then governed by the collagen fibres.

The strain-energy function of the Holzapfel material model is written as:

$$\overline{\Psi}(\overline{\mathbf{C}}, \mathbf{a}_{01}, \mathbf{a}_{02}) = \overline{\Psi}_{iso}(\overline{\mathbf{C}}) + \overline{\Psi}_{aniso}(\overline{\mathbf{C}}, \mathbf{a}_{01}, \mathbf{a}_{02}) \tag{2.28}$$

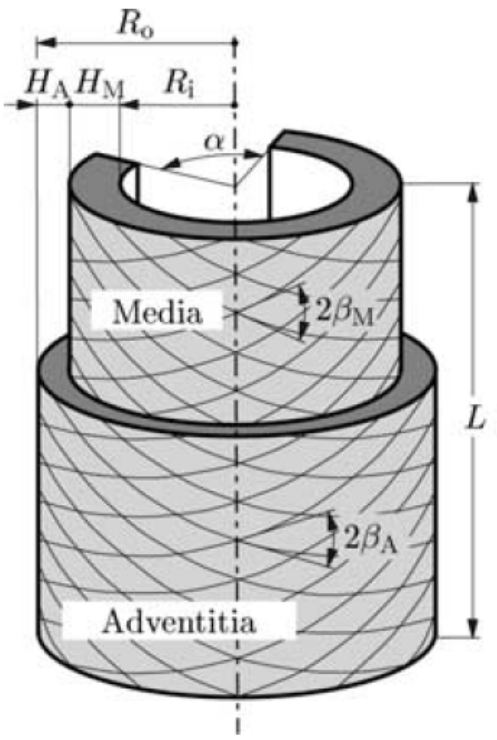

Figure 2.6: Geometry assumed by the Holzapfel material model [7]

where $\overline{\mathbf{C}}$ is the modified right Cauchy-Green tensor. The $\mathbf{a}_{01}$ and $\mathbf{a}_{02}$ are two direction vectors which can characterize the two families of collagenous fibers. These two direction vectors can be written in a cylindrical polar coordinate system. In 3 dimensional case, they are written as:

$$\mathbf{a}_{01} = \begin{bmatrix} 0 \\ cos\beta \\ sin\beta \end{bmatrix} \tag{2.29}$$

$$\mathbf{a}_{01} = \begin{bmatrix} 0 \\ cos\beta \\ -sin\beta \end{bmatrix} \tag{2.30}$$

where β is the angle between the collagen fibres and the circumferential direction in the arterial wall. This angle differs between different arterial layers. The first entry of the direction vectors represent the planar orientation of the arterial wall. Since, in Holzapfel material model, there is no radial fibres in the arterial wall, the value in the first entry is zero. In this thesis, only two-dimensional cases are considered. And the corresponding direction vectors are expressed as:

$$\mathbf{a}_{01} = \begin{bmatrix} cos\beta \\ sin\beta \end{bmatrix} \tag{2.31}$$

$$\mathbf{a}_{01} = \begin{bmatrix} cos\beta \\ -sin\beta \end{bmatrix} \tag{2.32}$$

Two structure tensors, which are based on the characteristics of the arterial wall, are defined to describe the response of the arterial wall. Each of them can be expressed as the tensor product of the corresponding direction vector.

$$\mathbf{A}_1 = \mathbf{a}_{01} \otimes \mathbf{a}_{01} \tag{2.33}$$

$$\mathbf{A}_2 = \mathbf{a}_{02} \otimes \mathbf{a}_{02} \tag{2.34}$$

Then two invariants $\bar{I}_4$ and $\bar{I}_6$ are introduced. They are the squares of the stretches in the directions of $\mathbf{a}_{01}$ and $\mathbf{a}_{02}$, which can be regarded as the stretch measures for the two families of collagen fibres. They can be expressed as:

$$\bar{I}_4(\overline{\mathbf{C}}, \mathbf{a}_{01}) = \overline{\mathbf{C}} : \mathbf{A}_1 \tag{2.35}$$

$$\bar{I}_6(\overline{\mathbf{C}}, \mathbf{a}_{02}) = \overline{\mathbf{C}} : \mathbf{A}_2 \tag{2.36}$$

The strain-energy density function for the anisotropic part is then written as:

$$\overline{\Psi}_{aniso}(\bar{I}_4, \bar{I}_6) = \frac{k_1}{2k_2} \sum_{i=4,6} \{exp[k_2(\bar{I}_i - 1)^2] - 1\} \tag{2.37}$$

where k_1 is a stress-like parameter and k_2 is a dimensionless parameter[7]. These two parameters are associated with the anisotropic contribution of collagen to the arterial response[2]. They can be regarded as a combination of the collagen fibre stiffness and collagen volume fraction[2].

The expression for Cauchy stress of the anisotropic part can be obtained through the following two equations:

$$\overline{\sigma} = J^{-1} dev(\overline{\mathbf{F}} \frac{\partial \overline{\Psi}}{\partial \overline{\mathbf{E}}} \overline{\mathbf{F}}^T) \tag{2.38}$$

with

$$dev(\cdot) = (\cdot) - \frac{1}{3}[(\cdot) : \mathbf{I}]\mathbf{I} \tag{2.39}$$

So, the final expression for the Cauchy stress of the anisotropic part is:

$$\overline{\sigma} = \sum_{i=4,6} 2\overline{\Psi}_i dev(\mathbf{a}_i \otimes \mathbf{a}_i) \tag{2.40}$$

where $\overline{\Psi}_i = \frac{\partial \overline{\Psi}_{aniso}}{\partial \bar{I}_i}$ denotes scalar response function and $\mathbf{a}_i = \overline{\mathbf{F}}\mathbf{a}_{0i}, i = 1, 2$ allows $\mathbf{a}_{0i}$ to be expressed in an Eulerian setting. The second-Piola Kirchhoff stress can be obtained through the following expression:

$$\mathbf{S} = J\mathbf{F}^{-1} \cdot \overline{\sigma} \cdot \mathbf{F}^{-T} \tag{2.41}$$

So, the final expression for the Second-Piola Kirchhoff stress is:

$$\mathbf{S}_{aniso} = J\mathbf{F}^{-1} \cdot (\sum_{i=4,6} 2\overline{\Psi}_i dev(\mathbf{a}_i \otimes \mathbf{a}_i)) \cdot \mathbf{F}^{-T} \tag{2.42}$$

The strain-energy density function for the isotropic part is taken from the Neo-Hookean material model which can be expressed as:

$$\Psi_{iso}(\mathbf{C}) = \frac{1}{2}\lambda_0 (lnJ)^2 - \mu_0 lnJ + \frac{1}{2}\mu_0 (trace\mathbf{C} - 3) \tag{2.43}$$

In the isotropic part, the strain-energy density function is expressed through the right Cauchy-Green tensor, not the modified counterpart.

Since the strain-energy density function for the isotropic part is taken from the Neo-Hookean material model, the Second-Piola Kirchhoff stress for the isotropic part is the same as the Neo-Hookean material model:

$$\mathbf{S}_{iso} = \lambda_0 lnJ\mathbf{C}^{-1} + \mu_0(\mathbf{I} - \mathbf{C}_{-1}) \tag{2.44}$$

Altogether, the Second-Piola Kirchhoff stress for the Holzapfel material model is $\mathbf{S} = \mathbf{S}_{iso} + \mathbf{S}_{aniso}$.

The elasticity tensor for the anisotropic part can be obtained through the equation (2.15). As a result, the elasticity tensor for the anisotropic part can be expressed as:

$$D_{aniso_{ijkl}} = 2k_1(a_{01_i}a_{01_j}a_{01_k}a_{01_l} + a_{02_i}a_{02_j}a_{02_k}a_{01_l}) \tag{2.45}$$

The elasticity tensor for the isotropic part can be taken from the Neo-Hookean material model which is:

$$D_{iso_{ijkl}} = \lambda C_{ij}^{-1}C_{kl}^{-1} + \mu(C_{ik}^{-1}C_{jl}^{-1} + C_{il}^{-1}C_{kj}^{-1}) \tag{2.46}$$

The elasticity tensor for the Holzapfel material model is $D_{ijkl} = D_{iso_{ijkl}} + D_{aniso_{ijkl}}$.

2.5.3. Gasser material model

In the Holzapfel material model, the collagen fibres in the arterial wall are assumed to be perfectly aligned. This is a realistic assumption for the media. However, based on the experiment results which are obtained by Canham[3], it is observed that there is an obvious dispersion of the structural orientation in the intima and adventitia. As a result, the Holzapfel material model cannot be applied to model the mechanical behaviour of the intima and adventitia. And, the intima is position where the plaque is formed. So, a new material model needs to be set up, in which the influence of the dispersion can be included. In this thesis, the Gasser material model is applied to analysis the mechanical behaviour of the arterial wall with dispersion. The Gasser material model can be regarded as an extension of the Holzapfel material model by adding a parameter which is related to the dispersion of the collagen fibres into the constitutive framework. The geometry of the Gasser material model is shown in Figure 2.7.

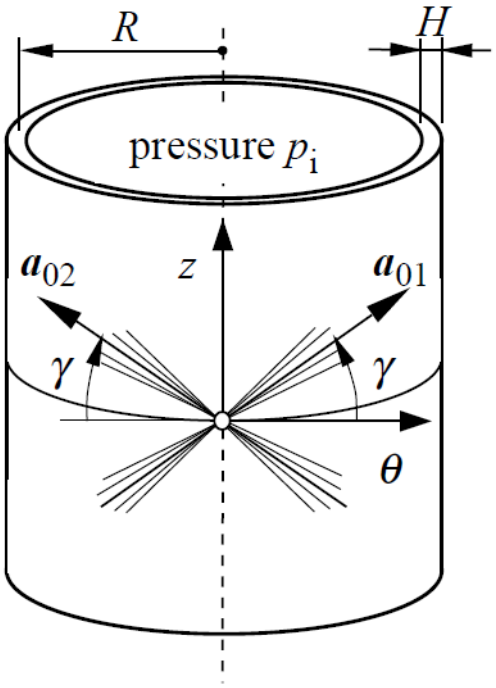

Figure 2.7: Geometry of the Gasser material model (Thin-wall approximation of the inflation of the adventitial layer with two embedded families of fibers. The mean orientations and the dispersion of the collagen fibers are characterized by γ and κ.)

In order to include the influence of the collagen fiber dispersion, a *generalized structure tensor* ***H*** is introduced.

It is assumed that there is a density function $\rho(\boldsymbol{M})$ which is referred as an orientation function[9]. It can be applied to represent the fibers' distribution in the reference configuration Ω_0 with respect to the referential orientation ***M***. ***M*** is an arbitrary unit vector which is located in the three dimensional Eulerian space[6]. ***M*** can be expressed by two Eulerian angles $\Theta \in [0, \pi]$ and $\Phi \in [0, 2\pi]$:

$$\boldsymbol{M}(\Theta,\Psi) = sin\Theta cos\Phi \mathbf{e}_1 + sin\Theta sin\Psi \mathbf{e}_2 + cos\Theta \mathbf{3}_3 \tag{2.47}$$

where $\{\mathbf{e}_1, \mathbf{e}_2, \mathbf{e}_3\}$ are the axes of a rectangular Cartesian coordinate system (Figure 2.10)[6].

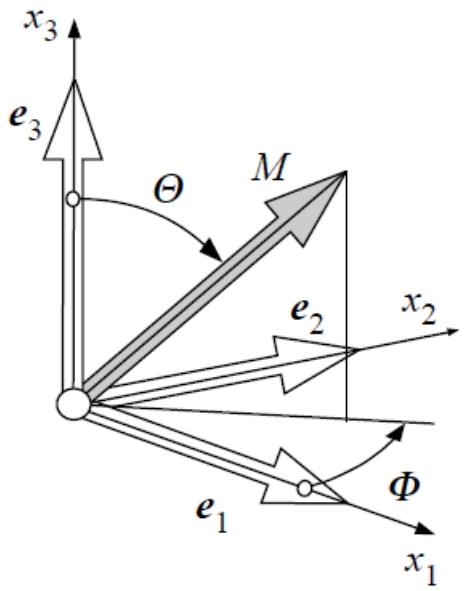

Figure 2.8: Characterization of an arbitrary unit direction vector ***M*** by means of Eulerian angels $\Theta \in [0,\pi]$ and $\Phi \in [0,2\pi]$ in a three-dimensional Cartesian coordinate system $\{\mathbf{e}_1, \mathbf{e}_2, \mathbf{e}_3\}$ [6]

So, the generalized structure tensor can be expressed by the density function $\rho(\boldsymbol{M})$ and the arbitrary unit vector ***M***:

$$\boldsymbol{H} = \frac{1}{4\pi}\int_{\omega} \rho(\boldsymbol{M}(\Theta,\Psi))\boldsymbol{M}(\Theta,\Psi) \otimes \boldsymbol{M}(\Theta,\Psi) d\omega \tag{2.48}$$

where ω is the unit sphere and $d\omega = sin\Theta d\Theta d\Psi$.

It can be observed from (2.48) that, the density function ρ is associated with two parameters Θ and Ψ. Since fiber of a given family are distributed with rotational symmetry about a mean referential direction, say $\boldsymbol{a}_0$, this family of fibers contributes a transversely isotropic character to the overall mechanical response of the arterial wall[6]. If the mean referential direction $\boldsymbol{a}_0$ is taken to coincide with the Cartesian basis vector $\boldsymbol{e}_3$, the density function is independent of Ψ. And the generality is still not lost. Then, the density function becomes $\rho(\Theta)$. It is assumed that the collagen fibers are distributed according to a transversely isotropic and π-periodic *von Mises* distribution[6]. So, the density function can be expressed as:

$$\rho(\Theta) = 4\sqrt{\frac{b}{2\pi}}\frac{exp[bcos(2\Theta)+1]}{erfi(\sqrt{2b})} \tag{2.49}$$

where b is the concentration parameter associated with the von Mises distribution. And, $erfi(x) = -ierf(x)$ is the imaginary error function[6]. The error function is expressed as:

$$erf(x) = \frac{2}{\sqrt{\pi}}\int_0^x exp(-t^2)dt \tag{2.50}$$

Then a dispersion parameter κ is introduced. It can be expressed by the density function:

$$\kappa = \frac{1}{4}\int_0^{\pi} \rho(\Theta) sin^3\Theta d\Theta \tag{2.51}$$

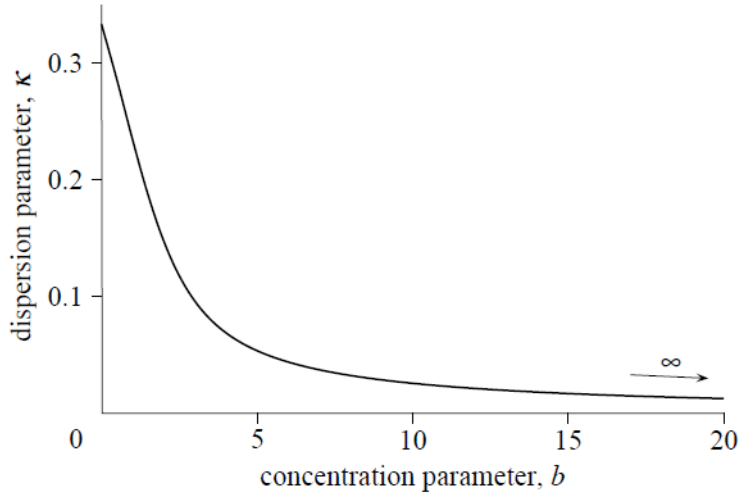

Figure 2.9: Relation between the dispersion parameter κ and the concentration parameter b [6]

The relation between the dispersion parameter κ and the concentration parameter b is shown in Figure 2.9 [6].

The upper limit of the dispersion parameter is $\frac{1}{3}$ which represents an isotropic distribution of the collagen fibre, and the corresponding value of the concentration parameter is 0. And the generalized structure tensor will become $\boldsymbol{I}$.The lower limit of the dispersion parameter is 0 which represents a perfect aligned distribution of the collagen fibres, in which case the corresponding value of the concentration parameter is positive infinity and the generalized structure tensor becomes $\mathbf{a}_0 \otimes \mathbf{a}_0$.

A graphical representation of the orientation of the collagen fibres based on the dispersion parameter is shown in Figure 2.10 [6].

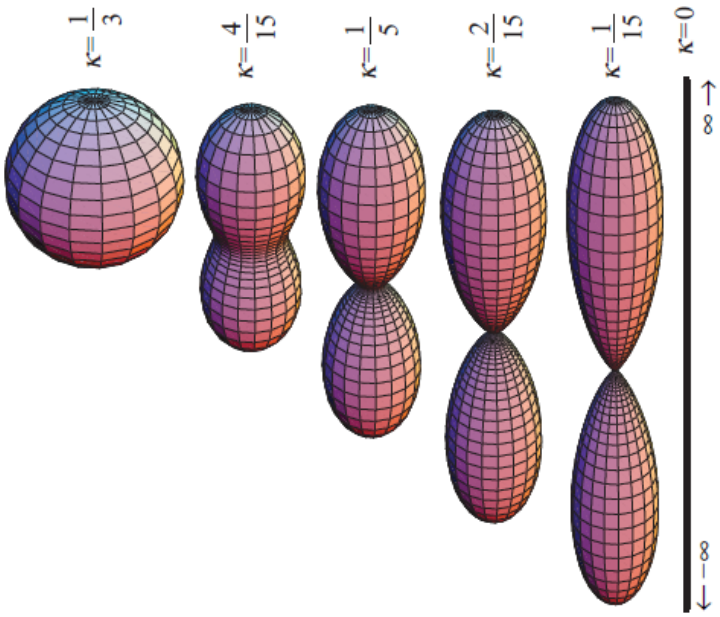

Figure 2.10: A graphical representation of the orientation of the collagen fibers based on the dispersion parameter [6]

It can be observed from Figure 2.10 that when the dispersion parameter $\kappa = \frac{1}{3}$, a sphere is observed. For the ideal aligned case in which the dispersion parameter is 0, an infinitely long line is observed. As for the other cases, ”bone-like” surfaces can be observed.

The relation between the probability density function ρ and the dispersion parameter is illustrated

in Figure 2.11[6].

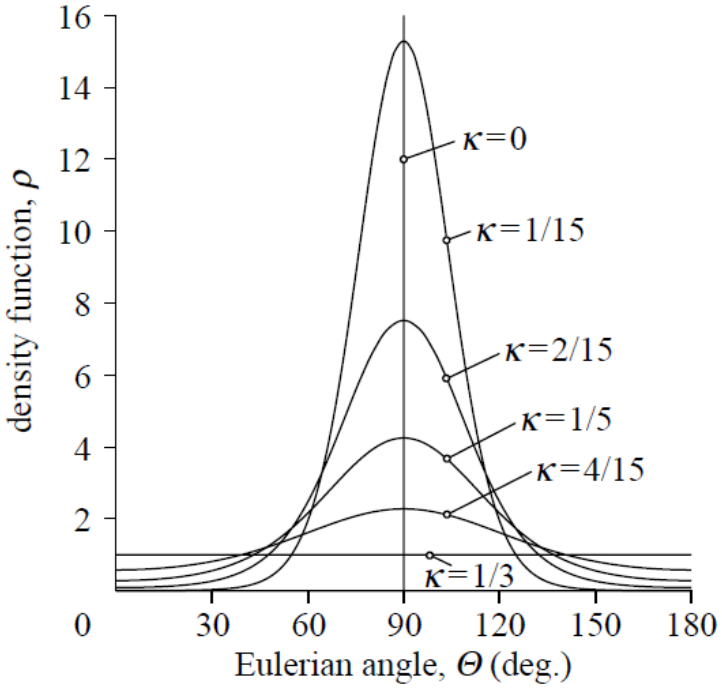

Figure 2.11: The probability density function of the von Mises distribution with different dispersion parameter [6]

It can be observed from Figure 2.11 that when the collagen fibers have an isotropic distribution with $\kappa = \frac{1}{3}$, the probability density function becomes a line with $\rho = 1.0$. When the collagen fibre are perfectly aligned, the probability density function becomes a Dirac delta function with $\Theta = 90^o$. For other values which are between these two boundary values, the probability density function shows a ”bell-shaped” curve.

The generalized structure tensor can then be expressed through the dispersion parameter and the referential unit vector:

$$\boldsymbol{H} = \kappa \boldsymbol{I} + (1 - 3\kappa)\mathbf{a}_0 \otimes \mathbf{a}_0 \tag{2.52}$$

where $\boldsymbol{I}$ is the identity tensor.

The strain-energy function for anisotropic parts can be expressed as:

$$\Psi_{aniso} = \sum_{i=1,2} \overline{\Psi}_{fi}(\overline{\mathbf{C}}, \mathbf{H}_i) = \sum_{i=1,2} \frac{k_1}{2k_2}[exp\{k_2[\kappa \bar{I}_1 + (1 - 3\kappa)\bar{I}_{4i} - 1]^2\} - 1] \tag{2.53}$$

where $\overline{I_1} = Tr(\overline{\mathbf{C}}$ and $\bar{I}_{4i} = \mathbf{a}_{0i} \otimes \mathbf{a}_{0i} : \overline{\mathbf{C}}$. This expression is comparable to the strain-energy function of the Holzapfel material model with an introduction of the dispersion parameter κ.

As for the Gasser material model, the Kirchhoff stress tensor is applied, which is defined based on the new strain-energy function. The Kirchhoff stress for the anisotropic part is expressed as:

$$\overline{\tau}_{aniso} = \sum_{i=1,2} \mathbb{P} : \tilde{\tau}_{fi} \tag{2.54}$$

Where $\mathbb{P}$ is the fourth-order projection tensor. It can be expressed as:

$$\mathbb{P} = \mathbb{I} - \frac{1}{3}\boldsymbol{I} \otimes \boldsymbol{I} \tag{2.55}$$

And the $\mathbb{I}$ is the fourth-order identity tensor:

$$(\mathbb{I})_{ijkl} = \frac{\delta_{ik}\delta_{jl} + \delta_{il}\delta_{jk}}{2} \tag{2.56}$$

$\tilde{\tau}_{fi}$ is defined as:

$$\tilde{\tau}_{fi} = 2\Psi'_{fi}\overline{\mathbf{h}}_i \tag{2.57}$$

where $\overline{\mathbf{h}}_i$ is:

$$\overline{\mathbf{h}}_i = \overline{\mathbf{F}}\mathbf{H}_i\overline{\mathbf{F}}^T = \kappa\overline{\mathbf{b}} + (1-3\kappa)(\overline{\mathbf{a}}_i \otimes \overline{\mathbf{a}}_i) \tag{2.58}$$

And, Ψ'_{fi} is the scalar stress function, it is expressed:

$$\Psi'_{fi} = k_1\overline{E}_i exp(k_2\overline{E}_i^2) \tag{2.59}$$

Where $\overline{E}_i$ is the Green-Lagrange strain-like quantity which can be expressed as:

$$\overline{E}_i = (\overline{\mathbf{h}}_i - \mathbf{H}_i) : \mathbf{I} = tr\overline{\mathbf{h}}_i - 1 \tag{2.60}$$

Just like the Holzapfel material model, the strain-energy function for the isotropic part can be taken directly from the Neo-Hookean material model which is:

$$\Psi_{iso}(\mathbf{C}) = \frac{1}{2}\lambda_0(lnJ)^2 - \mu_0 lnJ + \frac{1}{2}\mu_0(trace\mathbf{C} - 3) \tag{2.61}$$

The Kirchhoff stress for the isotropic part, which is the matrix in the arterial wall can be taken form the Neo-Hookean material model. It can be expressed as:

$$\overline{\tau}_{iso} = \lambda_0 lnJ\mathbf{C}^{-1} + \mu_0(\mathbf{B} - \mathbf{I}) \tag{2.62}$$

So, the final expression for the Kirchhoff stress of the Gasser material model is $\overline{\tau} = \overline{\tau}_{aniso} + \overline{\tau}_{iso}$
The isochoric elasticity tensor for the collagen fibres is defined as:

$$\overline{D}_{aniso_{ijkl}} = 4J^{-\frac{4}{3}} \sum_{m=1,2} \Psi''_{fm_{ijkl}}(\mathbb{P}_{ijkl} : \overline{h}_{m_{ijkl}}) \otimes (\mathbb{P}_{ijkl} : \overline{h}_{m_{ijkl}}) \tag{2.63}$$

where Ψ''_{fm} is the scalar elasticity function which can be formulated as:

$$\Psi''_{fm} = k_1(1 + 2k_2\overline{E}_i^2)exp(k_2\overline{E}_i^2) \tag{2.64}$$

The elasticity tensor for the matrix can be taken form the Neo-Hookean material model is:

$$\overline{D}_{iso_{ijkl}} = \lambda\delta_{ij}\delta_{kl} + \mu(\delta_{ik}\delta_{jl} + \delta_{il}\delta_{kj}) \tag{2.65}$$

So, the final expression for the elasticity tensor of the Gasser material model is $\overline{D} = \overline{D}_{aniso} + \overline{D}_{iso}$

2.6. Failure model

In order to develop a constitutive model for failure of arterial wall tissue, failure models need to be included to be combined with the material models. There is one failure model included in this thesis. The failure model is first introduced in one dimension case and then extended to three dimensions.

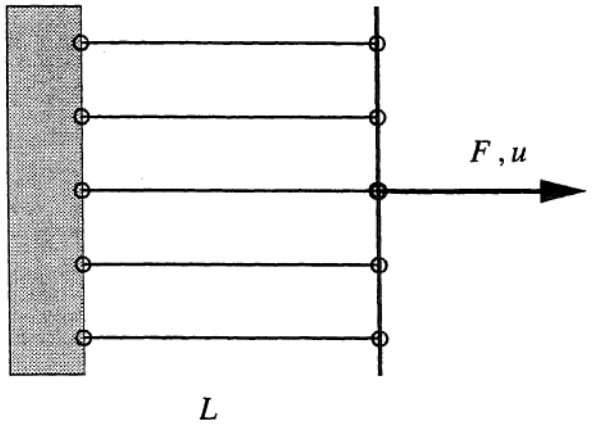

Figure 2.12: System of m parallel elastic-perfectly brittle bars [5]

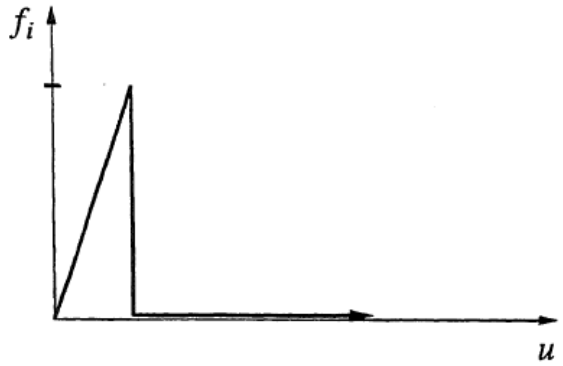

Figure 2.13: Elastic-perfectly brittle behaviour of bars [5]

2.6.1. An elementary failure model

A system which contains *m* parallel bars, which have the same stiffness *k* and different strength, is assumed (Figure 2.12). These bars all have a perfectly brittle mechanical behaviour (Figure 2.13), which means that the stress will drop directly to zero with no additional straining when failure happens. When one of the bars fails, the force at the moment when it fails is:

$$f_i = ku \tag{2.66}$$

Since all of the bars have a parallel arrangement, they all have the same displacement *u*. It is assumed that, for the displacement *u*, *n* bars are broken. The total force in the system can be expressed as:

$$F = \sum_{i=1}^{m-n} ku = (m-n)ku \tag{2.67}$$

The stiffness of the bar can be defined as: $k = \frac{EA_0}{ml}$. E is the total stiffness of the system. A_0 is the total cross-sectional area. l is the length of the bars. So, equation(2.67) can be rewritten as:

$$F = (1 - \frac{n}{m})EA_0\frac{u}{l} \tag{2.68}$$

In order to extend the discrete model to a continuous model, a damage parameter ω is defined which is equal to $\frac{n}{m}$. It follows from the elementary model that, the range of ω is from 0 to 1. And strain ϵ is applied to replace $\frac{u}{l}$. As a result, the equation(2.68) can be rewritten as:

$$F = (1 - \omega)EA_0\epsilon \tag{2.69}$$

The *damage parameter* can be regarded as an internal parameter reflecting how much of the system is still intact. The equation can also be written into a strain-stress format by using the expression $\sigma = \frac{F}{A_0}$

$$\sigma = \frac{F}{A_0} = (1 - \omega)E\epsilon \tag{2.70}$$

2.6.2. Generalization to three dimensions

In order to extend the elasticity-based failure model to three dimensions, it should start with the one-dimensional constitutive relation:

$$\sigma = (1 - \omega)E\epsilon \tag{2.71}$$

where ω is a scalar-valued internal parameter. It can characterize the total amount of the damage which the material has experienced. In order to extend the failure model into a two-dimensional case, the elastic modulus can be replaced by the stiffness matrix **D**:

$$\sigma = (1 - \omega)\mathbf{D}\epsilon \tag{2.72}$$

The growth of the damage is now controlled by the damage loading function:

$$f(\tilde{\epsilon}, \kappa) = \tilde{\epsilon} - \kappa \tag{2.73}$$

Where κ is a history-dependent parameter, which reflects the loading history. From an initial value κ_0 it grows, as it memorizes the largest value ever attained of the equivalent strain $\tilde{\epsilon}$. $\tilde{\epsilon}$ is the three-dimensional generalization of the uniaxial strain in the bars. In this thesis, the equivalent strain is defined by the principal strains which is proposed by Mazars for concrete:

$$\tilde{\epsilon} = \sqrt{\sum_{i=1}^{3} (\langle \epsilon_i \rangle)^2} \tag{2.74}$$

where ϵ_i is the principal strain, and $< \epsilon_i >= \epsilon_i$ if $\epsilon_i > 0$ and $< \epsilon_i >= 0$ otherwise.

Based on the definition of the history parameter, it will never decrease during the loading and its rate must be non-negative. If $\dot{\kappa} > 0$, the damage grows. And if the loading function is negative, unloading occurs, and $\dot{\kappa} = 0$.

The failure theory can be completed through defining an evolution law for the damage variable ω. ω can be regarded as a function of the history parameter κ.

$$\omega = \omega(\kappa) \tag{2.75}$$

The range of the ω is from 0 to 1. When ω is equal to 0, it represents that the material is fully intact. When ω is equal to 1, it represents that the material is fully damaged. In this thesis, the expression used for ω is:

$$\omega(\kappa) = \frac{\kappa_u(\kappa - \kappa_0)}{\kappa(\kappa_u - \kappa_0)} \tag{2.76}$$

With this relation, it is assumed that the uniaxial mechanical response of the material can be described by a bilinear strain-stress curve. In the first part, it is a linear elastic relation with a Young's modulus E up to a peak value of the stress $\sigma = f_t$. In the second part, it is a linear descending strain-stress curve which ends at an axial strain $\epsilon = \kappa_u$. κ_0 is the strain value where the strain-stress curve reaches the peak, and it can be expressed as: $\kappa_0 = \frac{f_t}{E}$.

3

Constitutive model for failure in hyperelastic material model

In order to model the plaque rupture, a new constitutive model for failure in hyperelastic materials need to be set up. The new constitutive model can be obtained by combining the material model and the failure model. It is assumed that the stress tensor for the hyperelastic material is $\mathbf{S}_h$ and the corresponding elasticity tensor is $\mathbf{C}_h$. This can be any of the three hyperelastic material models discussed in the previous chapter. As for the new constitutive model, the stress tensor is assumed to be $\mathbf{S}_n$ and the tangent stiffness matrix is assumed to be $\mathbf{C}_n$. $\mathbf{E}$ is the Green strain tensor.

By introducing damage in the hyperelastic material model, the stress tensor of the new constitutive model can be expressed as:

$$\mathbf{S}_n = (1-\omega)\mathbf{S}_h \tag{3.1}$$

where ω is the damage parameter which is mentioned in chapter 2 and it is also a function of the Green strain tensor. The elasticity tensor is $\mathbf{C} = \frac{\partial \mathbf{S}}{\partial \mathbf{E}}$. So, the stiffness matrix for the new constitutive model can be expressed as:

$$\mathbf{C}_n = \frac{\partial \mathbf{S}_n}{\partial \mathbf{E}} = (1-\omega)\frac{\partial \mathbf{S}_h}{\partial \mathbf{E}} - \frac{\partial \omega}{\partial \mathbf{E}}\mathbf{S}_h \tag{3.2}$$

It is known that the elasticity tensor for the hyperelastic model can be expressed as:

$$\mathbf{C}_h = \frac{\partial \mathbf{S}_h}{\partial \mathbf{E}} \tag{3.3}$$

So, the elasticity tensor for the new constitutive can be expressed as:

$$\mathbf{C}_n = \frac{\partial \mathbf{S}_n}{\partial \mathbf{E}} = (1-\omega)\mathbf{C}_h - \frac{\partial \omega}{\partial \mathbf{E}}\mathbf{S}_h \tag{3.4}$$

Since $\omega = \omega(\kappa)$, and the history parameter can be formulated by the equivalent strains. The equivalent strains can be obtained through the Green strain. According to the chain rule:

$$\frac{\partial \omega}{\partial \mathbf{E}} = \frac{\partial \omega}{\partial \kappa}\frac{\partial \kappa}{\partial \mathbf{E}} \tag{3.5}$$

From equation (2.76), the $\frac{\partial \omega}{\partial \kappa}$ can be expressed as:

$$\frac{\partial \omega}{\partial \kappa} = \frac{\kappa_u \kappa_0}{\kappa^2(\kappa_u - \kappa_0)} \tag{3.6}$$

According to equation (2.74), all the principal strains are strictly positive. The history parameter can be formulated as:

$$\kappa = \sqrt{< \epsilon_1 >^2 + < \epsilon_2 >^2 + < \epsilon_3 >^2} \tag{3.7}$$

So, $\frac{\partial \kappa}{\partial \mathbf{E}}$ can be rewritten as:

$$\frac{\partial \kappa}{\partial \mathbf{E}} = \frac{(\partial \sqrt{< \epsilon_1 >^2 + < \epsilon_2 >^2 + < \epsilon_3 >^2})}{\partial \mathbf{E}} = \sum_{i=1}^{3} \frac{< \epsilon_i >}{\sqrt{< \epsilon_1 >^2 + < \epsilon_2 >^2 + < \epsilon_3 >^2}} \frac{\partial \epsilon_i}{\partial \mathbf{E}} \tag{3.8}$$

The $\frac{\partial \epsilon_i}{\partial \mathbf{E}}$ can be expressed through the principal invariants of the Green strain tensor:

$$\frac{\partial \epsilon_i}{\partial \mathbf{E}} = \frac{1}{(3\epsilon_i^2 - 2\mathbf{I}_1 \epsilon_i + \mathbf{I}_2)} (\epsilon_i^2 \frac{\partial \mathbf{I}_1}{\partial \mathbf{E}} - \epsilon_i \frac{\partial \mathbf{I}_2}{\partial \mathbf{E}} + \frac{\partial \mathbf{I}_3}{\partial \mathbf{E}}) \tag{3.9}$$

Where $\mathbf{I}_1, \mathbf{I}_2$ and $\mathbf{I}_3$ are the principal invariants of the Green strain tensor. And the corresponding derivatives are explained in equation (2.16) (2.17) and (2.18).

So, the final expression for the new constitutive model is:

$$\mathbf{C}_n = \frac{\partial \mathbf{S}}{\partial \mathbf{E}} = (1-\omega)\mathbf{C}_h - \frac{\kappa_u \kappa_0}{\kappa^2(\kappa_u - \kappa_0)} \sum_{i=1}^{3} \left(\{ \frac{< \epsilon_i >}{\sqrt{< \epsilon_1 >^2 + < \epsilon_2 >^2 + < \epsilon_3 >^2}} \frac{1}{(3\epsilon_i^2 - 2\mathbf{I}_1 \epsilon_i + \mathbf{I}_2)} \left((\epsilon_i^2 \frac{\partial \mathbf{I}_1}{\partial \mathbf{E}} - \epsilon_i \frac{\partial \mathbf{I}_2}{\partial \mathbf{E}} + \frac{\partial \mathbf{I}_3}{\partial \mathbf{E}}) \right) \} \right) \mathbf{S}_h \tag{3.10}$$

Since three material models are included in this thesis, three constitutive models for failure can be inferred. The stress tensors and the elasticity tensors have already been obtained in chapter 2. The failure model is also explained in chapter 2. By combining the material model and the failure model through the method which is explained above. The three constitutive models for failure can be obtained.

3.1. Constitutive model for failure of the Neo-hookean material model

The second Piola-Kirchhoff stress for the new constitutive model can be expressed by combining equation (2.24) and equation (3.1), as:

$$\mathbf{S} = (1-\omega)[\lambda_0 ln J \mathbf{C}^{-1} + \mu_0 (\mathbf{I} - \mathbf{C}^{-1})] \tag{3.11}$$

The Kirchhoff stress can be formulated as:

$$\tau = (1-\omega)[\lambda_0 ln J \mathbf{C}^{-1} + \mu_0 (\mathbf{B} - \mathbf{I})] \tag{3.12}$$

The corresponding elasticity tensor can be expressed as:

$$\mathbf{C} = (1-\omega)\mathbf{C}_{Neo} - \frac{\kappa_u \kappa_0}{\kappa^2(\kappa_u - \kappa_0)} \sum_{i=1}^{3} \left(\{ \frac{< \epsilon_i >}{\sqrt{< \epsilon_1 >^2 + < \epsilon_2 >^2 + < \epsilon_3 >^2}} \frac{1}{(3\epsilon_i^2 - 2\mathbf{I}_1 \epsilon_i + \mathbf{I}_2)} \left((\epsilon_i^2 \frac{\partial \mathbf{I}_1}{\partial \mathbf{E}} - \epsilon_i \frac{\partial \mathbf{I}_2}{\partial \mathbf{E}} + \frac{\partial \mathbf{I}_3}{\partial \mathbf{E}}) \right) \} \right) \mathbf{S}_{Neo} \tag{3.13}$$

3.2. Constitutive model for failure of the Holzapfel material model

The second Piola-Kirchhoff stress for the new constitutive model can be expressed by combining equation (2.43), equation (2.44) and equation (3.1), as:

$$\mathbf{S} = (1-\omega_m)[\lambda_0 ln J \mathbf{C}^{-1} + \mu_0 (\mathbf{I} - \mathbf{C}^{-1})] + (1-\omega_f)[J \mathbf{F}^{-1} \cdot (\sum_{i=4,6} 2\overline{\Psi}_i dev(\mathbf{a}_i \otimes \mathbf{a}_i)) \cdot \mathbf{F}^{-T}] \tag{3.14}$$

The corresponding elasticity can be expressed as:

$$\mathbf{C} = (1-\omega_m)\mathbf{C}_{Hol_{aniso}} + (1-\omega_f)\mathbf{C}_{Hol_{iso}}$$
$$-\frac{\kappa_{um}\kappa_{0m}}{\kappa^2(\kappa_{um}-\kappa_{0m})}\sum_{i=1}^{3}\left(\{\frac{<\epsilon_i>}{\sqrt{<\epsilon_1>^2+<\epsilon_2>^2+<\epsilon_3>^2}}\frac{1}{(3\epsilon_i^2-2\mathbf{I}_1\epsilon_i+\mathbf{I}_2)}\left((\epsilon_i^2\frac{\partial\mathbf{I}_1}{\partial\mathbf{E}}-\epsilon_i\frac{\partial\mathbf{I}_2}{\partial\mathbf{E}}+\frac{\partial\mathbf{I}_3}{\partial\mathbf{E}})\right)\}\right)\mathbf{S}_{Hol_{aniso}}$$
$$-\frac{\kappa_{uf}\kappa_{0f}}{\kappa^2(\kappa_{uf}-\kappa_{0f})}\sum_{i=1}^{3}\left(\{\frac{<\epsilon_i>}{\sqrt{<\epsilon_1>^2+<\epsilon_2>^2+<\epsilon_3>^2}}\frac{1}{(3\epsilon_i^2-2\mathbf{I}_1\epsilon_i+\mathbf{I}_2)}\left((\epsilon_i^2\frac{\partial\mathbf{I}_1}{\partial\mathbf{E}}-\epsilon_i\frac{\partial\mathbf{I}_2}{\partial\mathbf{E}}+\frac{\partial\mathbf{I}_3}{\partial\mathbf{E}})\right)\}\right)\mathbf{S}_{Hol_{iso}} \quad (3.15)$$

3.3. Constitutive model for failure of the Gasser material model

The Kirchhoff stress for the new constitutive model can be expressed by combining equation (2.55), equation (2.62) and equation (3.1), as:

$$\mathbf{S} = (1-\omega_m)[\lambda_0 ln\mathbf{J}\mathbf{C}^{-1} + \mu_0(\mathbf{B}-\mathbf{I})] + (1-\omega_f)[\sum_{i=1,2}\mathbb{P}:\tilde{\tau}_{fi}] \quad (3.16)$$

The corresponding elasticity can be expressed as:

$$\mathbf{C} = (1-\omega_m)\mathbf{C}_{Gas_{aniso}} + (1-\omega_f)\mathbf{C}_{Gas_{iso}}$$
$$-\frac{\kappa_{um}\kappa_{0m}}{\kappa^2(\kappa_{um}-\kappa_{0m})}\sum_{i=1}^{3}\left(\{\frac{<\epsilon_i>}{\sqrt{<\epsilon_1>^2+<\epsilon_2>^2+<\epsilon_3>^2}}\frac{1}{(3\epsilon_i^2-2\mathbf{I}_1\epsilon_i+\mathbf{I}_2)}\left((\epsilon_i^2\frac{\partial\mathbf{I}_1}{\partial\mathbf{E}}-\epsilon_i\frac{\partial\mathbf{I}_2}{\partial\mathbf{E}}+\frac{\partial\mathbf{I}_3}{\partial\mathbf{E}})\right)\}\right)\mathbf{S}_{Gas_{aniso}}$$
$$-\frac{\kappa_{uf}\kappa_{0f}}{\kappa^2(\kappa_{uf}-\kappa_{0f})}\sum_{i=1}^{3}\left(\{\frac{<\epsilon_i>}{\sqrt{<\epsilon_1>^2+<\epsilon_2>^2+<\epsilon_3>^2}}\frac{1}{(3\epsilon_i^2-2\mathbf{I}_1\epsilon_i+\mathbf{I}_2)}\left((\epsilon_i^2\frac{\partial\mathbf{I}_1}{\partial\mathbf{E}}-\epsilon_i\frac{\partial\mathbf{I}_2}{\partial\mathbf{E}}+\frac{\partial\mathbf{I}_3}{\partial\mathbf{E}})\right)\}\right)\mathbf{S}_{Gas_{iso}} \quad (3.17)$$

4

Numerical analysis

Numerical analyses are performed on the constitutive models for failure in the three hyperelastic material models which are Neo-hookean material model, Holzapfel material model and Gasser material model. The numerical analyses are performed on a two-dimensional single finite element test. The single element is constrained in x and y directions on the left side. The force is applied on the right side of the element in x-direction, and the force is applied by displacement control method(Figure 4.1). The model is assumed to be in plain strain state. The Newton-Raphson method is applied to be the solution method for these non-linear problems. The analyses are performed by using *Jive* which is C++ programming toolkit for advanced numerical simulations.

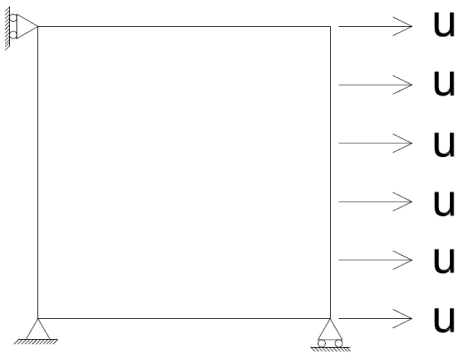

Figure 4.1: Geometry and boundary conditions of the single element

4.1. Neo-Hookean material model

First, the behaviour of the Neo-Hookean material combined with damage is investigated.

The load-displacement response for the new constitutive model for failure in the Neo-Hookean material model is shown in Figure(4.2) with $\mu = 6000, \lambda = 5000, \kappa_0 = 1.0, \kappa_u = 1.5$.

It can be observed from Figure(4.2) that the load-displacement curve can be divided into two parts. The first part is the curve before the failure starts. The second part is the curve after the failure starts. As for the first part, it can be observed that the curve is non-linear. The slope of the curve in the first part decreases with the increase of the displacement which means that the stiffness of the material will decrease with the increase of the deformation. As for the second part, another non-linear curve is observed. This curve represents the failure behaviour of the material. The beginning point of the curve represents where the material begins to fail. The end point of the curve represents where the material is totally damaged.

Since there are four parameters which can influence the response of the material which are λ, μ, κ_0 and κ_u. The λ and μ are related to the material properties. The κ_0 and κ_u are related to the failure behaviour. As a result, parameter sensitivity analyses need to be performed to see how these four

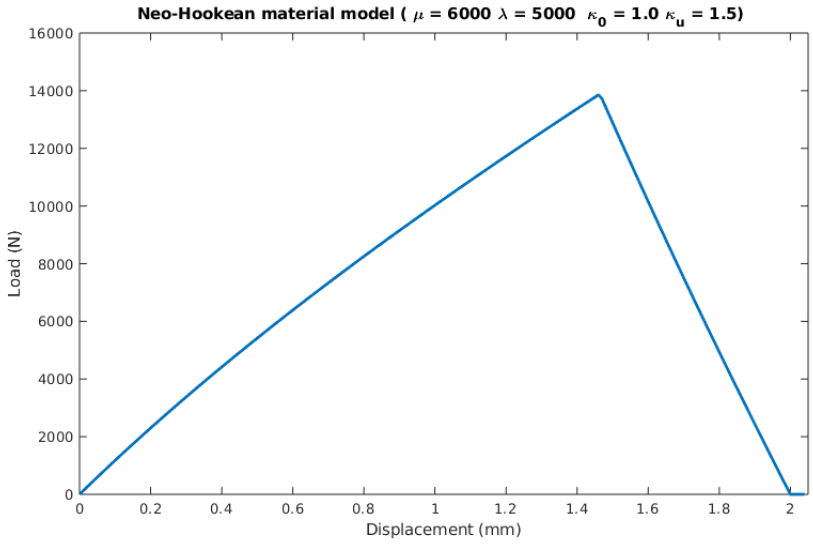

Figure 4.2: Load-displacement response for the constitutive model for failure in the Neo-Hookean material model

parameters can influence the response of the material. First, the influence of λ is analysed (Figure 4.3).

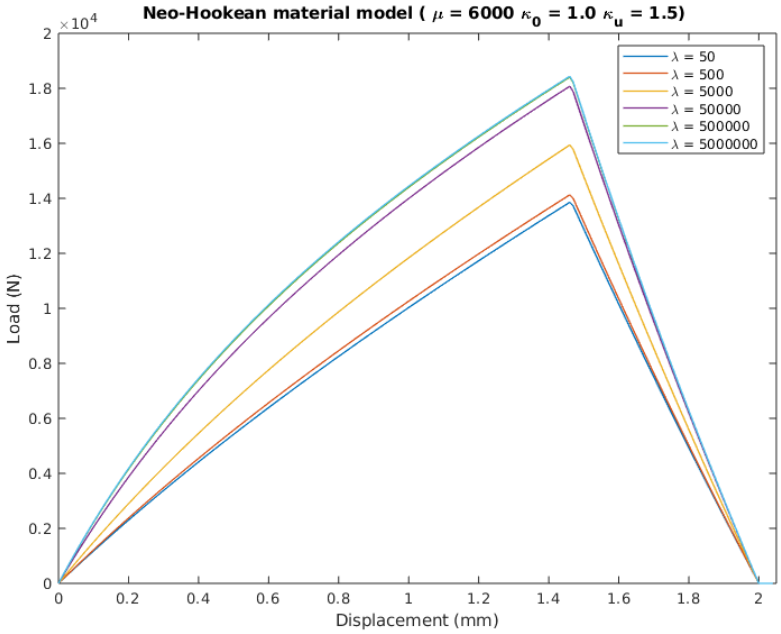

Figure 4.3: Influence of the λ on the load-displacement response of the Neo-Hookean material

It can be observed from Figure 4.3 that, in general, the overall load-displacement curve will get higher with the increase of λ. However, when λ is greater than 500000, the load-displacement responses are almost the same. This phenomenon can be explained through the expression of the Poisson's ratio (4.1). With the increase of λ, the Poisson's ratio increases. However, there is an upper limit of the Poisson's ratio which is 0.5. When λ goes to infinity, the Poisson's ratio reaches its upper limit 0.5, in which case incompressible material behaviour is obtained. As a result, when the value of λ is big enough, it cannot influence the load-displacement response of the Neo-Hookean material model.

$$\nu = \frac{\lambda}{2(\lambda + \mu)} = \frac{1}{2(1 + \frac{\mu}{\lambda})} \tag{4.1}$$

As for the parameter μ which is also related to the material properties, its influence on the load-displacement response is shown in Figure 4.4.

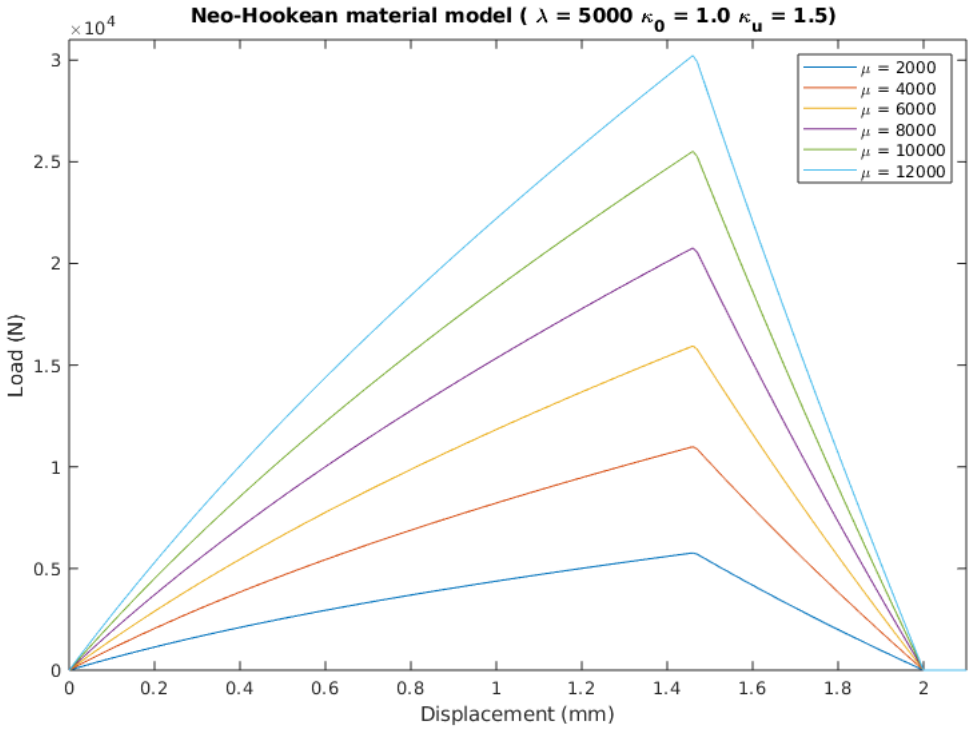

Figure 4.4: Influence of the μ on the load-displacement response of the Neo-Hookean material

The parameter μ is a parameter which is related to the stiffness of the material. It can be observed from Figure 4.4 that with the increase of μ, the stiffness of the material increases and the load-displacement curve gets higher.

The other two parameters which are κ_0 and κ_u are related to the failure behaviour. According to section 2.6, the κ_0 determines when the material begins to fail. Figure 4.5 is a reflection of this. In Figure 4.5, for a higher value of κ_0, the failure of the material begins later. The other parameter κ_u can determine when the failure finishes. This is reflected by Figure 4.6. With a same κ_0, the failure begins at the same time. However, since the value of κ_u is different, the failure finishes at different time.

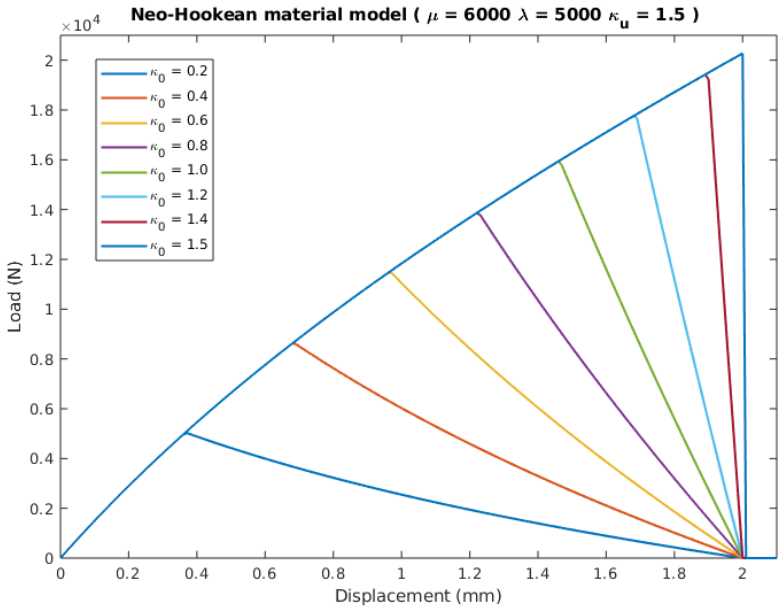

Figure 4.5: Influence of the κ_0 on the load-displacement response of the Neo-Hookean material

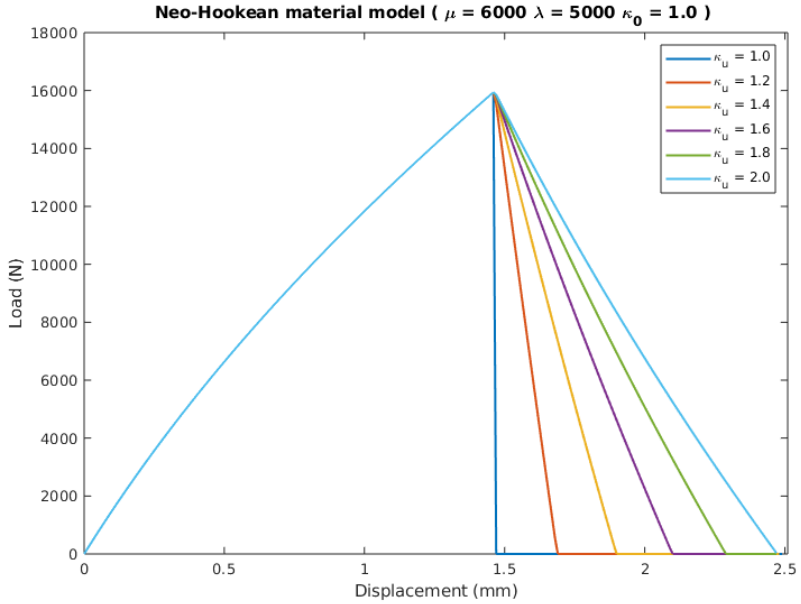

Figure 4.6: Influence of the κ_u on the load-displacement response of the Neo-Hookean material

4.2. Holzapfel material model

Next, the damage version of the Holzapfel material is investigated.

The load-displacement response for the new constitutive model for failure in the Holzapfel material model is shown in Figure 4.7 $\mu = 6000, \lambda = 5000, k_1 = 6000, k_2 = 1.0, \beta = 30^o, \kappa_{m0} = 0.5, \kappa_{mu} = 0.9, \kappa_{f0} = 0.7, \kappa_{fu} = 0.9$.

It can be observed form Figure 4.7 that the load-displacement response can be divided into three stages by two points(A and B) which are indicated in the figure. In the first stage, both the matrix and the collagen fibres do not start to fail. The slope of the curve in stage keeps increasing which means that the stiffness of the material keeps increasing. When the curve reaches point A, it comes to the second stage. In this stage, the matrix starts to fail and the collagen fibres do not. A sudden decrease of slope

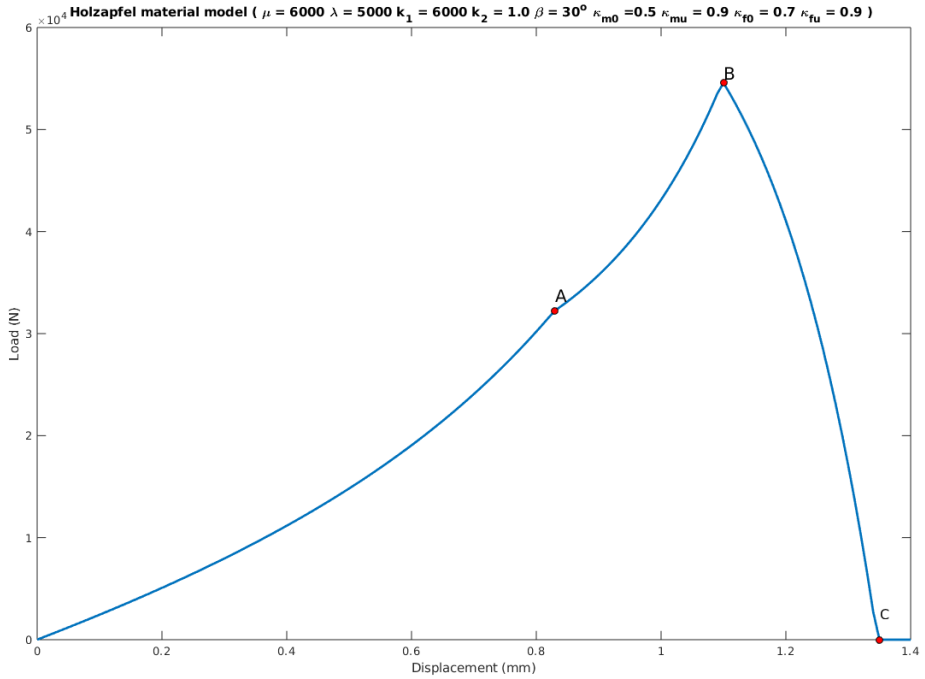

Figure 4.7: Load-displacement response for the constitutive model for failure in the Holzapfel material model

can be observed in point A. After that, the slope of the curve in the second stage keeps increasing. It can also be concluded from this phenomenon that, compared with the contribution of collagen fibres, the contribution of the matrix is small. After point B, it comes to the third stage where the collagen fibres start to fail. After point B, the curve goes down, which means that the material starts to fail as a whole. This can also illustrate that the collagen fibres play the main role in the strength of the arterial wall. Since κ_{mu} and κ_{fu} are equal to each other, the matrix and the collagen fibers will totally fail at the same point which is point C in the figure.

Compared with the Neo-Hookean material model, three new parameters are added in the Holzapfel material model. They are β, k_1 and k_2. According to Section 2.5.2, the β is the angle between the collagen fibres and the circumferential direction in the arterial wall. k_1 and k_2 are parameters which are related to the strength of the collagen fibres. k_1 is a stress-like parameter and k_2 is a dimensionless parameter. Parameter sensitivity analyses are also performed for the Holzapfel material model. First, the influence of β is analysed(Figure 4.8).

It can be observed from Figure 4.8 that the stiffness of the material reaches the highest value when the direction of the fibres is parallel to the direction in which the load is applied ($\beta = 0^o$). With the increase of the angle β, the stiffness of the material decreases. When the angle β is equal to 50^o, the response curve goes down after stage one. This means that, in this state, the matrix plays the main role in the mechanical behaviour of the material. When the angle is in between 60^o and 90^o, the load-displacement response remains the same. And the response curve coincides with the load-displacement curve in which only the contribution of the matrix is included. It can be concluded that, when the angle is in between 60^o and 90^o, the contribution of the collagen fibres can be neglected compared with the contribution of the matrix.

The influence of the stress-like parameter k_1 is shown in Figure 4.9. It can be observed , with the increase of k_1, the stiffness of the material increases. By comparing with the load-displacement response curve of the matrix, the higher of the value of k_1, the more contribution of collagen fibres is obtained. According to equation (2.37), the contribution of the collagen fibers can be set to zero by setting k_1 equal to zero which is also indicated by Figure 4.9.

The influence of the dimensionless parameter k_2 is shown in Figure 4.10. Just like the influence of k_1, with the increase of k_2, the stiffness of the material increases. By comparing with the load-displacement response curve of the matrix, the higher of the value of k_2, the more contribution of the collagen fibres is obtained. Another phenomenon can be observed that, for a small value of k_2, the

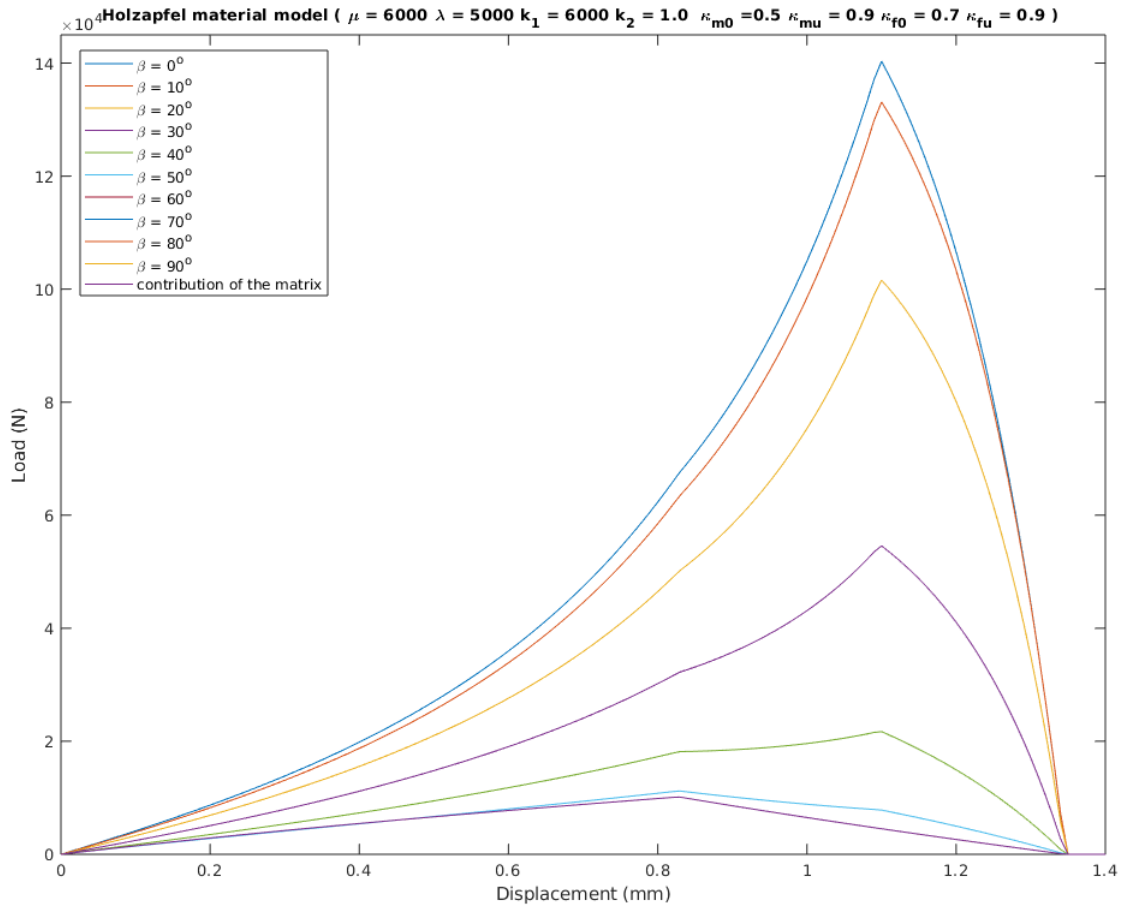

Figure 4.8: Influence of the angle β on the load-displacement response of the Holzapfel material model

curve in stage three is close to a linear curve. With the increase of k_2, the curve in stage three becomes more non-linear.

As for a real arterial wall, when it is loaded in tension, the matrix will fail first. After that, the collagen fibres will start to fail. In the end, the material will completely separate. This is only for normal case. As the arterial wall can be influenced by a lot of internal and external factors, some special cases may happen. In this thesis, three special cases are assumed. The first case (Figure 4.11) is that the collagen fibres will fail at first, then the matrix will start to fail. This cased can be realised by setting $\kappa_{m0} > \kappa_{f0}$. The second case (Figure 4.12) is that the collagen fibres will get fully damaged at first, and the matrix will get fully damaged later. This case can be realised by setting $\kappa_{mu} > \kappa_{fu}$. The third case (Figure 4.13) is a combination of the first case and the second case. In the third case, the collagen fibres will start to fail at first and will get fully damaged at first. This case can be realised by setting $\kappa_{m0} > \kappa_{f0}$ and $\kappa_{mu} > \kappa_{fu}$.

It can be observed from Figure 4.11 that, after the collagen fibres start to fail, the load-displacement response curve will go down gradually. This is due to that the collagen fibres contribute the main part of the strength of the material. After the matrix start to fail, the decline of the slope will become more significant. Since the matrix and the collagen will get fully damaged at the same time, the response curve will go directly to the end point.

In figure 4.12, the collagen fibres will get fully damaged before the matrix. In the first two stages, the load-displacement curve is the same as the normal load-displacement curve. However, when the collagen fibres are fully damaged, the load is not equal to zero. This is due to the fact that there is still a contribution which is from the matrix and an inflexion point can be observed in the figure. After the inflexion point, the absolute value of the slope will become quite small compared with the absolute value before the inflection point, and the curve will steadily decline to the end point.

The third case can be regarded as a combination of the first case and second case. In Figure

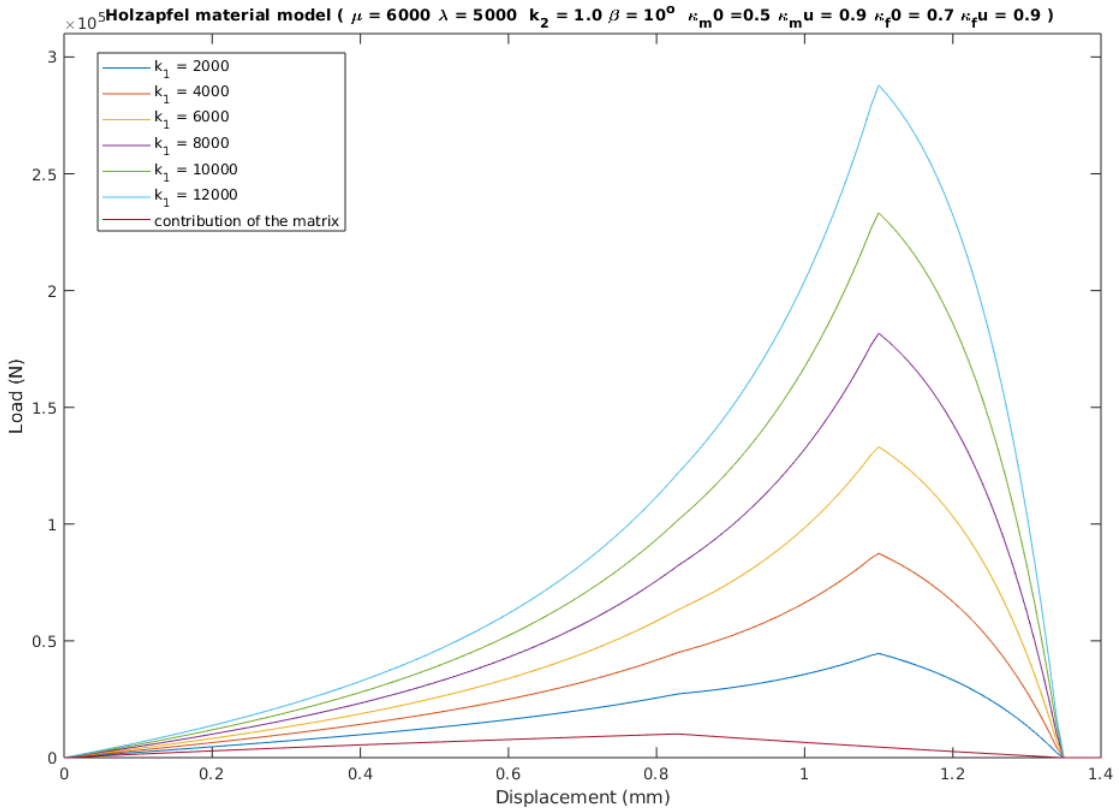

Figure 4.9: Influence of k_1 on the load-displacement response of the Holzapfel material model(add k1=0)

4.13, two inflexion points can be observed. After the first inflexion point, the collagen fibres start to fail. Since it contributes the main part of the strength of the material. Then, it comes to the second inflexion point. In this point, the collagen fibres are fully damaged. Since the matrix is not fully damaged and the material still have some strength to bear the load, the load will not be equal to zero immediately. The response curve will decline much more slowly. When the material is fully damaged, the load will become zero and the curve will reach the end point.

4.3. Gasser material model

Finally, the damage version of the Gasser material is investigated.

The load-displacement response for the new constitutive model for failure in the Gasser material model is shown in Figure 4.14.

By comparing Figure 4.14 with Figure 4.7, it can be observed that the load-displacement response of the Gasser material model is similar to the load-displacement response of the Holzapfel material model. There are also three stages which are divided by two points (A,B) in the response curve of Gasser material model. The features of the response curve in the three stages are the same as the features in the Holzapfel material model. This is due to that the Gasser material model is set up based on the Holzapfel material model. It can be regarded as an extension of the Holzapfel material model. So, the response curves are similar with each other.

In the Gasser material model, there are two parameters which are related to the arrangement of the collagen fibres. They are the angle β and the dispersion parameter κ. The influence of these two parameters on the mechanical behaviour of the arterial wall is analyzed. First, the influence of the dispersion parameter κ is analyzed for five given values of β. The results are shown in Figure 4.15, Figure 4.16, Figure 4.17, Figure 4.18 and Figure 4.19.

It can be observed from Figure 4.15, Figure 4.16 and Figure 4.17 that, for a given value of the angle β, the stiffness of the material reaches the highest value when the dispersion parameter is equal to zero. With the increase of the dispersion parameter, the stiffness decreases. When the dispersion

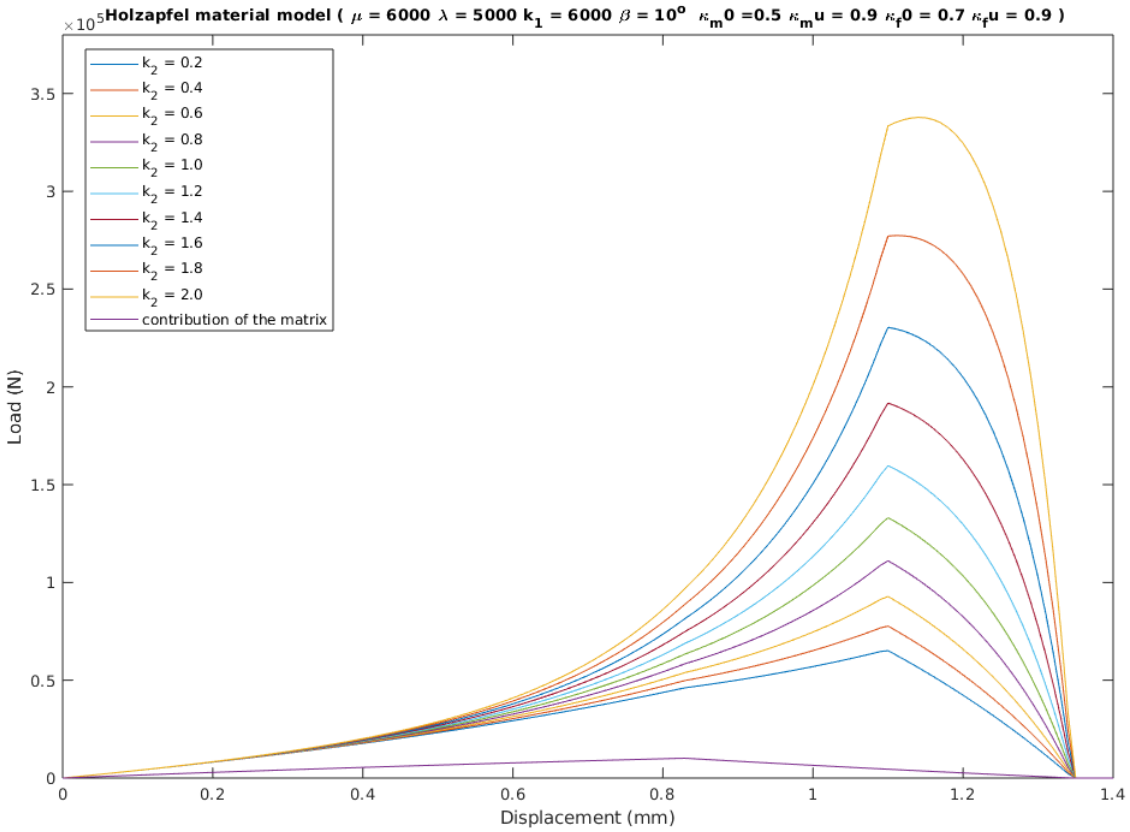

Figure 4.10: Influence of k_2 on the load-displacement response of the Holzapfel material model

parameter is higher than 0.3, the contribution of the collagen fibres is quite small which makes the response curve really close to the response curve of the matrix. According to Figure 4.8, it is known that when the angle is between 60^o and 90^o, the contribution of the collagen fibres can be neglected. This can also be proved by Figure 4.18, and Figure 4.19. In these two figures, only one response curve can be observed, which means that, compared with the contribution of the matrix, the contribution of the collagen fibres can be neglected. This also indicates that when β is between 60^o and 90^o, the dispersion rate have an ignorable influence on the overall mechanical behaviour of the arterial wall.

The influence of the angle β is then analyzed for five given values of the dispersion parameter κ. The results are shown in Figure 4.20, Figure 4.21, Figure 4.22, Figure 4.23 and Figure 4.24.

As for Figure 4.20, Figure 4.21 and Figure 4.22, they can be compared with Figure 4.8. It can be concluded that, for a given value of the dispersion parameter, the influence of the angle β is the same as the influence of the angle β in the Holzapfel material model. The stiffness of the material reaches the highest value when the angle is equal to 0^o. Then, it decreases with the increase of the angle. When the angle is between 60^o and 90^o, the contribution of the collagen fibres can be neglected and the corresponding curves are close to each other. In Figure 4.23 and Figure 4.24, it can be observed that all of the curves are close each other. In this two figures, the values of the dispersion parameter are large enough which makes the collagen fibres in the arterial wall cannot be divided into two groups. In this state, the collagen fibres can be regarded to be randomly arranged in every possible direction. So, the angles can only have a quite small on the overall mechanical response of the arterial wall. As a result, there is only a slight difference between different curves.

4.4. Verification of different material models

Three material models are included in this thesis. The Neo-Hookean material model is an extension of the Hooke's law which can be applied to model the mechanical behaviour of the matrix in the arterial wall. In order to model the overall mechanical behaviour of the arterial wall, the Holzapfel material model is set up by adding the contribution of the collagen fibres in the arterial wall to the Neo-Hookean

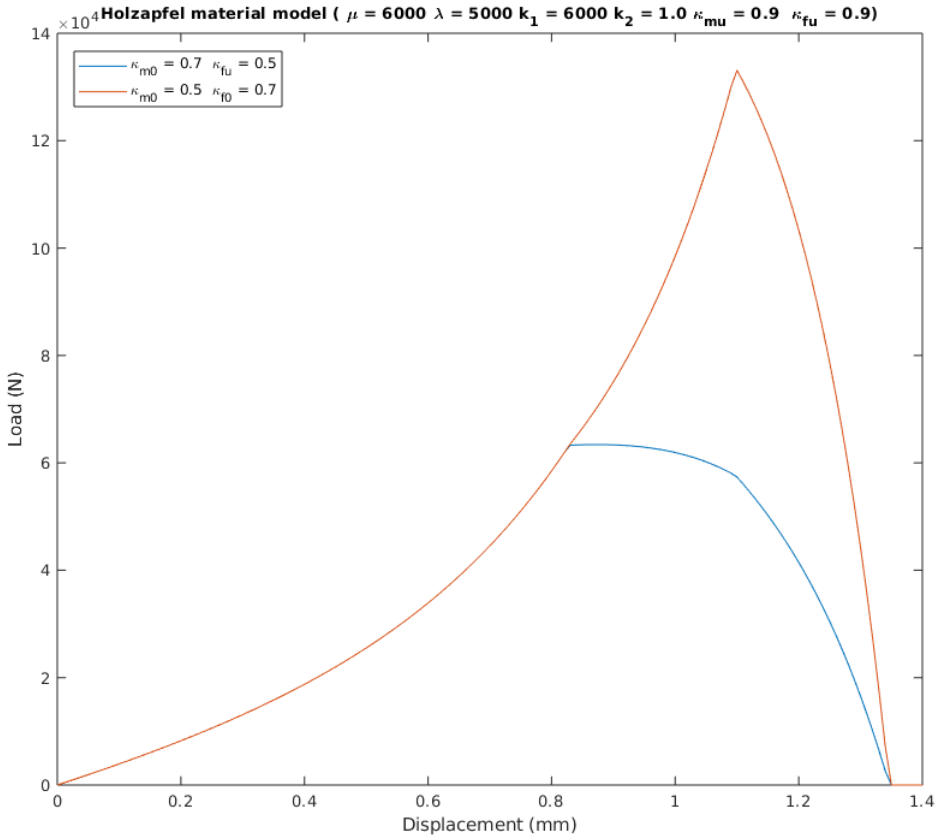

Figure 4.11: First case: the collagen fibers will start to fail before the matrix

material model. Since there is dispersion existing in the arterial wall, in order to include the influence of the dispersion in the material model, the Gasser material model is set up by adding the dispersion parameter to the Holzapfel material model. Based on this relation, the Neo-Hookean material model can be regarded as a special case of the Holzapfel material model and the Gasser material model. The Holzapfel material model can be regarded as a special case of the Gasser material model. As a result, the Neo-Hookean material model can be verified by the Holzapfel material model and the Gasser material model. The Holzapfel material model can be verified by the Gasser material model.

4.4.1. Verification of the Neo-Hookean material model by the Holzapfel material model and the Gasser material model

In the Holzapfel material model, if the value of k_1 is set equal to zero, the contribution of the collagen fibres will be equal to zero. As a result, only the matrix contributes to the strength of the material which means that the Holzapfel material becomes Neo-Hookean material. By setting the material parameters of the isotropic part in the Holzapfel material equal to the material parameters of the Neo-Hookean material. The Neo-Hookean material model can be verified. The corresponding load-displacement response curves are shown in Figure 4.25.

It can be observed from Figure 4.25 that the load-displacement response of the Neo-Hookean material model coincides with the load-displacement response of the Holzapfel material model. According to equation 2.24 and equation 2.44, in the Holzapfel material model, the expression for the Second-Piola Kirchhoff stress of the isotropic part (matrix) is the same as the expression for the Second-Piola Kirchhoff in the Neo-Hookean material model. According to equation 2.26 and equation 2.45, the expressions for the elasticity tensor are also the same. As a result, by neglecting the contribution of the collagen fibres, the load-displacement response curves coincide with each other.

Just like the Holzapfel material model, in the Gasser material model, the contribution of the collagen fibres can be neglected by setting the value of k_1 equal to zero. In this way, only the matrix contributes to the strength of the Gasser material model. Setting the material parameters of the matrix equal to each

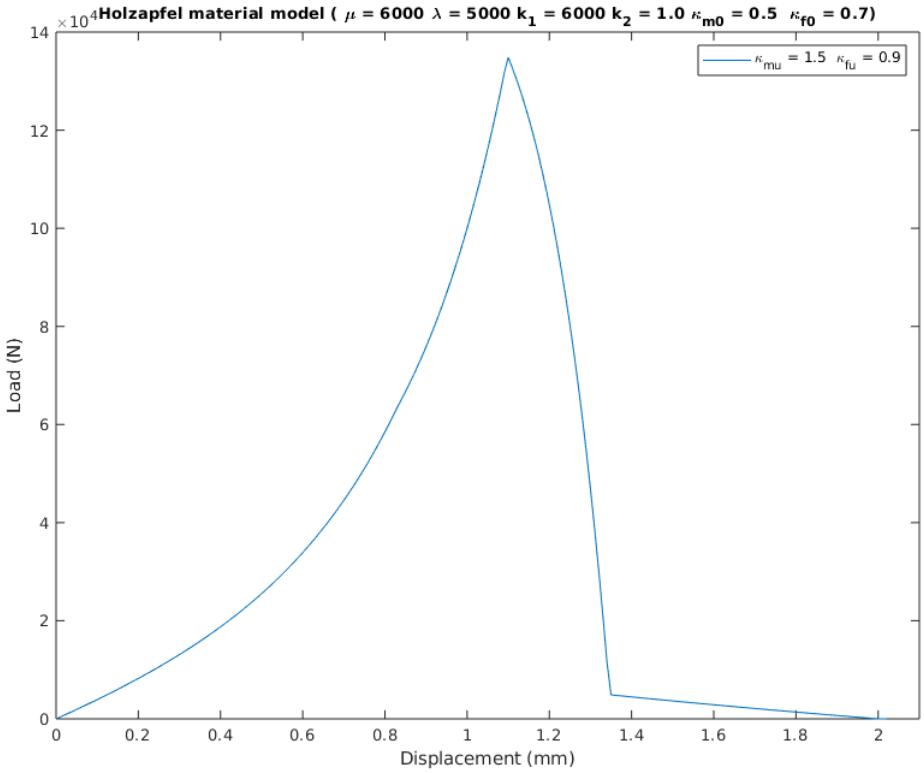

Figure 4.12: Second case: the collagen fibers will get fully damaged before the matrix

other, the Neo-Hookean material model is verified by the Gasser material model. The corresponding load-displacement response curves are shown in Figure 4.26.

The load-displacement curve of the Gasser material model is higher than the response curve of the Neo-Hookean material model. According to equation 2.24 and equation 2.62, the Second-Piola Kirchhoff stress is applied in the Neo-Hookean material model. However, the Kirchhoff stress is applied in the Gasser material model. The expressions for the elasticity tensor are also different. As a result, the load-displacement response curves are different. As for the Gasser material model, it can be observed from the figure that the slope in the first part increases with the increase of the displacement. This means that the stiffness of the matrix will increase with the increase of the deformation. This phenomenon is caused by the different expressions for the stress and elasticity tensor.

4.4.2. Verification of the Holzapfel material model by the Gasser material model

Compared with the Holzapfel material model, a dispersion is added in the Gasser material model. In the Holzapfel material model, the collagen fibres are assumed to be perfectly aligned with each other. As for the Gasser material model, if the dispersion parameter is set to be zero, the collagen fibres are perfect aligned with each other. If the other material parameters are the same, the Gasser material model can be applied to verify the Holzapfel material model. The corresponding load-displacement curves are shown in Figure 4.27.

It can be observed from Figure 4.27 that the load-displacement response curve for the Gasser material model is higher than the curve of the Neo-Hookean material model. According to equation 2.37 and equation 2.53, there is a two times relation for the strain-energy function between these two material model. If the dispersion parameter is set to be zero and other parameters are the same, the strain energy function of the Gasser material model is twice than the strain energy function of the Holzapfel material model. This influence can be avoided by setting the value k_2 of the Gasser material model equal to half of the value of the Holzapfel material model. The corresponding response curves are shown in Figure 4.28

In Figure 4.28, the load-displacement response curve gets lower compared with Figure 4.27. However, it is still higher than the response curve of the Holzapfel material model. They do not coincide with

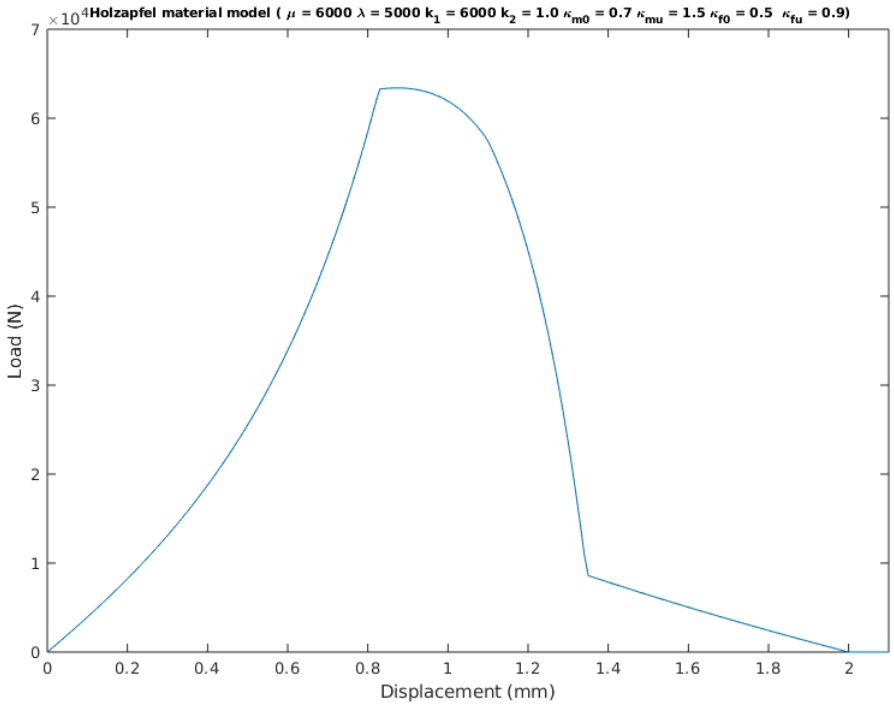

Figure 4.13: Third case:the collagen fibers will start to fail at first and will get fully damaged at first

each other. According to section 4.4.1, the response curve of the matrix in the Gasser material model is higher than the curve of the matrix in the Holzapfel material model. This may lead to the response curve of the Gasser material model higher than the curve of the Holzapfel material model. As a result, the contribution of the matrix should be removed. The corresponding curves are shown in Figure 4.29.

It can be observed from Figure 4.29 that there is not too much difference between Figure 4.28 and Figure 4.29 which indicates that the contribution of the matrix is quite small compared with the contribution of the collagen fibres. The response curve of the Gasser material model is still higher than the response curve of the Holzapfel material model. This phenomenon indicates that even the strain energy functions are equal to each other, the response curves are still different. Since the methods which are applied to get the expressions for stress and elasticity tensor are different. So, the expressions for stress and elasticity tensor are critical in setting up material models.

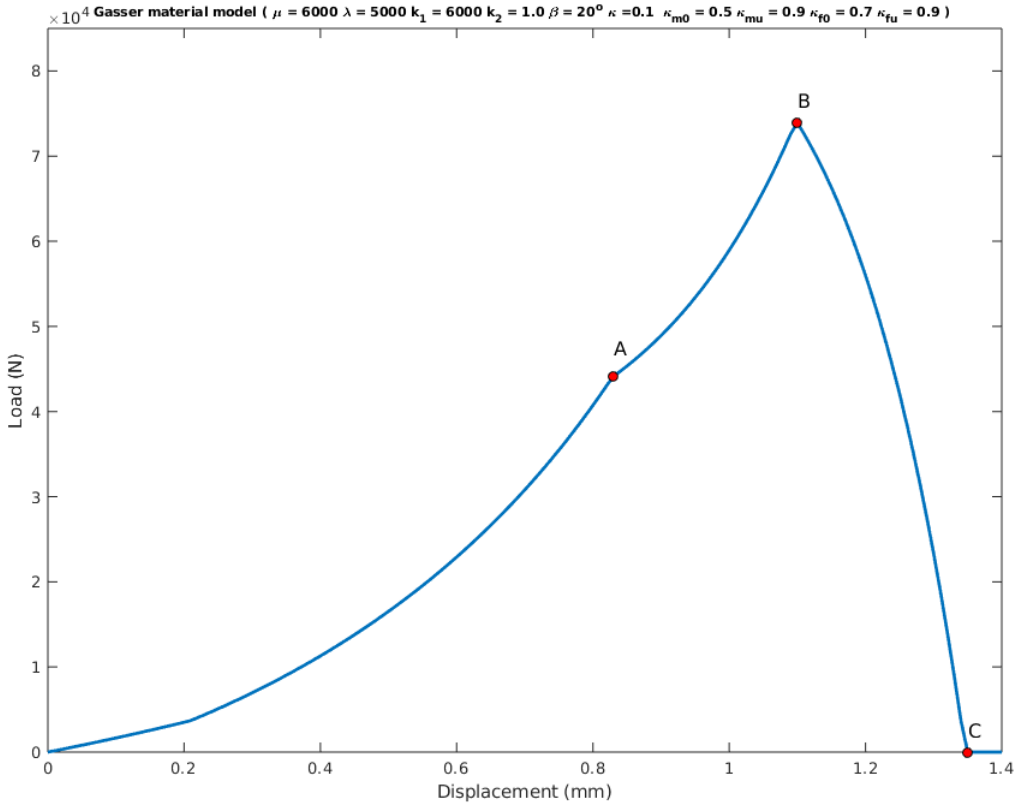

Figure 4.14: Load-displacement response for the constitutive model for failure in the Gasser material model

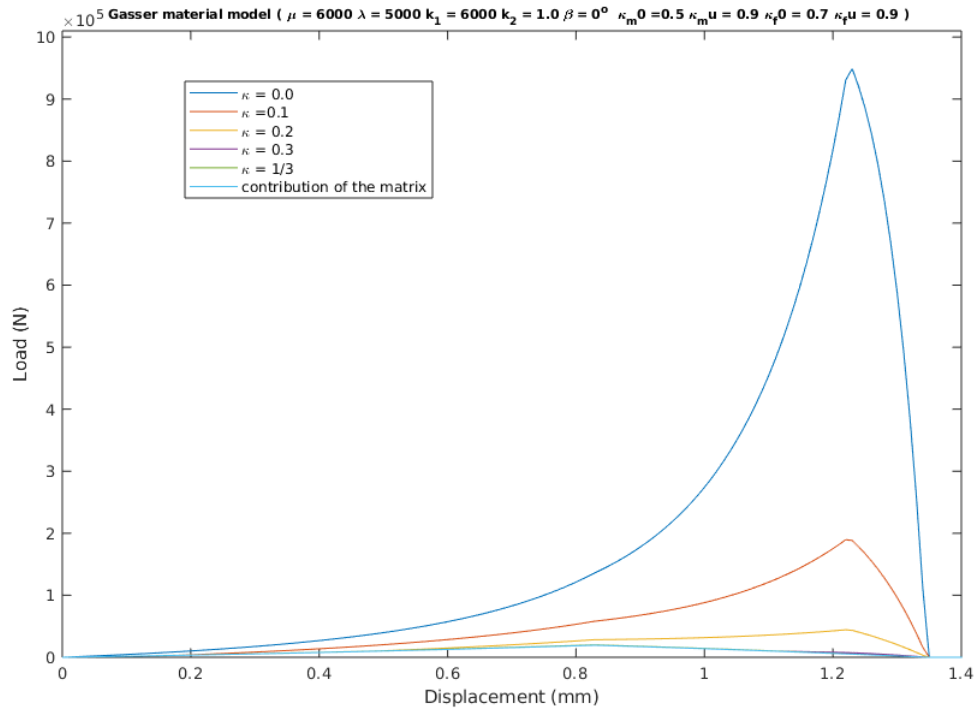

Figure 4.15: Influence of the dispersion parameter κ when $\beta = 0^o$

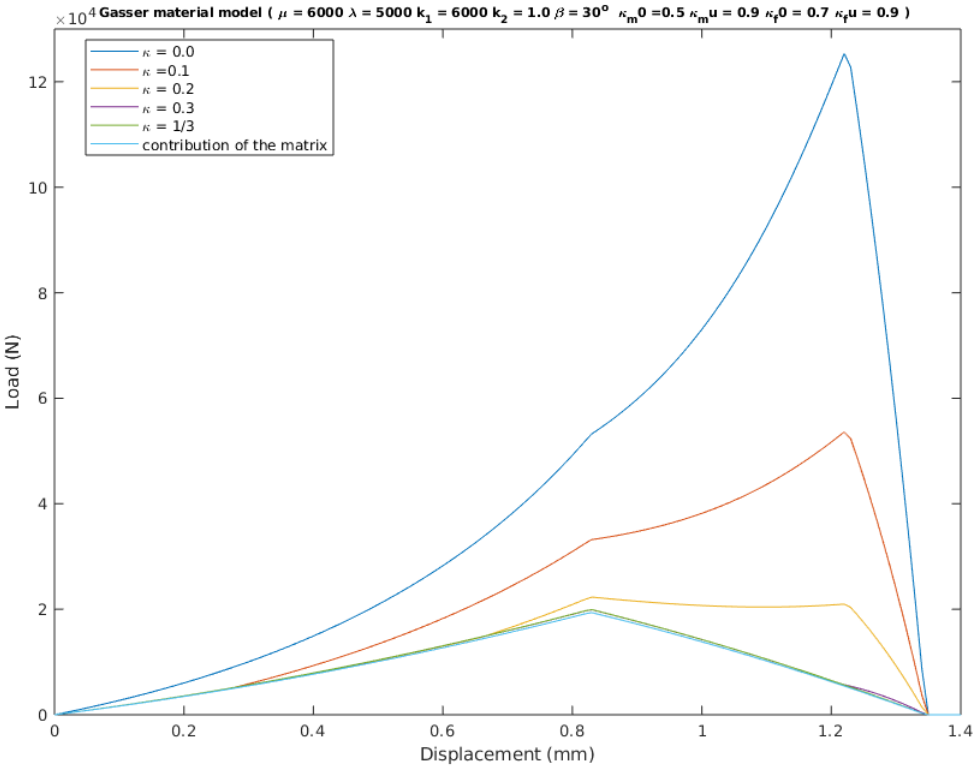

Figure 4.16: Influence of the dispersion parameter κ when $\beta = 30^o$

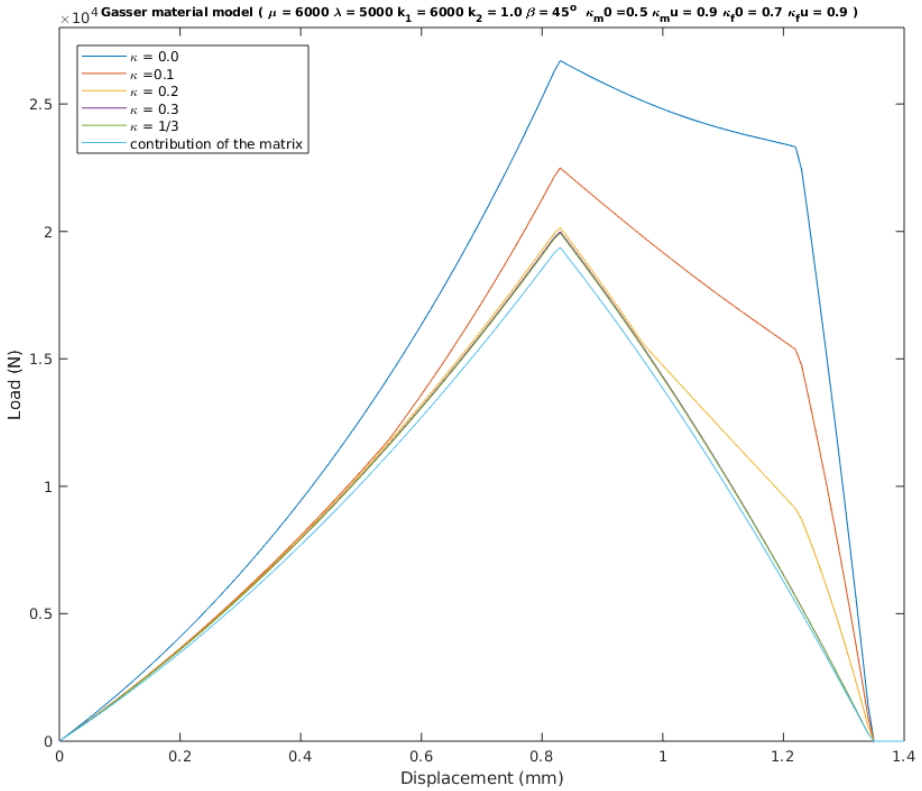

Figure 4.17: Influence of the dispersion parameter κ when $\beta = 45^o$

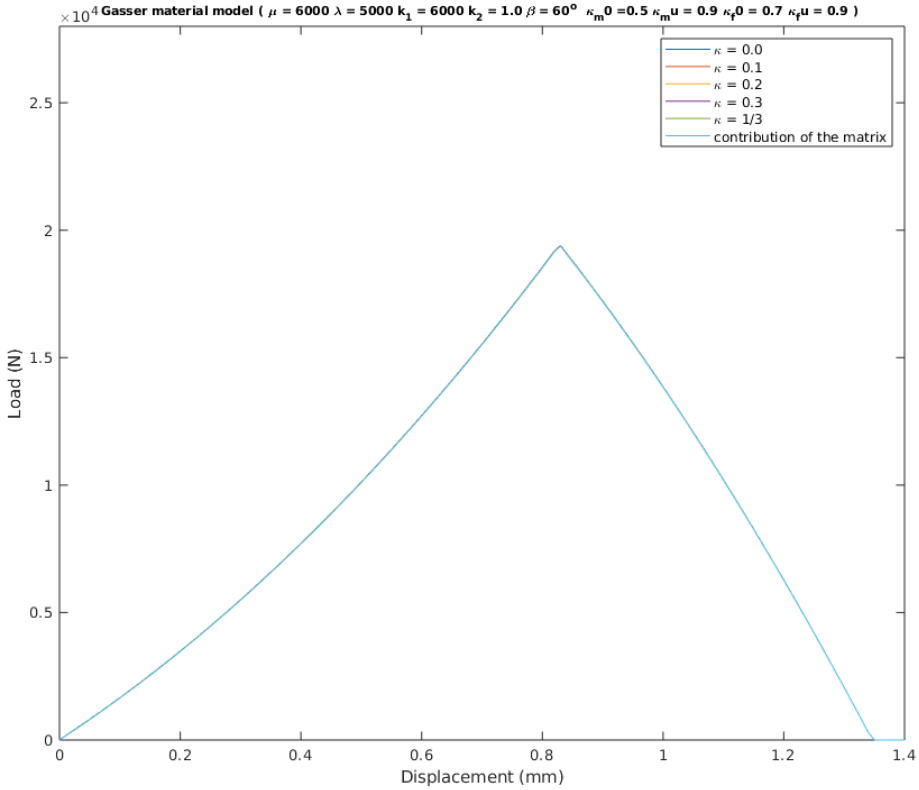

Figure 4.18: Influence of the dispersion parameter κ when $\beta = 60^o$

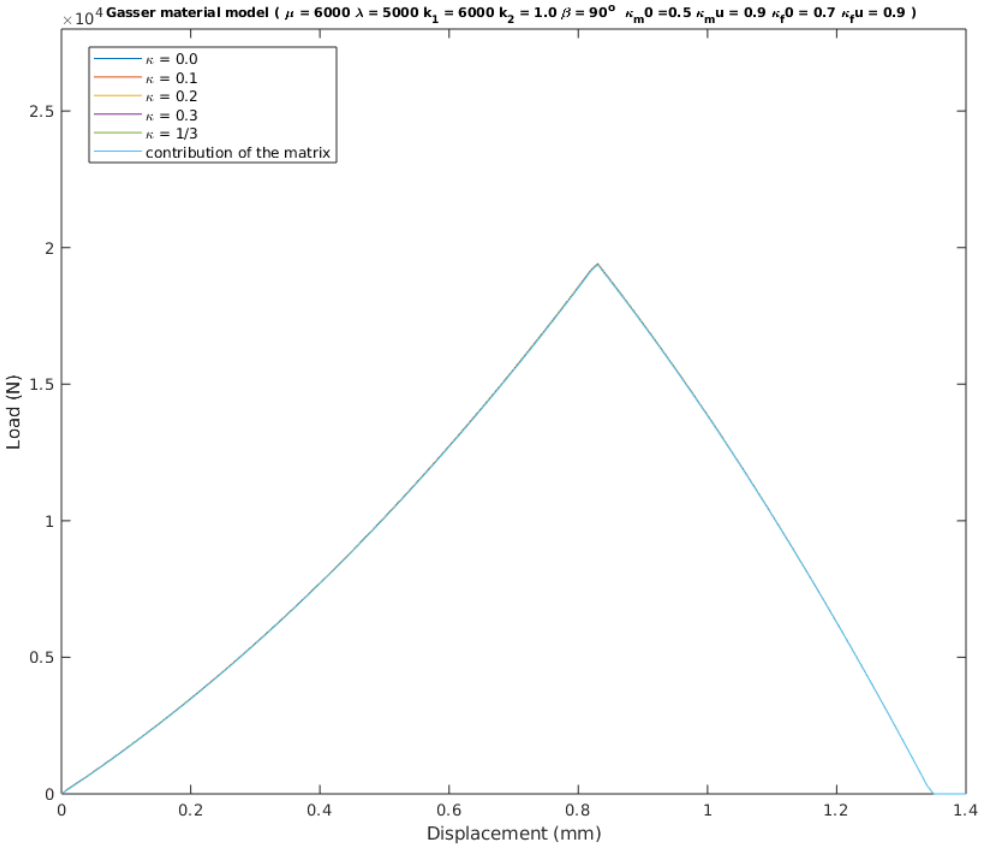

Figure 4.19: Influence of the dispersion parameter κ when $\beta = 90^o$

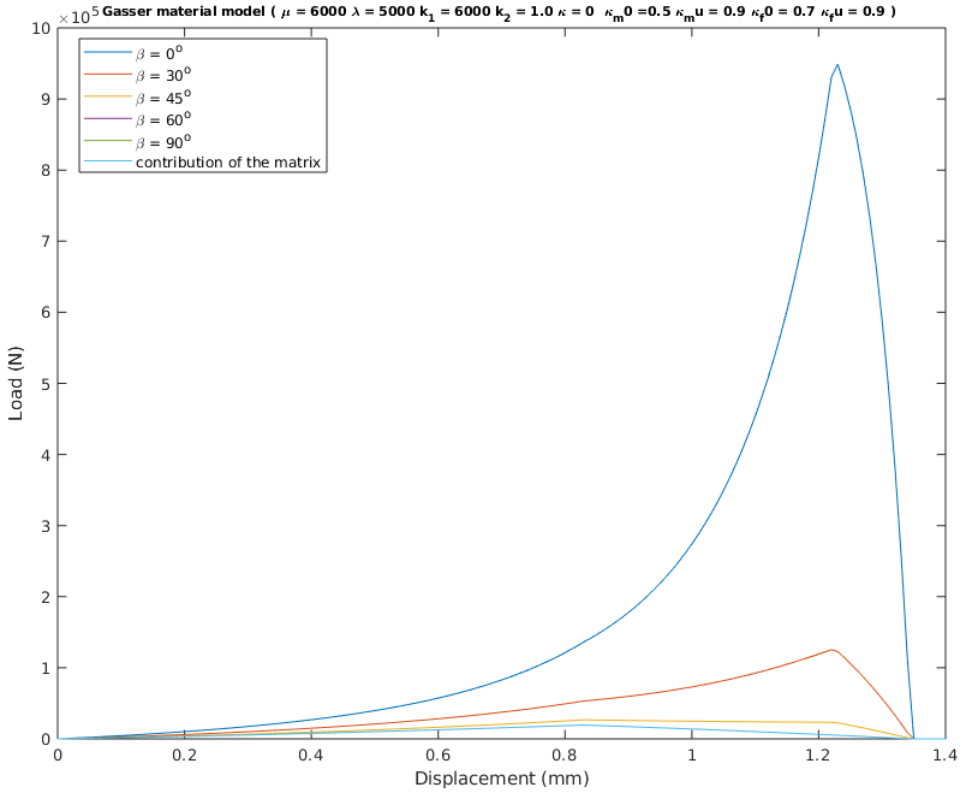

Figure 4.20: Third case:the collagen fibers will start to fail at first and will get fully damaged at first

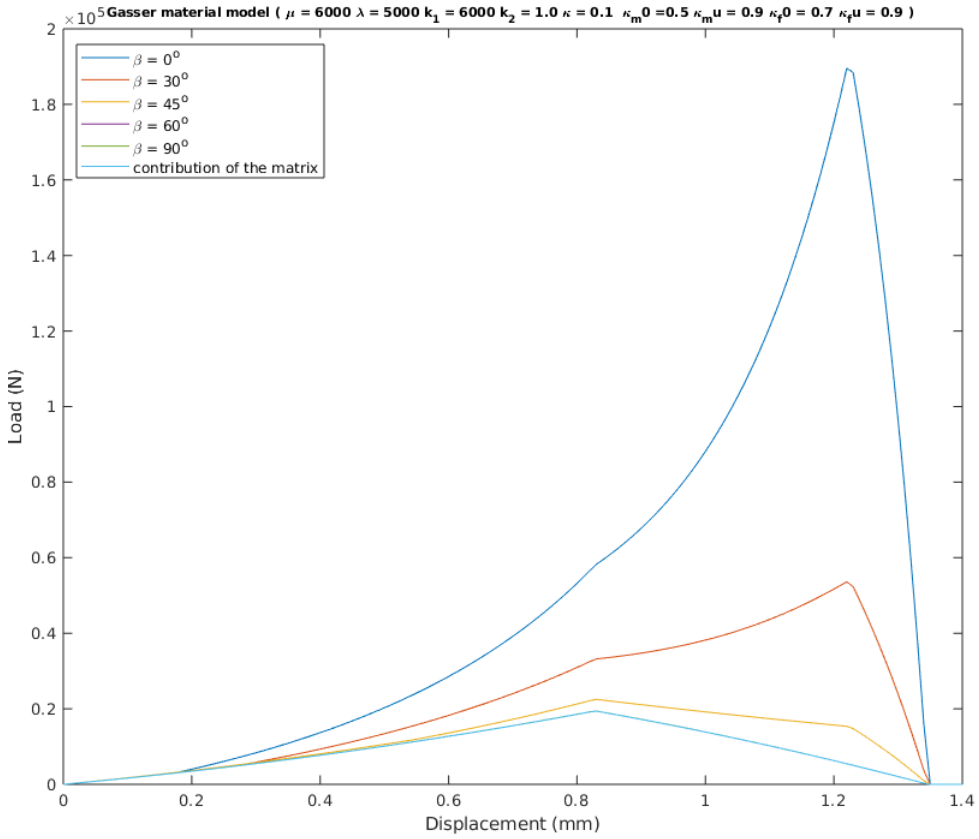

Figure 4.21: Third case:the collagen fibers will start to fail at first and will get fully damaged at first

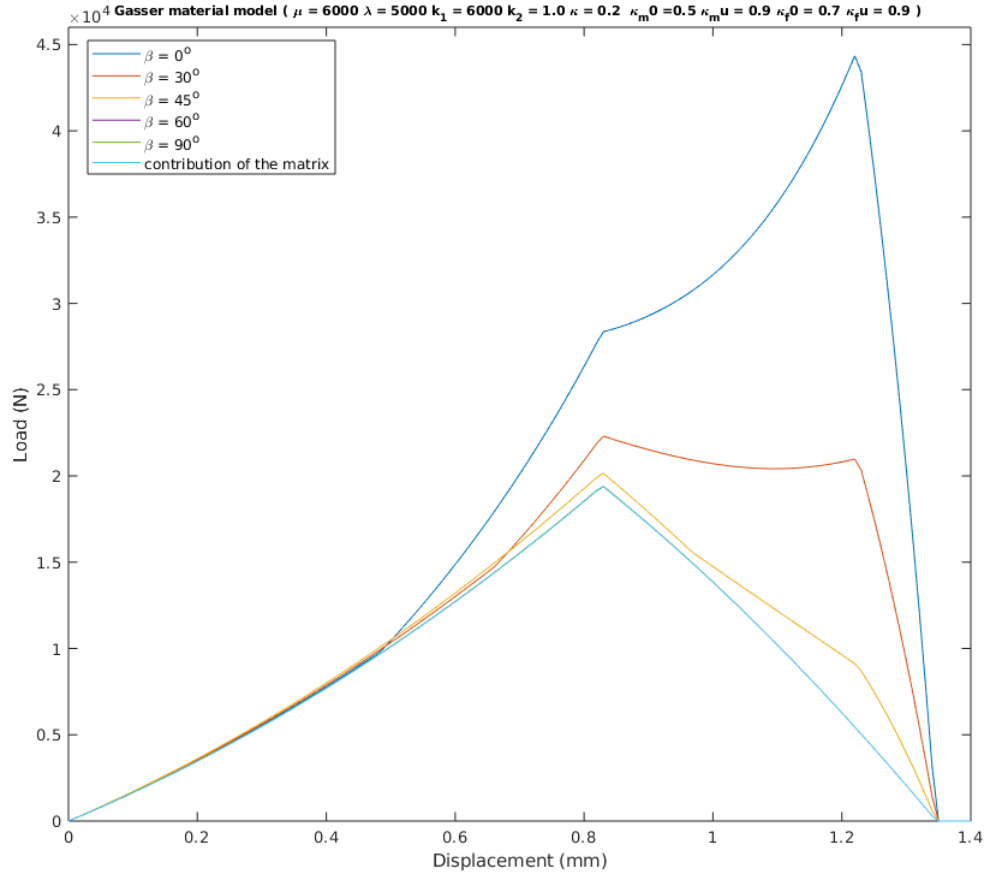

Figure 4.22: Third case:the collagen fibers will start to fail at first and will get fully damaged at first

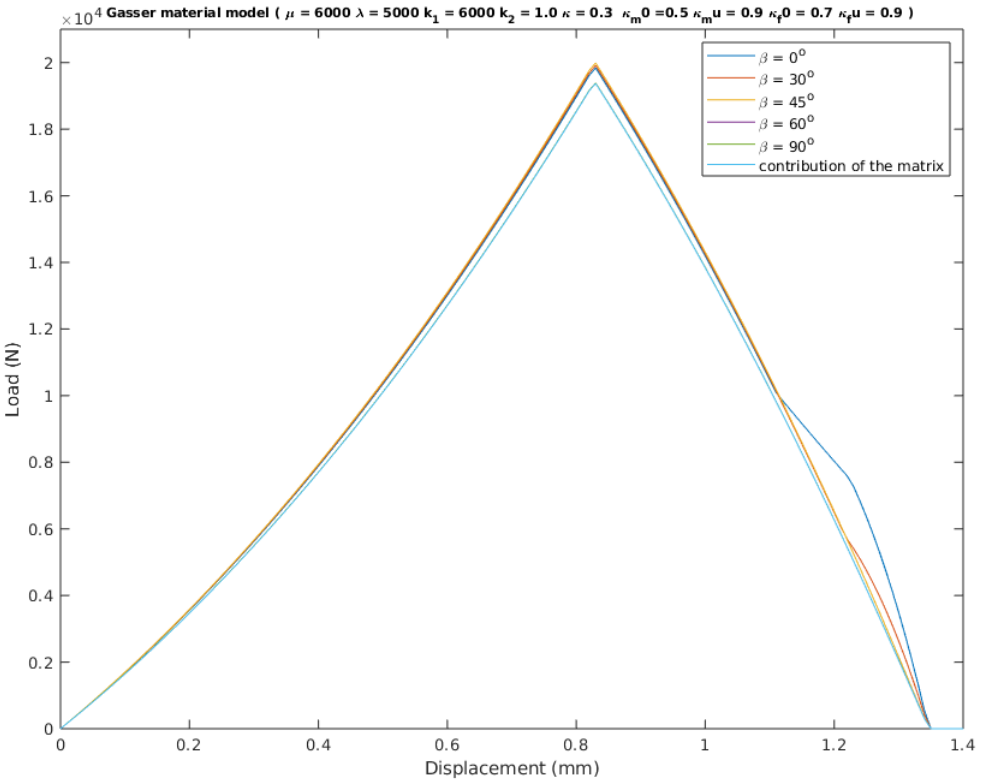

Figure 4.23: Third case:the collagen fibers will start to fail at first and will get fully damaged at first

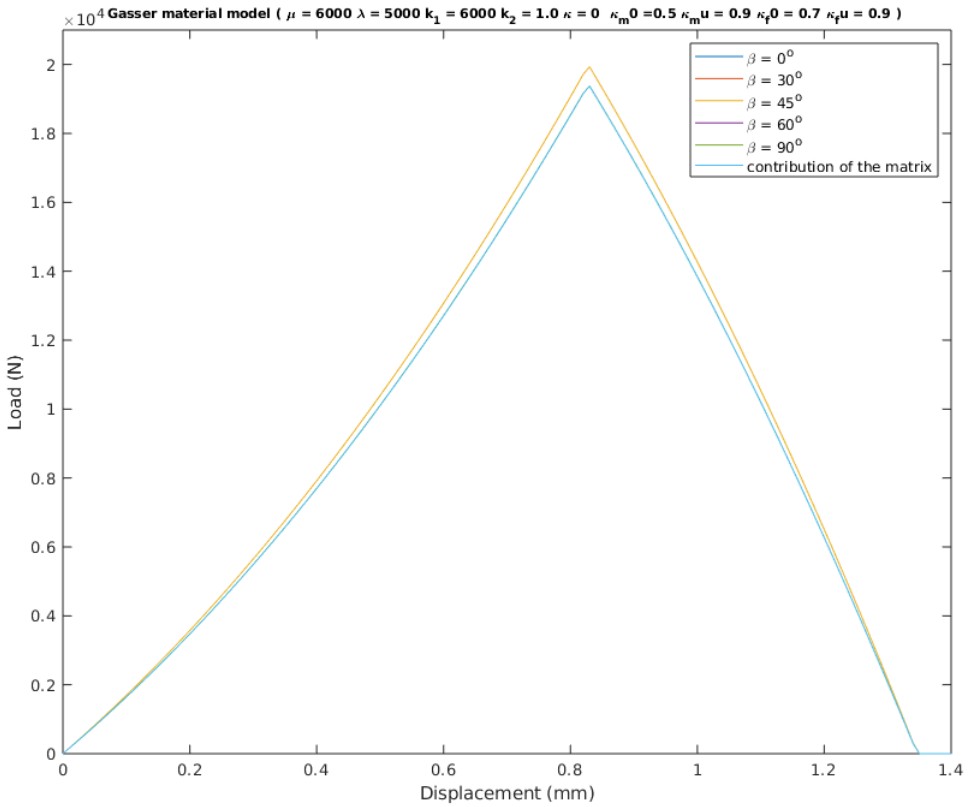

Figure 4.24: Third case:the collagen fibers will start to fail at first and will get fully damaged at first

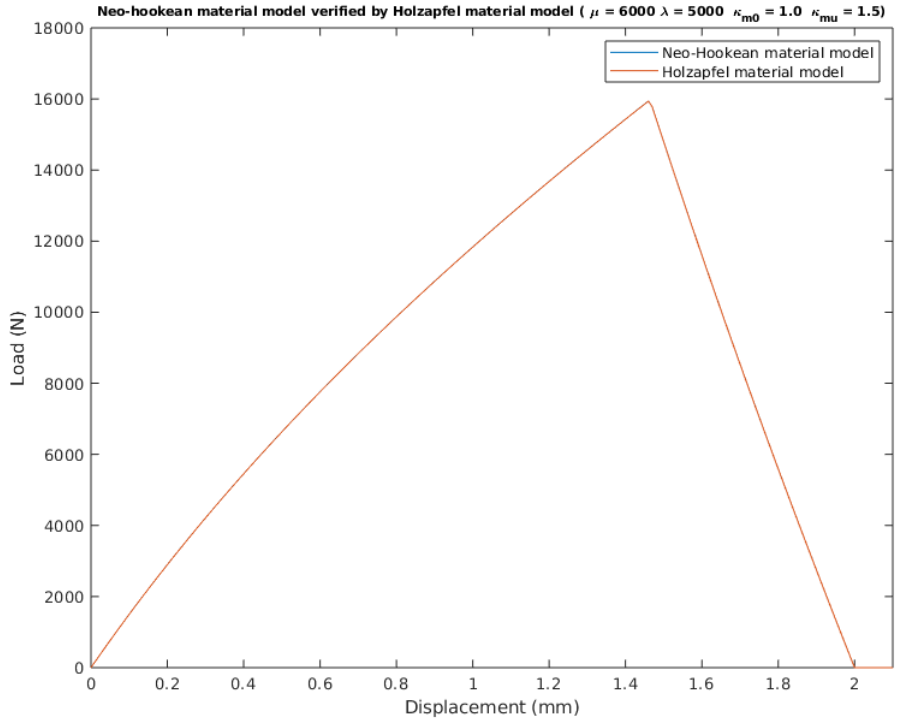

Figure 4.25: Load-displacement response for Neo-Hookean material model and Holzapfel material model

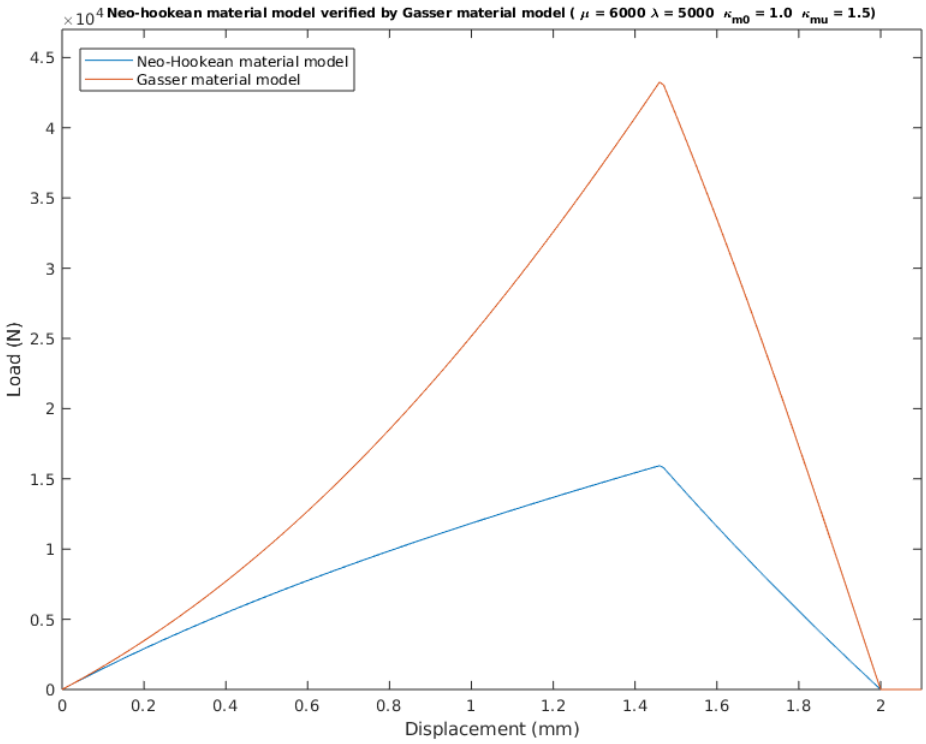

Figure 4.26: Load-displacement response for Neo-Hookean material model and Gasser material model

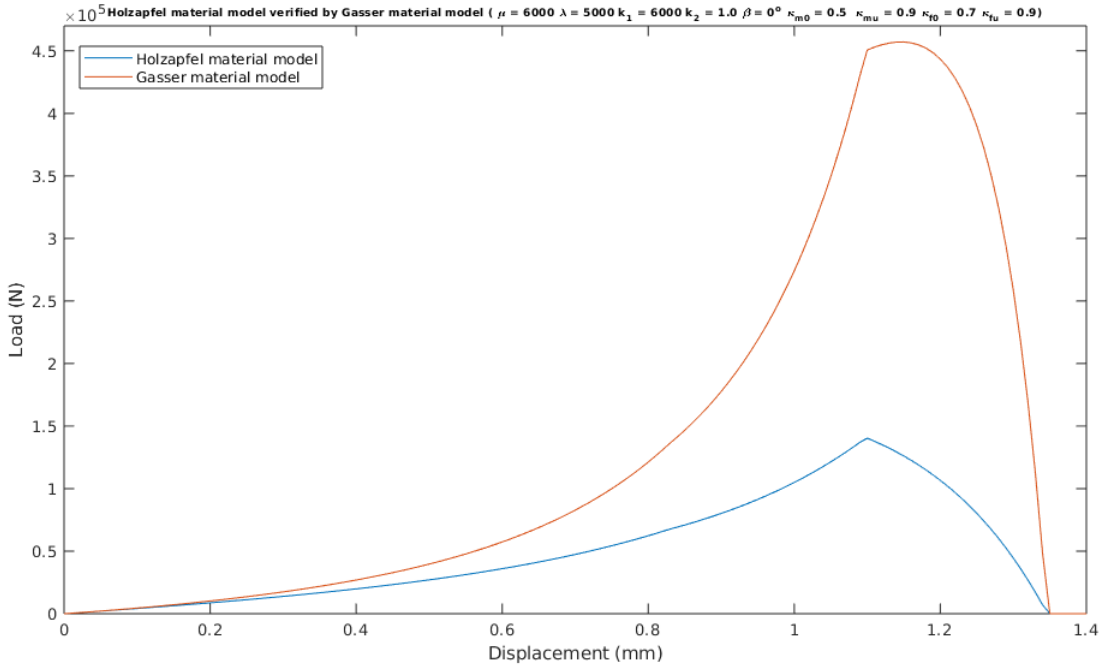

Figure 4.27: Load-displacement curves for Holzapfel material model and Gasser material model

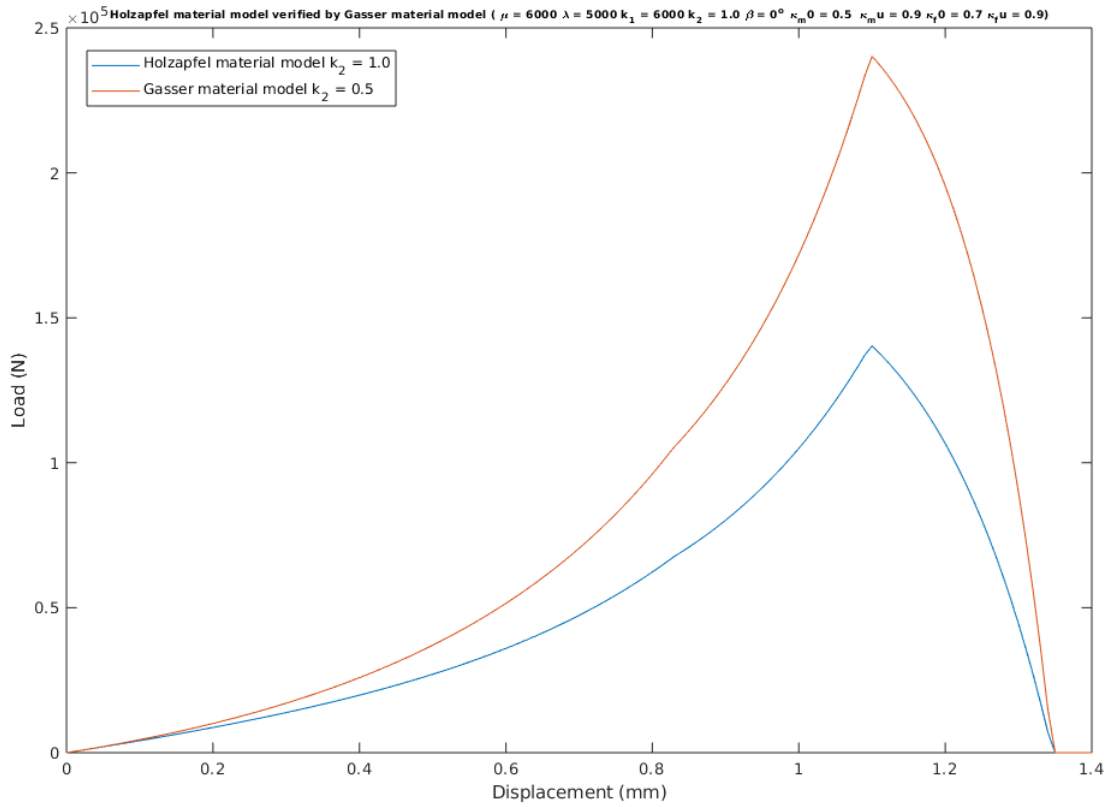

Figure 4.28: Load-displacement curves for Holzapfel material model and Gasser material model ($k_{2h} = 2k_{2g}$)

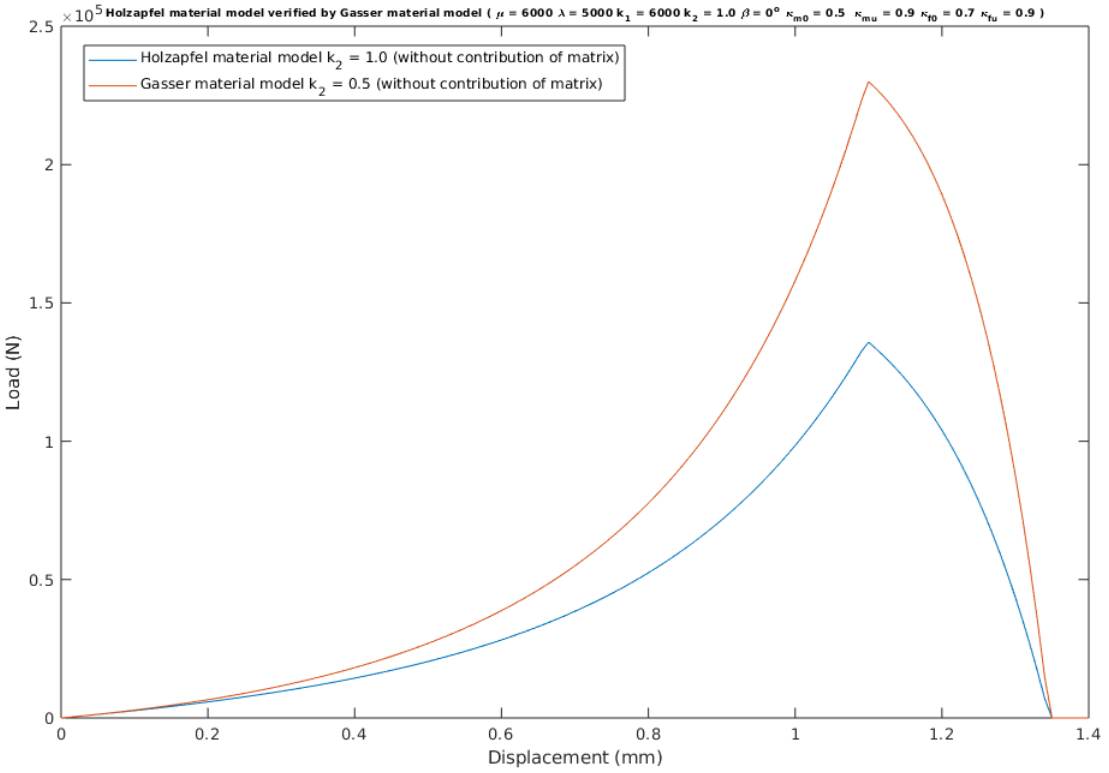

Figure 4.29: Load-displacement curves for Holzapfel material model and Gasser material model ($k_{2h} = 2k_{2g}$, without contribution of the matrix)

5

Failure analysis

In this chapter, failure analyses are performed on four models. They are a simple plane, a bar, a plane with an imperfection and a plane with a rectangular hole. As for the first and second model, the failure analyses are performed with the three developed models. As for the third model, the failure analyses are performed based on Neo-Hookean material model. In addition, the influences of the mesh size, location of the imperfection and the depth of the imperfection are analyzed. As for the fourth model, the failure analyses are performed based on the Neo-Hookean material model. In addition, the influences of the mesh size, size of the rectangular hole and location of the rectangular are analyzed.

5.1. Model of a simple plane

5.1.1. Model description

The geometry and boundary conditions are shown in Figure 5.1. The length of the plane is 40 mm and the height is 16 mm. The displacement of the nodes at the left side is constrained in x direction. The bottom node on the left side is also constrained in y direction. The force is applied on the right side of the plane in x direction. The force is applied by displacement control method. The plane is assumed to be in plane strain state.

Figure 5.1: Geometry and boundary conditions of the plane model

5.1.2. Neo-Hookean material

First, the Neo-Hookean material is applied to the plane model. The deformation of the plane is shown in Figure 5.2, and the corresponding load-displacement response curve is shown in Figure 5.3.

It can be observed from Figure 5.2 that the crack appears on the right side of the model. The load-displacement curve is similar to the response curve of a single element test of the Neo-Hookean material model in chapter 4.

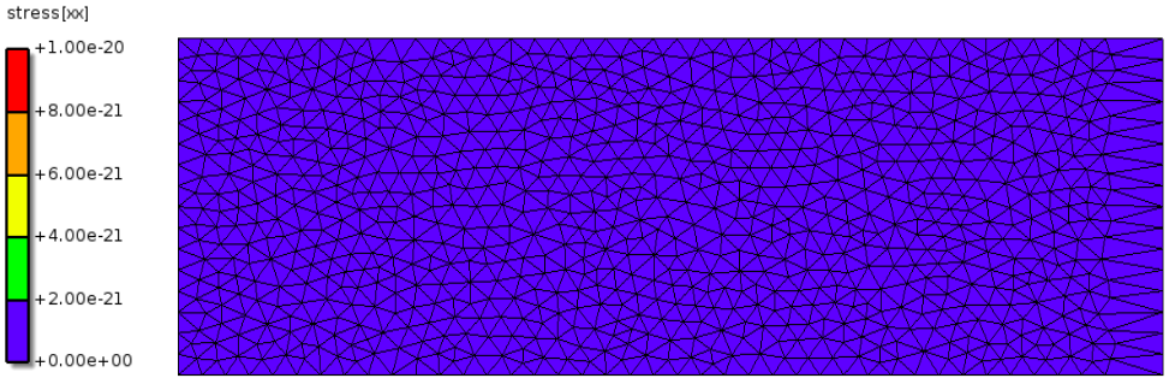

Figure 5.2: Deformation of the plane (Neo-Hookean material)

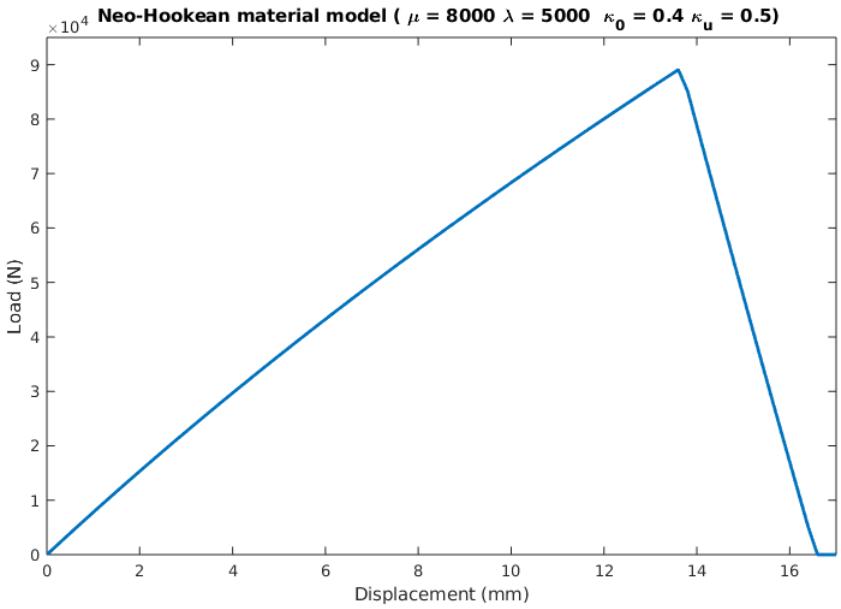

Figure 5.3: Load-displacement response curve for the plane model (Neo-Hookean material)

5.1.3. Holzapfel material

Then, the Holzapfel material is applied to the plane model. The deformation of the plane is shown in Figure 5.4. and the corresponding load-displacement response curve is shown in Figure 5.5.

It can be observed from the figure that, just like the Neo-Hookean material model, the crack appears on the right side of the plane. The load-displacement curve is similar to the response curve of a single element test of the Holzapfel material model in chapter 4. The only difference is that the failure behaviour is brittle in the plane model. This phenomenon is caused by the limitation of the implementation.

5.1.4. Gasser material

In the end, the Gasser material is applied to the plane model. The deformation of the plane is shown in Figure 5.6, and the corresponding load-displacement response curve is shown in Figure 5.7.

Just like the Neo-Hookean material model and the Holzapfel material model, the crack appears on the right side of the plane. The load-displacement response curve is also similar to the response curve of a single element test of the Gasser material model. Just like the response curve of the plane model with Holzapfel material, the failure behaviour is also brittle due to the same reason.

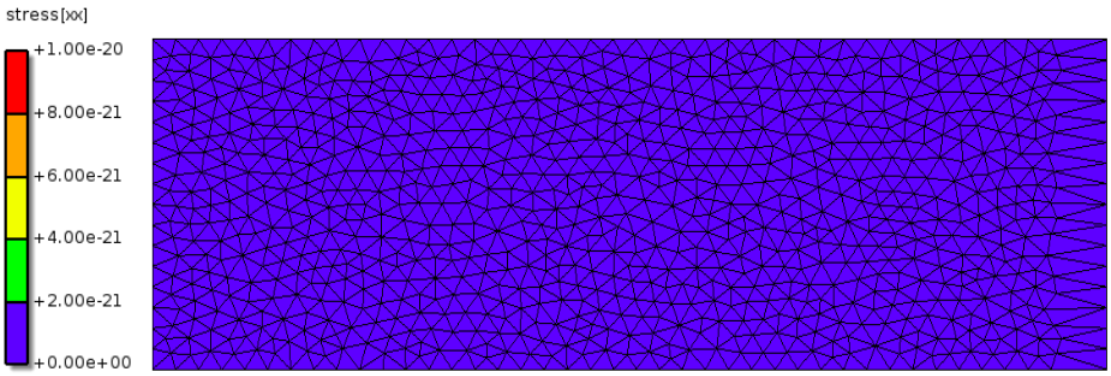

Figure 5.4: Deformation of the plane (Holzapfel material)

5.2. Model of a simple bar

5.2.1. Model description

The geometry and boundary conditions are shown in Figure 5.8. The length of the bar is 10 mm and the height of the bar is 2 mm. The displacement of the nodes at the left side is constrained in X direction. The bottom node on the left side is constrained in y direction. The force is applied on the right side of the bar in x direction. The force is applied by displacement control method.

5.2.2. Mesh size dependence

The influence of the mesh size is analyzed. The bar is meshed with one element, three elements, five elements and seven elements. The meshed models are shown in Figure 5.9 - Figure 5.12.

In the meshed models, all the elements have the same elastic properties. However, as for the element in the middle of the bar, it has a lower strength compared with other elements which makes the middle element become the critical element in the bar. The corresponding load-displacement response curves for the Neo-Hookean material model, the Holzapfel material model and the Gasser material model is shown in Figure 5.13, Figure 5.14 and Figure 5.15.

It can be observed from the figures that with the increase of the numbers of the elements, it will not influence the response curves before the damage begins. However, it does influence the material behaviour after the damage begins. With the same damage parameters, when the total number of the elements is equal to 1, the distance between when the damage begins and when the damage finishes is large. With the increase of the total number of the elements, the distance gets narrower, which means that the damage behaviour becomes more brittle.

5.3. Model of a plane with an imperfection

5.3.1. Model description

The geometry and boundary conditions are shown in Figure 5.16. The length of the plane is 40 mm, and the height is 16 mm. The depth of the imperfection is 8 mm, and the width of the imperfection is 4 mm. The boundary conditions of the model are similar with boundary conditions of the simple plane model. The displacement of the nodes at the left side is constrained in x direction. The bottom node on the left side is also constrained in y direction. The force is applied on the right side of the model in x direction. The force is applied by displacement control method. The model is assumed to be in plane strain state. The material of the model is Neo-Hookean material model.

5.3.2. Damage behaviour

The damage behaviour of the model is analyzed. With the increase of the force applied on the model, cracks will appear on the model. The deformed model is shown in Figure 5.17, and the corresponding load-displacement response curve is shown in Figure 5.18.

It can be observed from Figure 5.19 that, in the beginning, the initial crack appears on the right bottom of the imperfection. Then, it propagates to the bottom of the plane. When the crack reaches

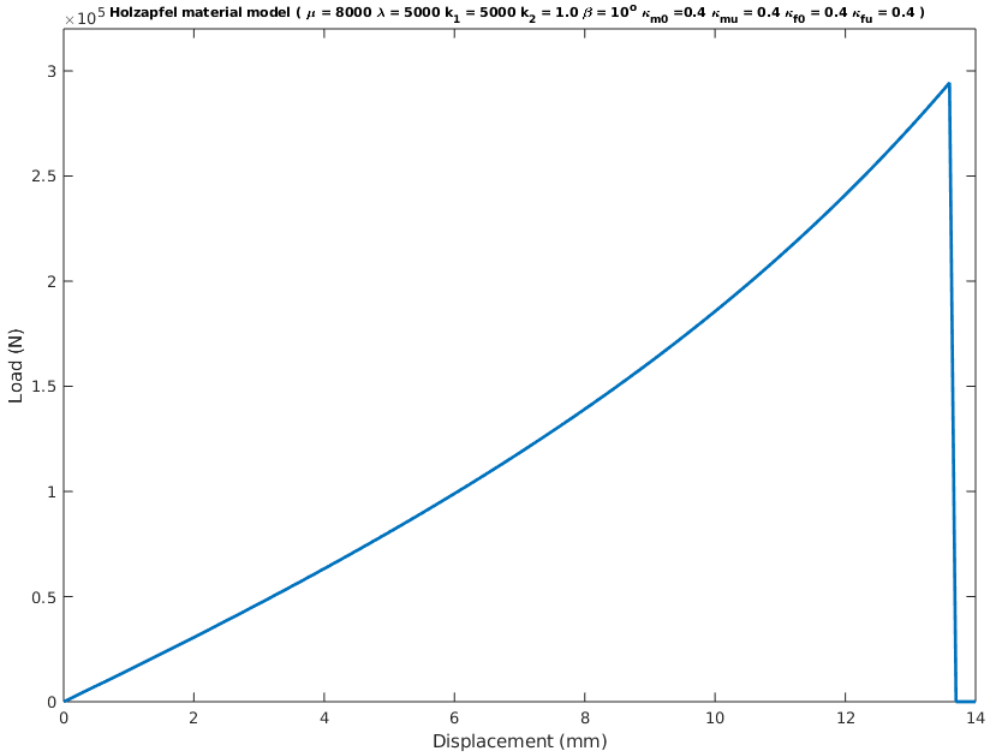

Figure 5.5: Load-displacement response curve for the plane model (Holzapfel material)

the bottom of the plane, the plane totally fails to two parts. It is known from Figure 5.18 that the damage behaviour of the model is a brittle damage behaviour.

5.3.3. Mesh size dependence

The influence of the mesh size is analyzed. The model will be meshed with three different sizes, and they are 2 mm, 1.5 mm and 1 mm. The deformed models are shown in Figure 5.19 (2 mm), Figure 5.20 (1.5 mm) and Figure 5.21 (1 mm). The corresponding load-displacement response curves are shown in Figure 5.14.

It can be concluded from Figure 5.19, Figure 5.20 and Figure 5.21 that the mesh size will not influence the crack pattern of the model. In these three figures, the initial crack appears at the right bottom of the imperfection and then propagates to the bottom of the plane. However, the mesh size can influence the load-displacement response of the model. In Figure 5.22, it can be observed that the mesh size can influence the mechanical behaviour after the failure begins. With the increase of the mesh size, the more load steps are needed to finish the damage behaviour. With a small mesh size, a smoother curve can be obtained.

5.3.4. Influence of the location of the imperfection

The influence of the location of the imperfection is also analyzed. The imperfection locates in the left, middle and right of the plane. The deformed models are shown in Figure 5.23, Figure 5.24 and Figure 5.25. The corresponding load-displacement response curves are shown in Figure 5.26.

It can be concluded from Figure 5.23, Figure 5.24 and Figure 5.25 that the location of the imperfection can affect the crack pattern of the model. When the imperfection locates at the left and middle of the plane, the initial crack appears at the right bottom of the imperfection. When the imperfection locates at the right of the plane, the initial crack appears at the left bottom of the imperfection. As for the load-displacement response curves, it can be observed from Figure 5.26 that the curves coincide with each other before the failure begins. The location of the imperfection will influence the response after the failure begins. When the imperfection locates at the left of the plane, the failure behaviour finishes in one load step. When it locates in the middle, the failure behaviour finishes in two load steps. When it locates in the right, the failure behaviour finishes in three load steps. As a result, the closer to

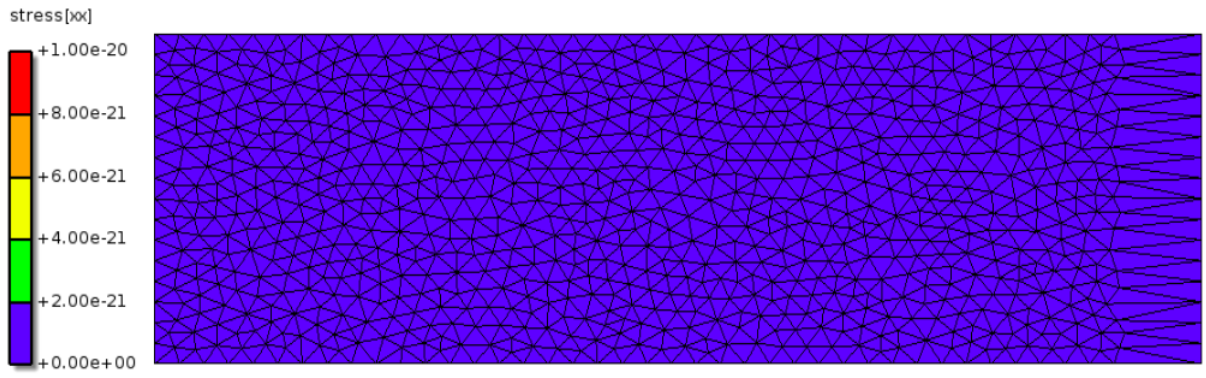

Figure 5.6: Deformation of the plane (Gasser material)

the right, the more load steps it is going to take to finish the failure behaviour.

5.3.5. Influence of the depth of the imperfection

In the end, the influence of the depth of the imperfection is analyzed. Three different depths are applied, which are 4 mm, 8 mm and 12 mm. The deformed models are shown in Figure 5.27, Figure 5.28 and Figure 5.29. The corresponding load-displacement response curves are shown in Figure 5.30.

It can be observed from Figure 5.27, Figure 5.28 and Figure 5.29 that the depth of the imperfection will not influence the crack pattern of the model. The initial crack appears at the right bottom of the imperfection and propagates to the bottom of the plane. It can be concluded from Figure 5.30 that the with the increase of the depth, the response curve will become lower, which means the load gets smaller. Because, for a higher value of the depth, the distance between the bottom of the imperfection and the bottom of the plane will become smaller. This distance can decide the strength of the plane. So, with a smaller value of the distance, a smaller value of strength can be obtained, which make the response curve becomes lower.

5.4. Model of the rectangular hole in the middle

5.4.1. Model description

The geometry and boundary conditions are shown in Figure 5.31. The length of the plane is 40 mm and the height is 16 mm. The size of the rectangular hole is 2 mm x 2mm. The boundary conditions of the model are similar to boundary conditions of the simple plane model. The displacement of the nodes at the left side is constrained in x direction. The bottom node on the left side is also constrained in y direction. The force is applied on the right side of the model in x direction. The force is applied by displacement control method. The model is assumed to be in plain strain state. The material of the model is Neo-Hookean material model.

5.4.2. Damage behaviour

The damage behaviour of the model is analyzed. The deformed model is shown in Figure 5.32, and the corresponding load-displacement response curve is shown in Figure 5.33.

There are two cracks appearing on the model. The initial cracks appear on the right top and left bottom of the rectangular hole. Then, they propagate to the top and bottom of the plane. When these two cracks propagate to the edges of the plane, the plane fails to two parts. The damage behaviour of the model is a brittle damage behaviour (Figure 5.33).

5.4.3. Mesh size dependence

The influence of the mesh size is analyzed. The model will be meshed with three different sizes, and they are 1 mm, 2 mm and 4 mm. The deformed models are shown in Figure 5.34 (1 mm), Figure 5.35 (2 mm) and Figure 5.36 (4 mm). The corresponding load-displacement response curves are shown in Figure 5.37.

It can be concluded from Figure 5.34, Figure 5.35 and Figure 5.36 that the mesh size will influence

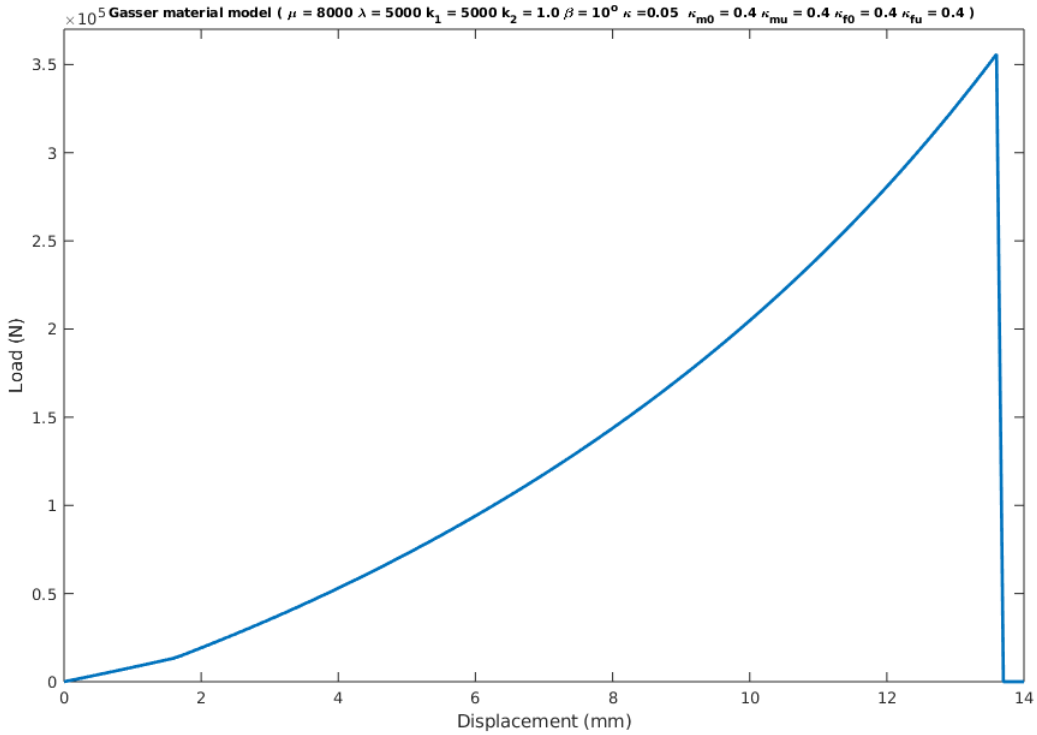

Figure 5.7: Load-displacement response curve for the plane model (Gasser material)

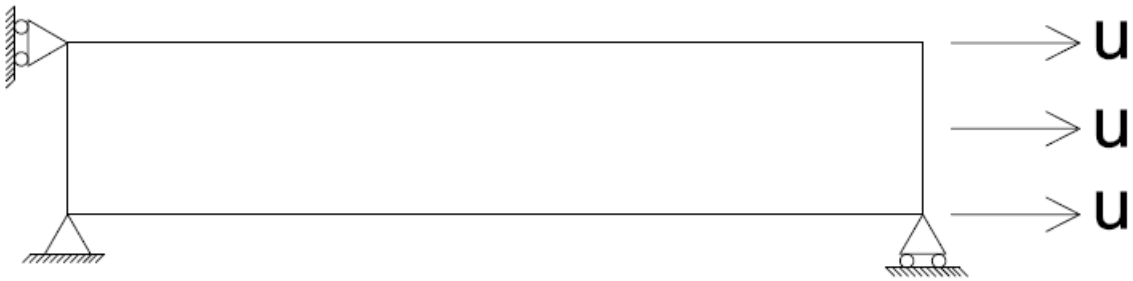

Figure 5.8: Geometry and boundary conditions of the bar model

the crack pattern of the model. When the mesh size is equal to 1 mm and 2 mm, the initial cracks appear on the right top and left bottom of the rectangular hole and propagate to the edges of the plane. However, when the mesh size is equal to 4 mm, the initial cracks appear on the left top and right bottom of the rectangular hole and propagate to the edges of the plane. In Figure 5.37, it can be observed that the response curves of mesh size equal to 1 mm and 2 mm are close to each other. However, the response curve of mesh size equal to 4 mm is too high compared with the other two curves. Since 4 mm is a little large compared with the geometry of the model, the results would be too rough to represent the actual response of the model.

5.4.4. Influence of the size of the rectangular hole

The influence of the size of the rectangular hole is analyzed. Three different sizes of the rectangular hole are applied to the model. They are 4 mm x 4 mm, 6 mm x 6 mm and 8 mm x 8 mm. The deformed models are shown in Figure 5.38 (4 mm x 4 mm), Figure 5.39 (6 mm x 6 mm) and Figure 5.40 (8 mm x 8 mm) and the corresponding load-displacement response curves are shown in Figure 5.41.

It can be concluded from Figure 5.38, Figure 5.39 and Figure 5.40 that the size of the rectangular hole could influence the crack pattern of the model. When the size of the rectangular hole is equal to

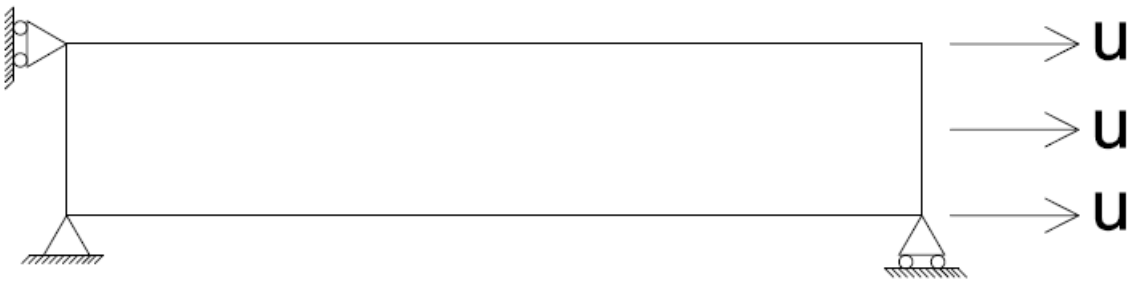

Figure 5.9: Meshed bar with one element

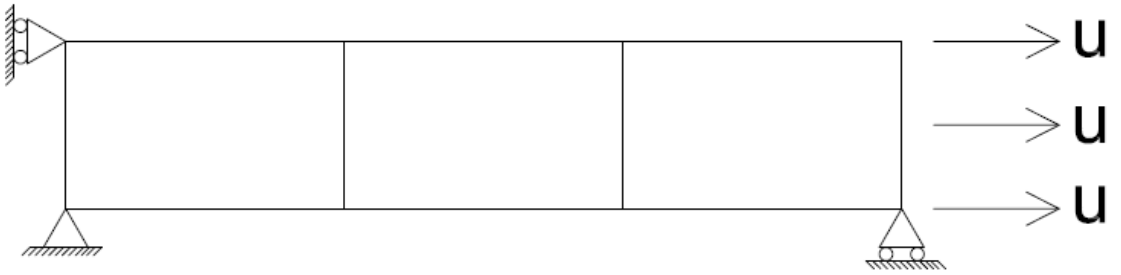

Figure 5.10: Meshed bar with three elements

4 mm x 4 mm and 6 mm x 6 mm, the crack patterns are the same. When the size gets bigger (8 mm x 8 mm), the crack pattern changes. The initial cracks appear on the left top and right bottom of the rectangular hole and propagate to the edges of the plane. It can be observed from Figure 5.41 that the bigger of the size of the rectangular hole, the lower of the corresponding load-displacement response curve. Since with the increase of the size of the rectangular hole, the effective height of the model decreases, which can influence of strength of the model. With the decrease of the effective height, the strength decreases and the response curve gets lower.

5.4.5. Influence of the location of the rectangular hole

In the end, the influence of the location of the rectangular hole is analyzed. It is analyzed in two parts. In the first part, the rectangular hole locates at the middle, top, bottom, left and bottom of the plane. The deformed models are shown in Figure 5.42 - Figure 5.46 and the corresponding load-displacement response curves are shown in Figure 5.47.

It can be concluded from Figure 5.42 - Figure 5.46 that the crack pattern of the left case and the crack pattern of the right case can be regarded as symmetry with the centre point of the plane. The crack pattern of the top case and the crack pattern of the bottom case are also symmetry with the centre point of the plane. This phenomenon is also reflected in Figure 5,53. In Figure 5.53, the response curve of the left and the response curve of the right coincides with each other. The response curve of the top and the response curve of the bottom coincides with each other. It can also be concluded from Figure 5.47 that the strengths of the five models are close to each other since they all have the same effective height.

In the second part, the rectangular hole locates at the middle, top-left, bottom-left, top-right and bottom-right of the plane. The deformed models are shown in Figure 5.48 - Figure 5.52 and the corresponding load-displacement response curves are shown in Figure 5.53.

Just like the first part, the crack pattern of left-top case and the crack pattern of the right-bottom case can be regarded as symmetry with the centre point of the plane. The crack pattern of the left-bottom case and the crack pattern of the right-top case are also symmetry with the centre point of the plane. These can also be proved by Figure 5.53. In Figure 5.53, the response curve of the left-top and the response curve of the right-bottom coincide with each other. The response curve of the left-bottom and

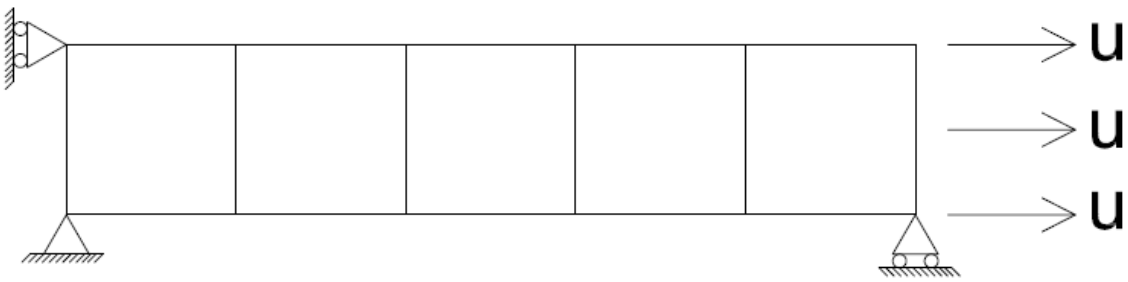

Figure 5.11: Meshed bar with five elements

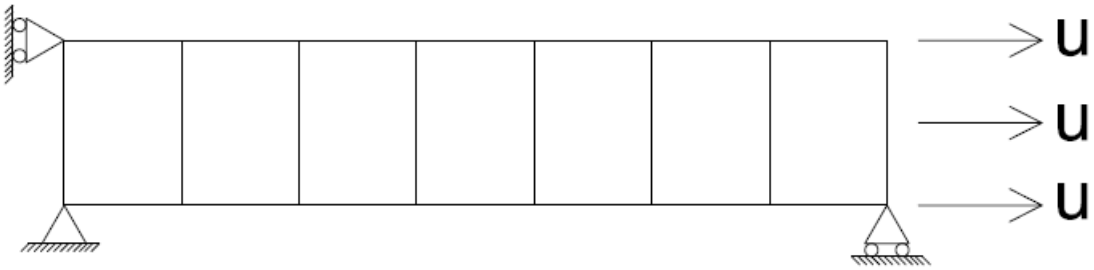

Figure 5.12: Meshed bar with seven elements

the response curve of the right-top coincide with each other. The strength of these five models is close to each other since they have the same effective height.

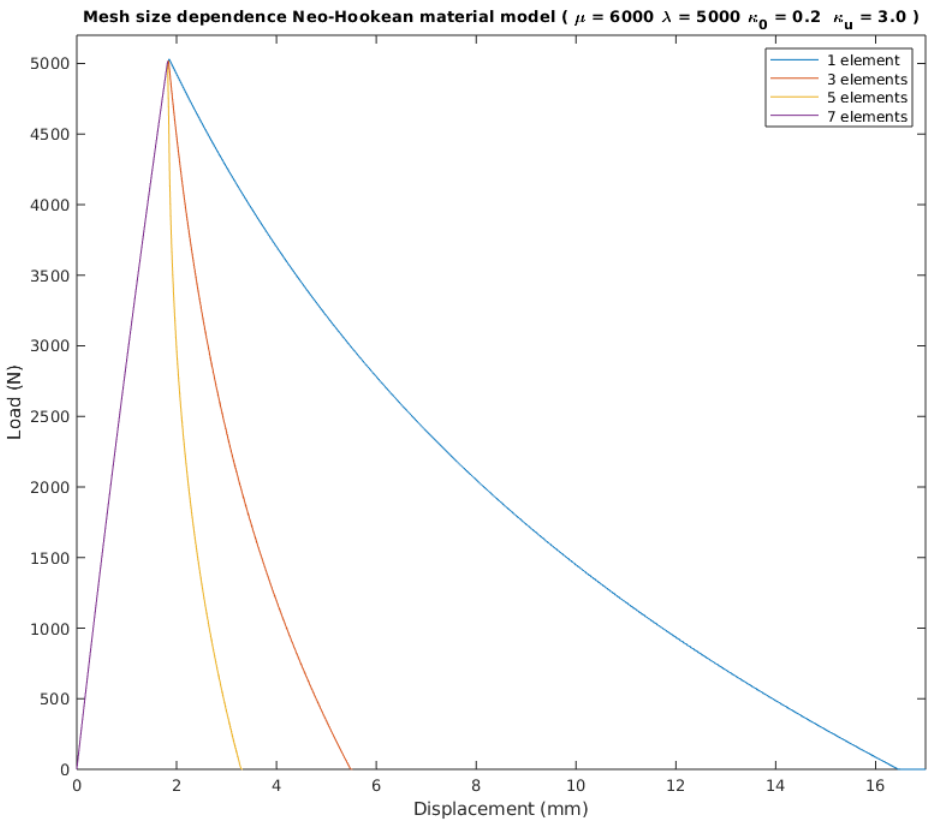

Figure 5.13: Load-displacement response curves for the Neo-Hookean material model

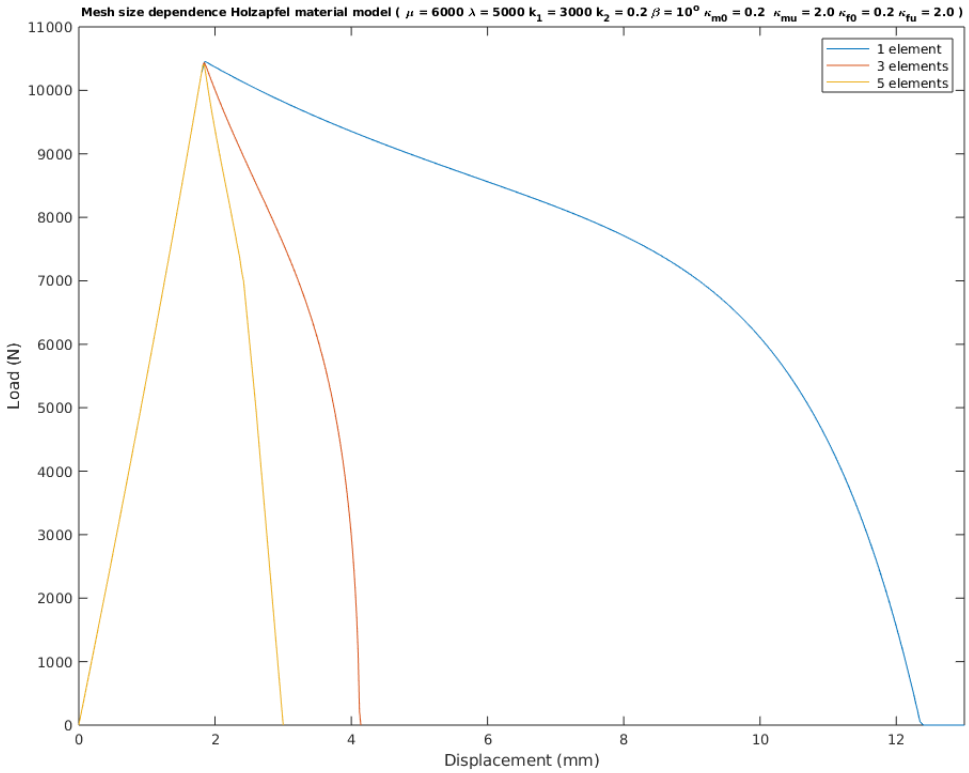

Figure 5.14: Load-displacement response curves for the Holzapfel material model

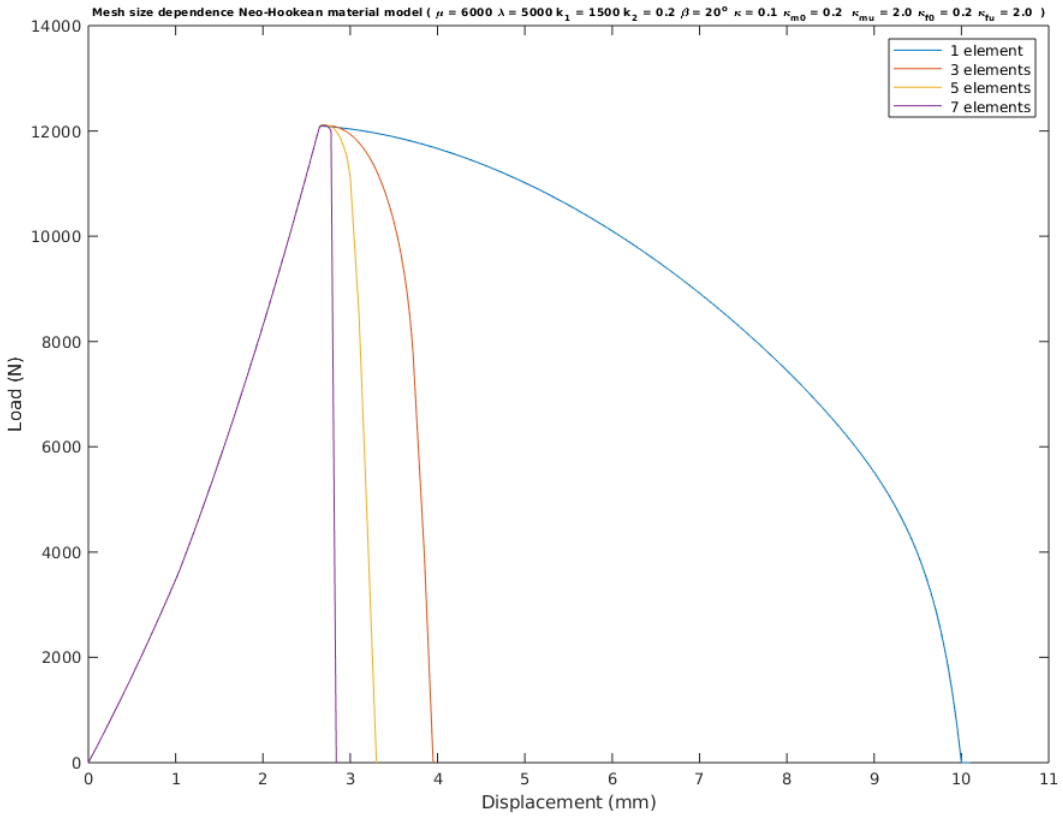

Figure 5.15: Load-displacement response curves for the Gasser material model

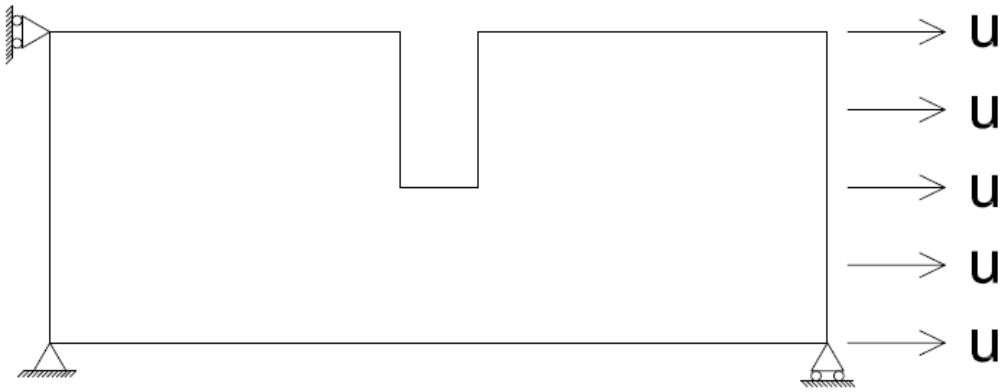

Figure 5.16: Geometry and boundary conditions of the plane model with an imperfection

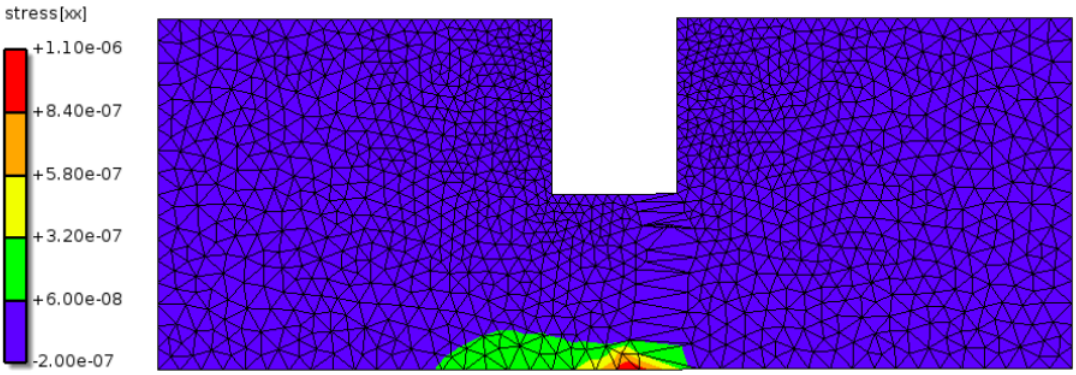

Figure 5.17: Deformation of the model (Neo-Hookean material)

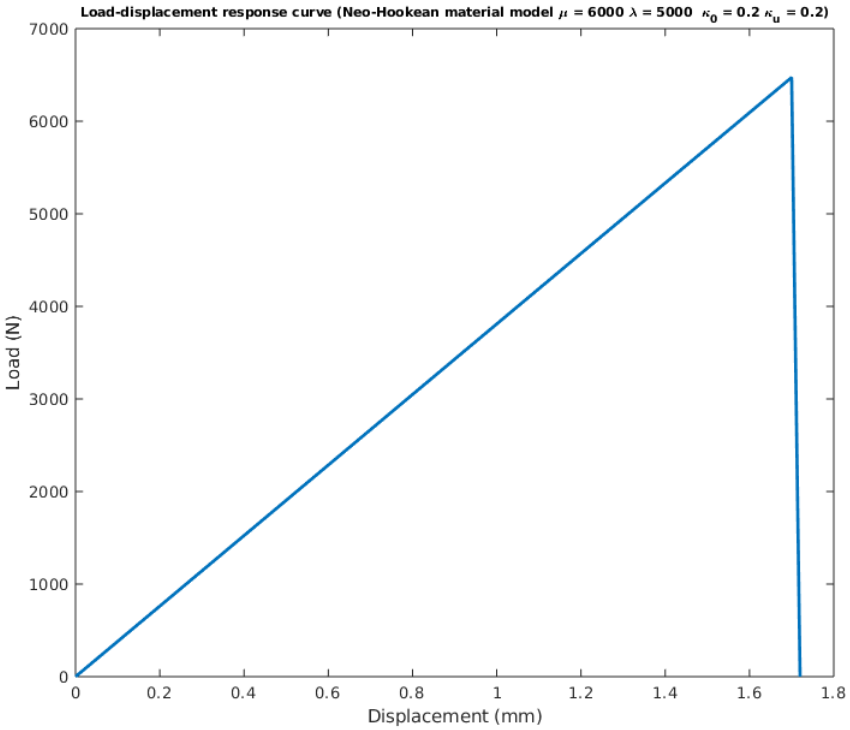

Figure 5.18: Load-displacement response curve for the plane model with imperfection (Neo-Hookean material)

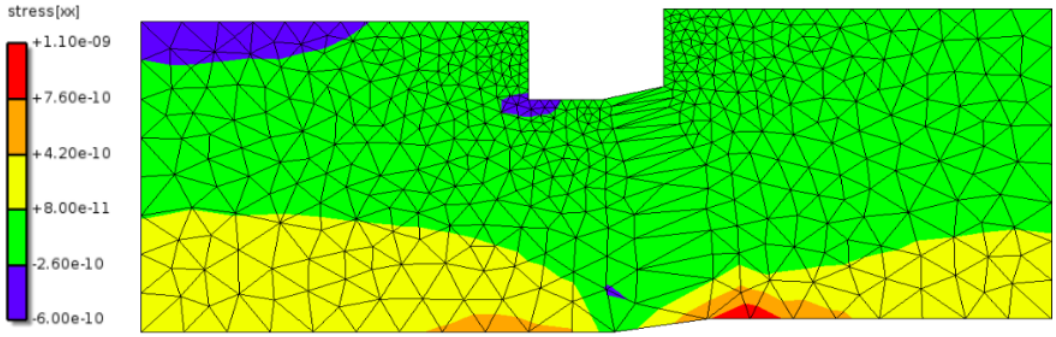

Figure 5.19: Deformed model with mesh size = 2 mm

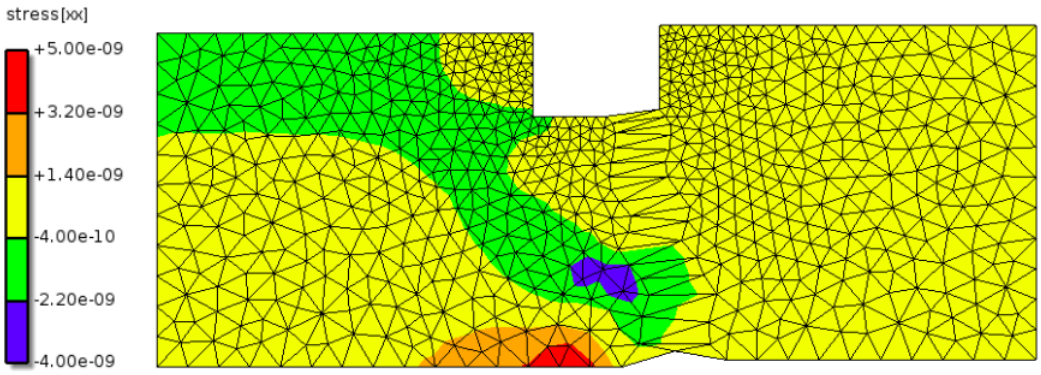

Figure 5.20: Deformed model with mesh size = 1.5 mm

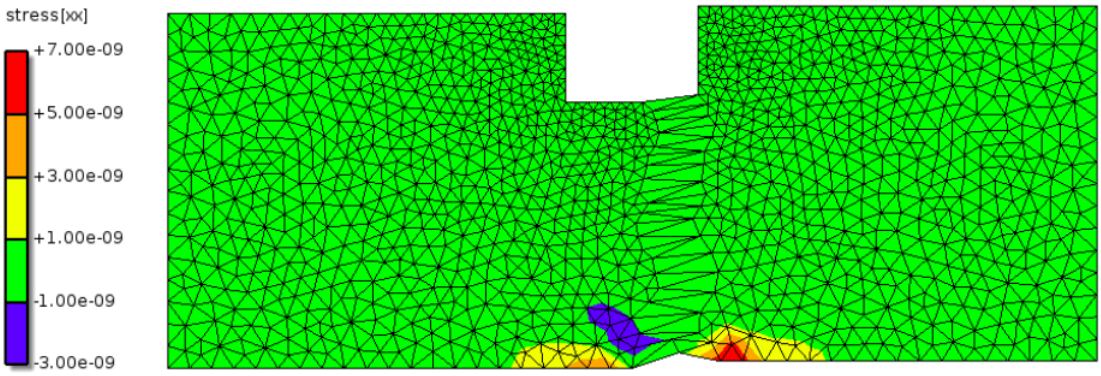

Figure 5.21: Deformed model with mesh size = 1 mm

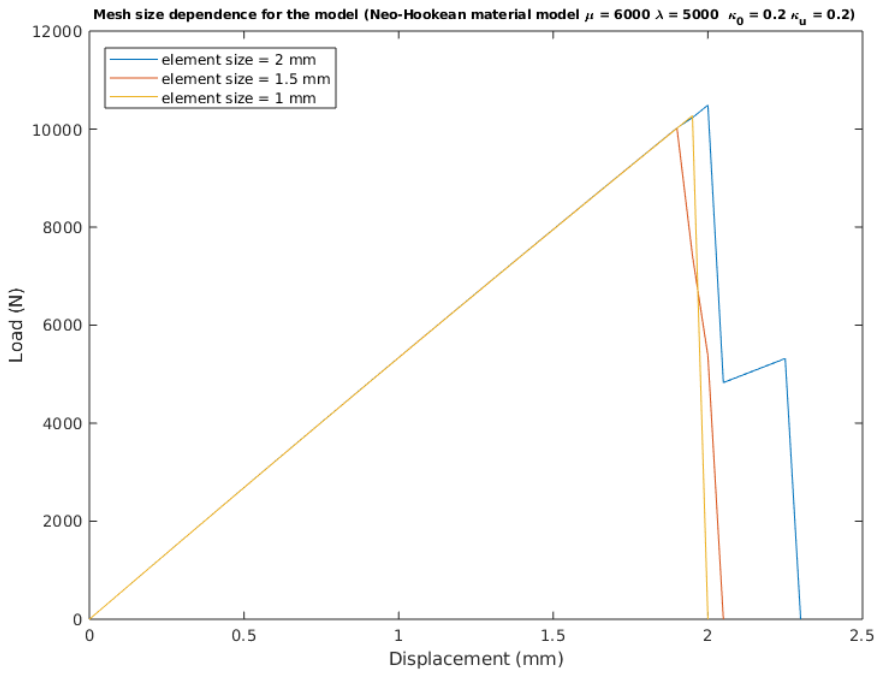

Figure 5.22: Load-displacement response curves for different mesh sizes

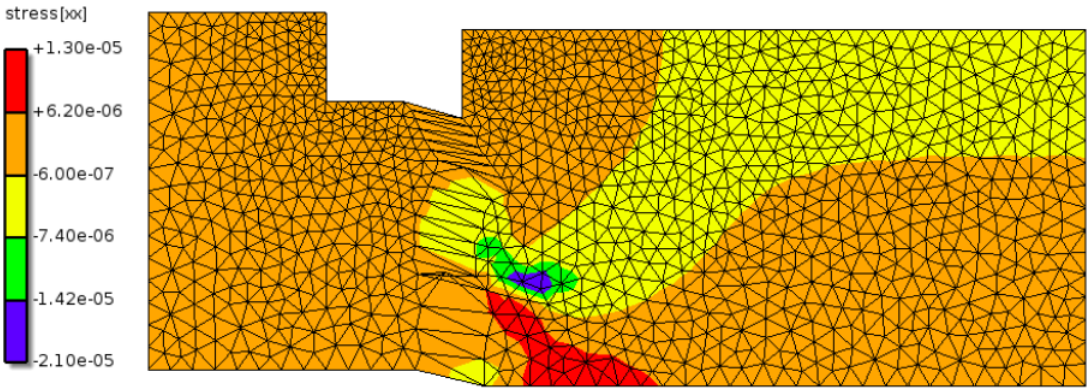

Figure 5.23: Deformed model with mesh size = 4 mm

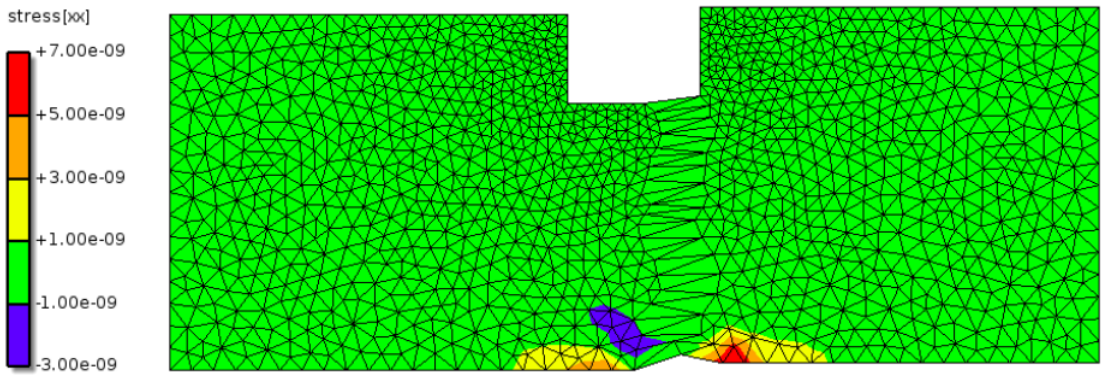

Figure 5.24: Deformed model with mesh size = 2 mm

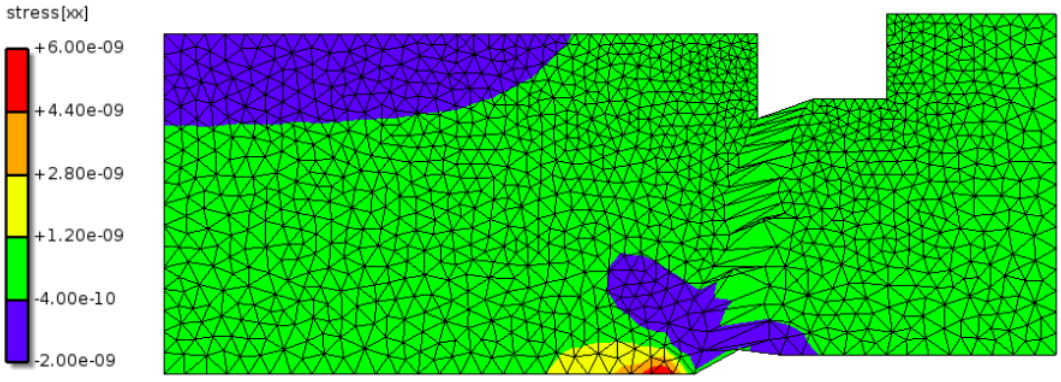

Figure 5.25: Deformed model with mesh size = 1 mm

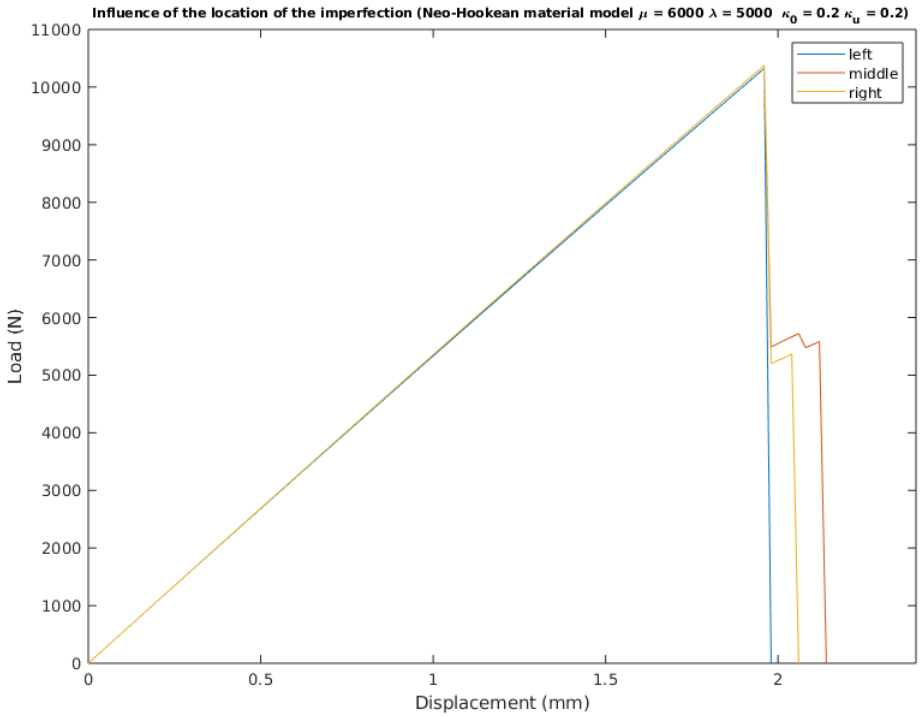

Figure 5.26: Load-displacement response curves for different mesh sizes

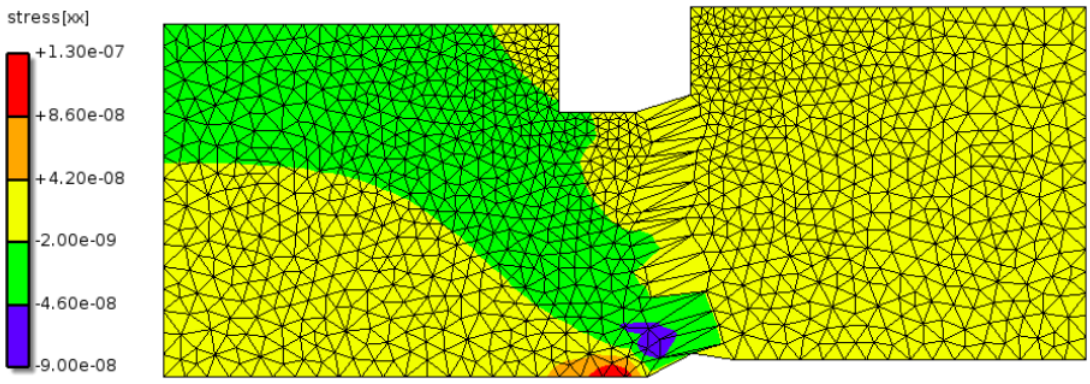

Figure 5.27: Deformed model with depth = 4 mm

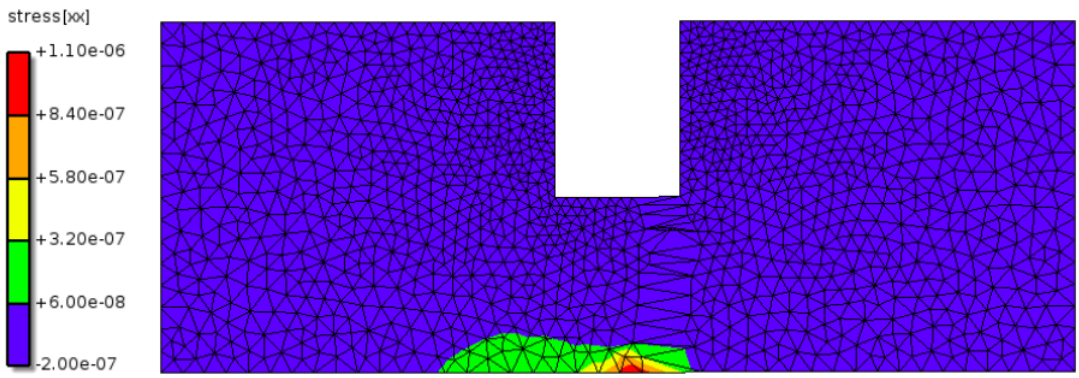

Figure 5.28: Deformed model with depth = 8 mm

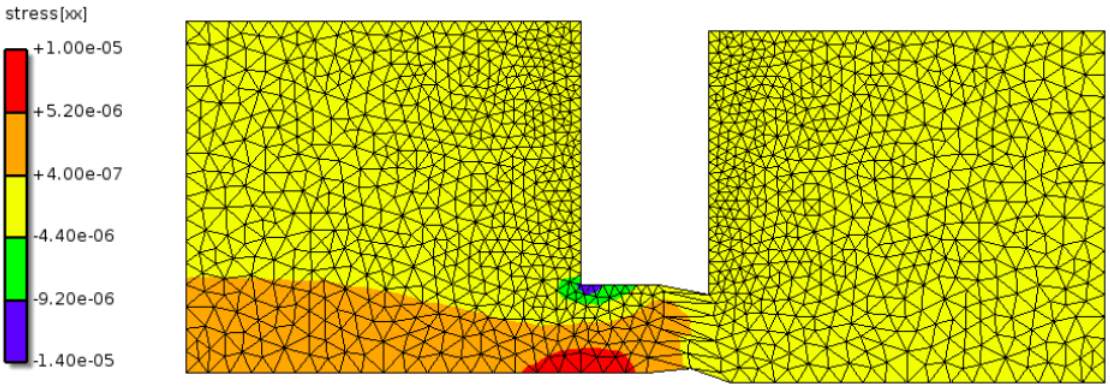

Figure 5.29: Deformed model with depth = 12 mm

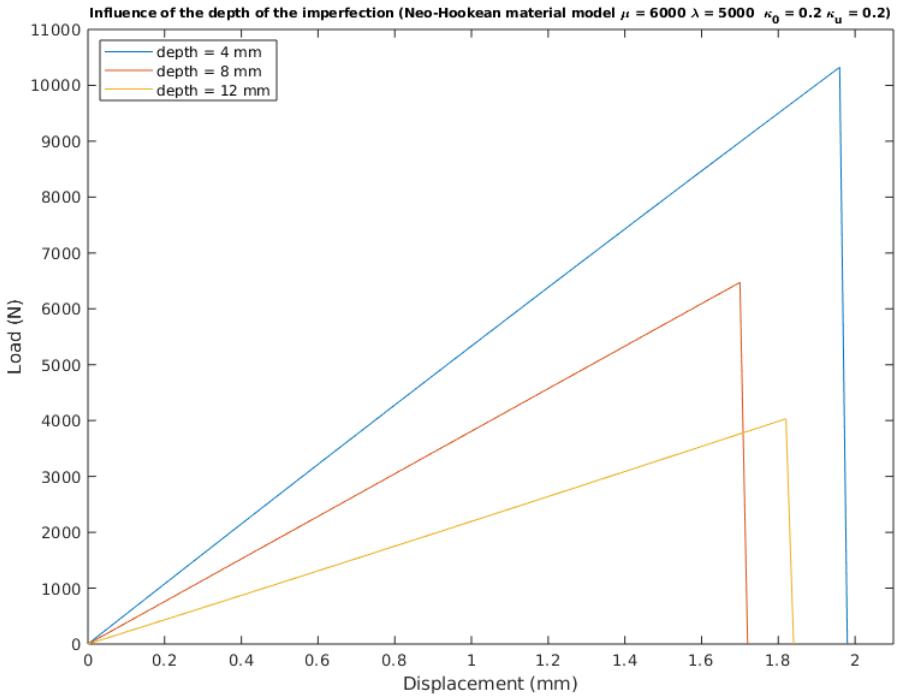

Figure 5.30: Load-displacement response curves for different mesh sizes

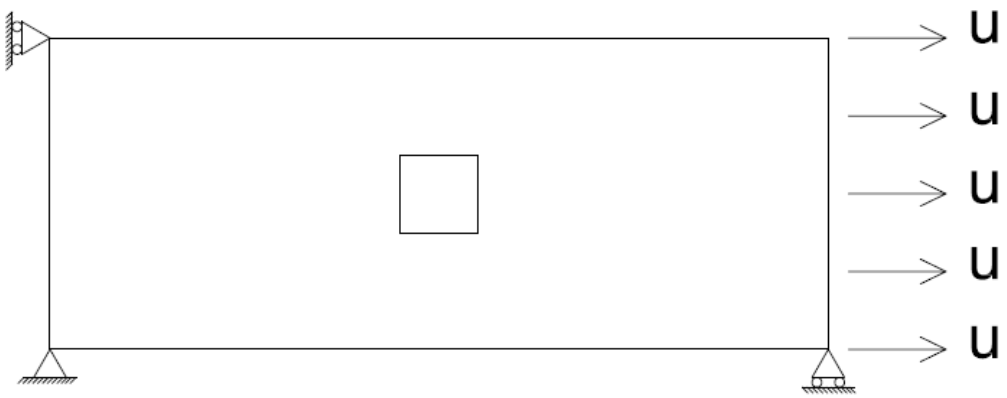

Figure 5.31: Geometry and boundary conditions of the plane model with an imperfection

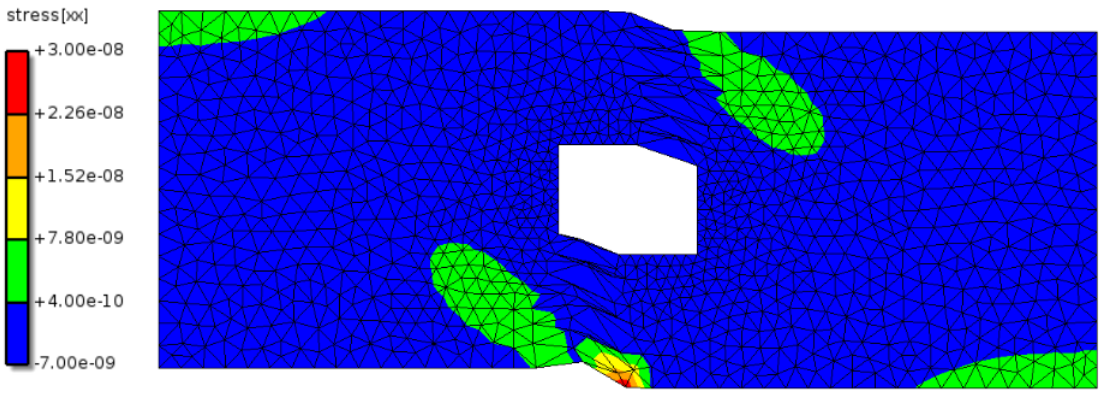

Figure 5.32: Deformation of the model (Neo-Hookean material)

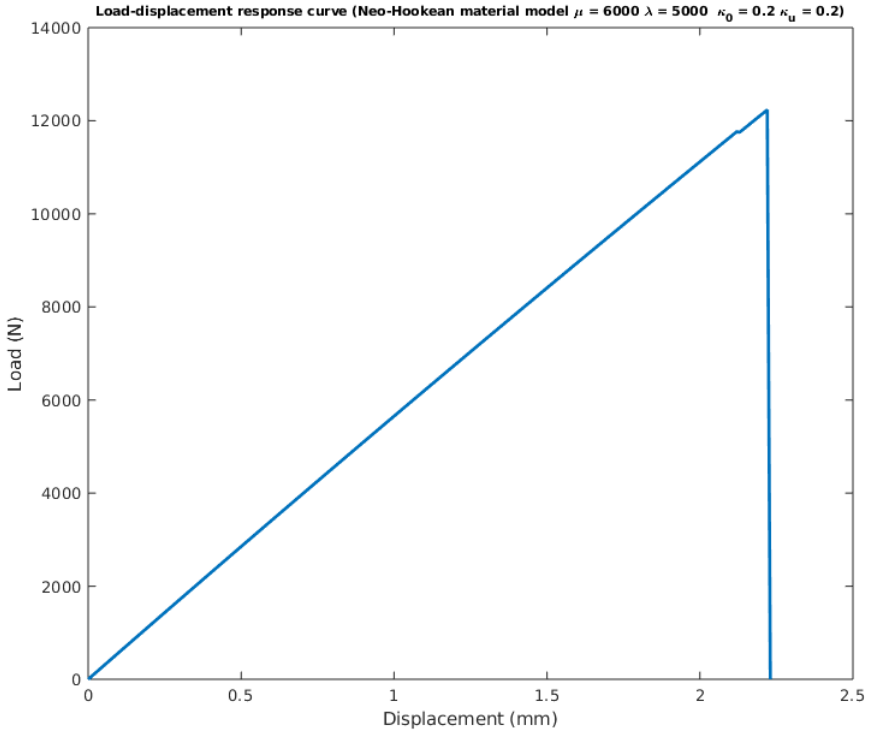

Figure 5.33: Load-displacement response curve for the plane model with imperfection (Neo-Hookean material)

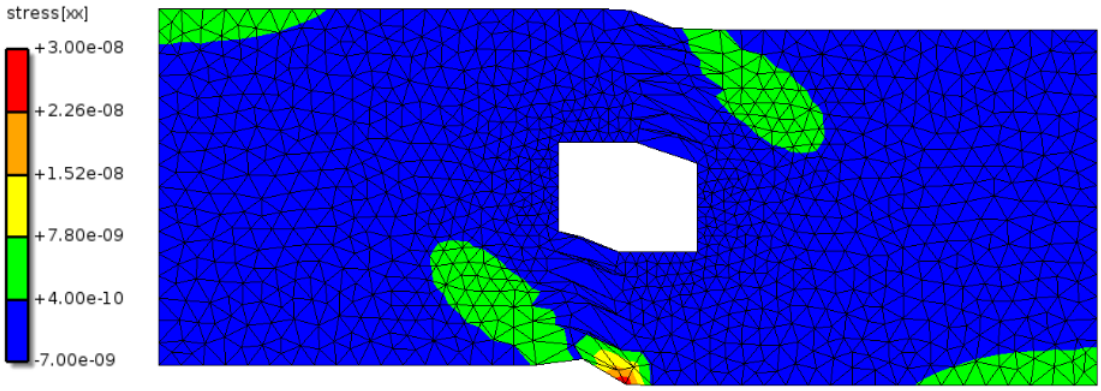

Figure 5.34: Deformed model with mesh size = 1 mm

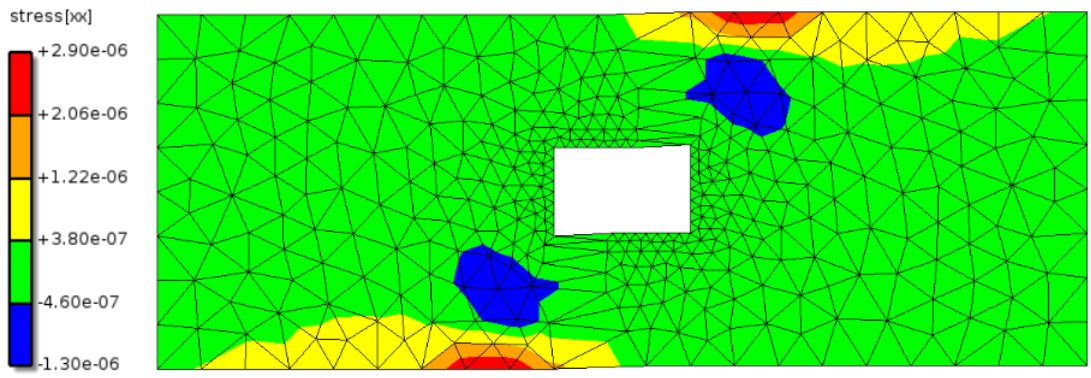

Figure 5.35: Deformed model with mesh size = 2 mm

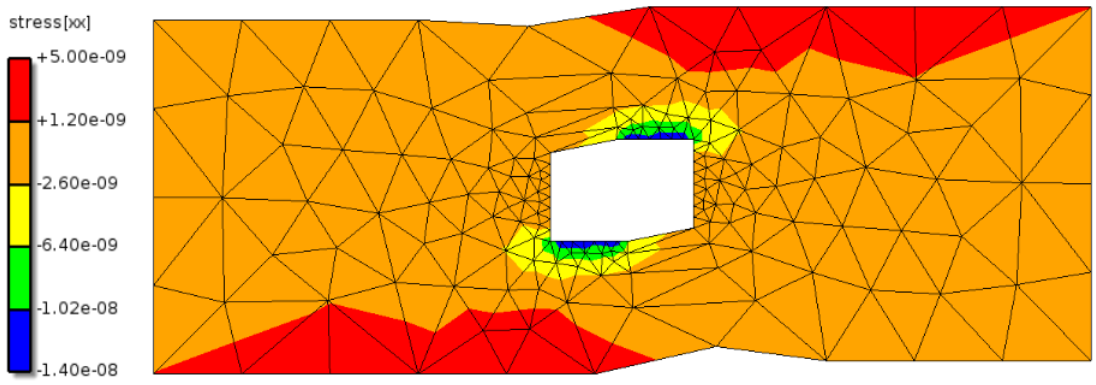

Figure 5.36: Deformed model with mesh size = 4 mm

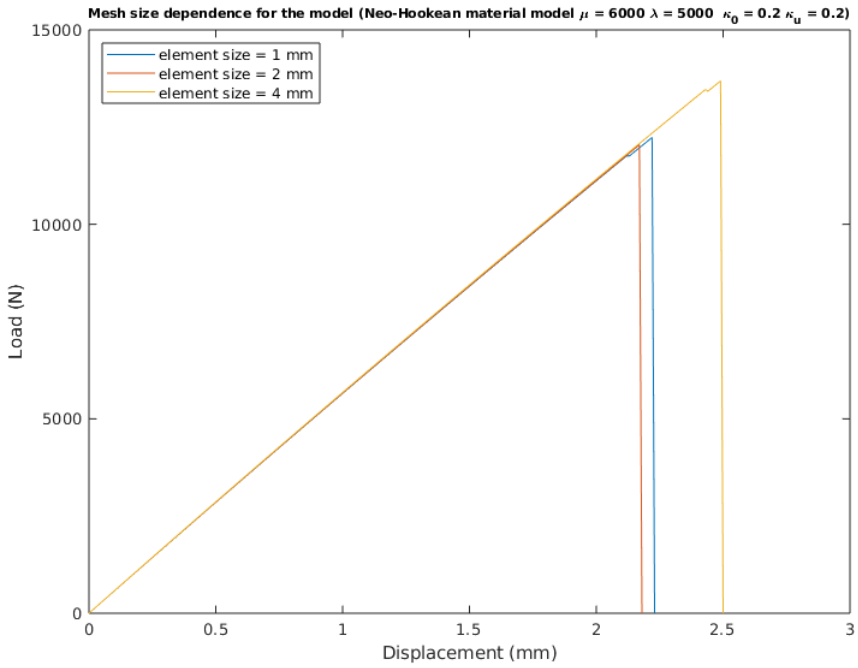

Figure 5.37: Load-displacement response curves for different mesh sizes

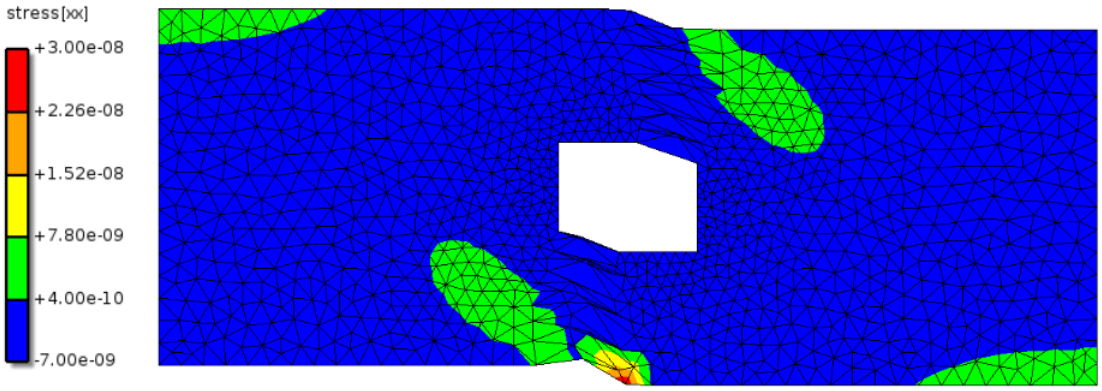

Figure 5.38: Deformed model with rectangular hole size = 4 mm x 4 mm

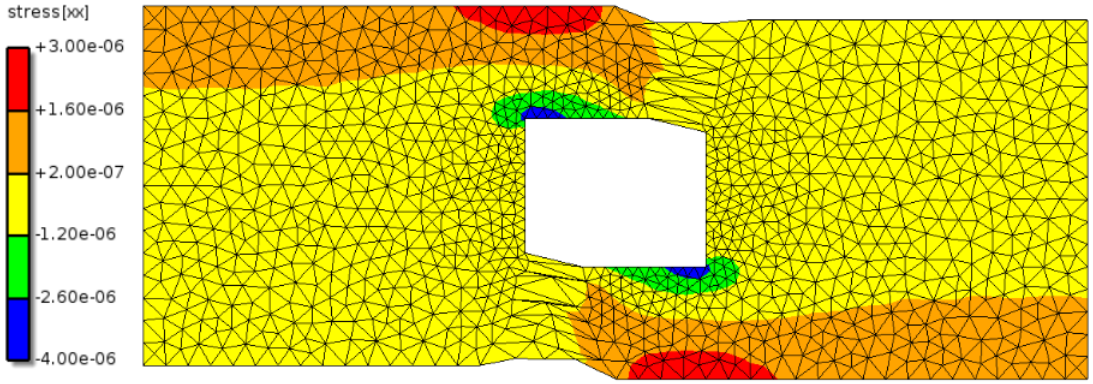

Figure 5.39: Deformed model with rectangular hole size = 6 mm x 6 mm

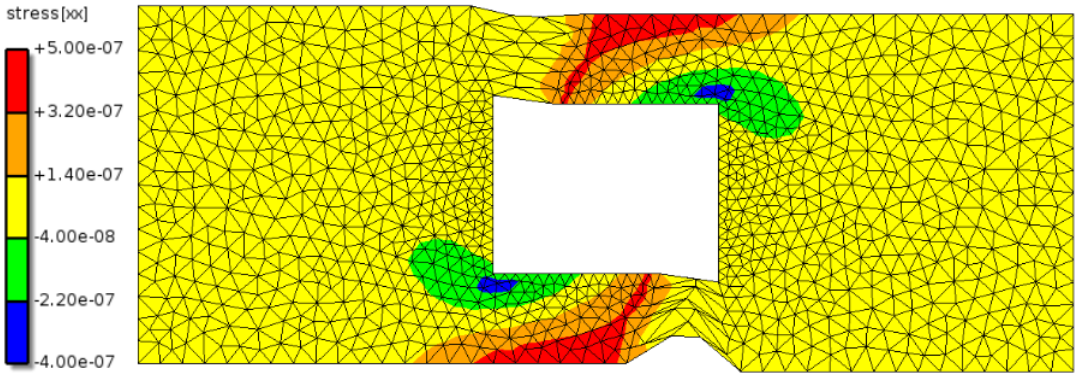

Figure 5.40: Deformed model with rectangular hole size = 8 mm x 8 mm

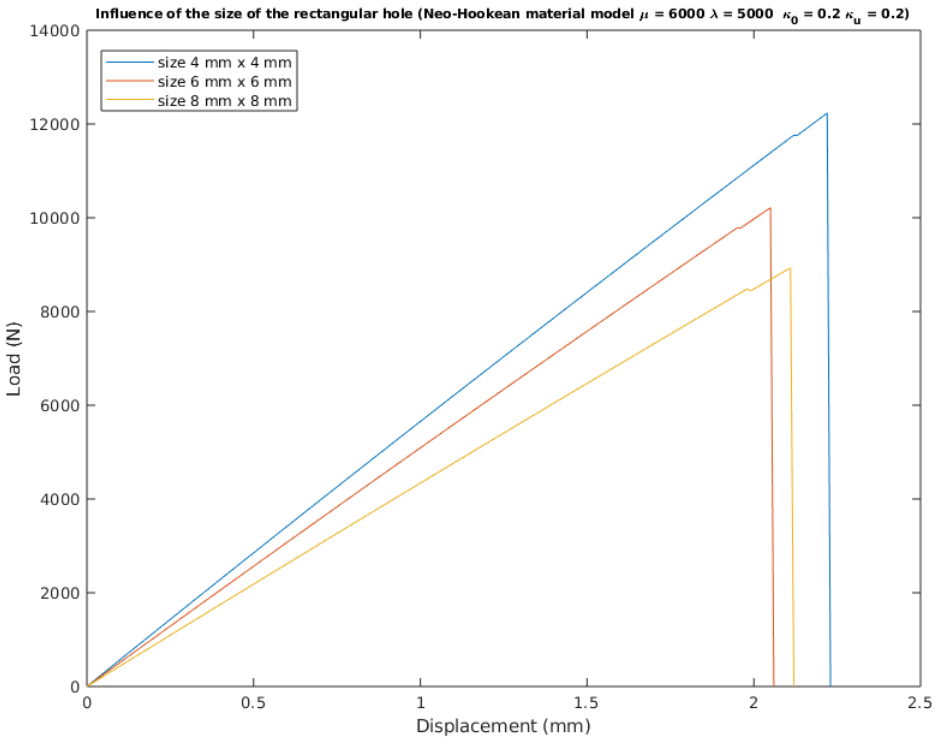

Figure 5.41: Load-displacement response curves for different sizes of the rectangular hole

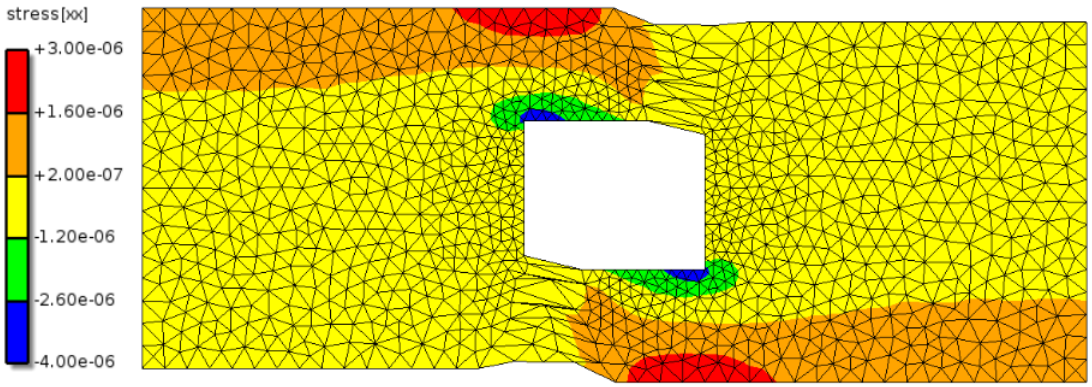

Figure 5.42: Deformed model with rectangular hole at the middle

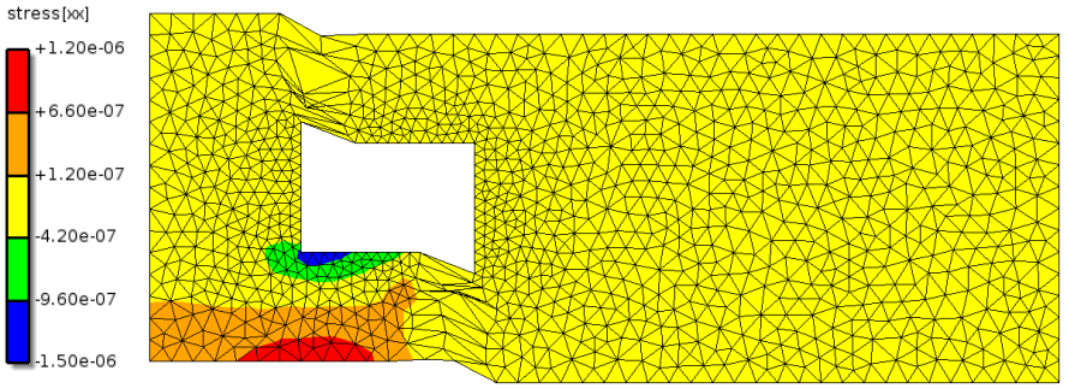

Figure 5.43: Deformed model with rectangular hole at the left

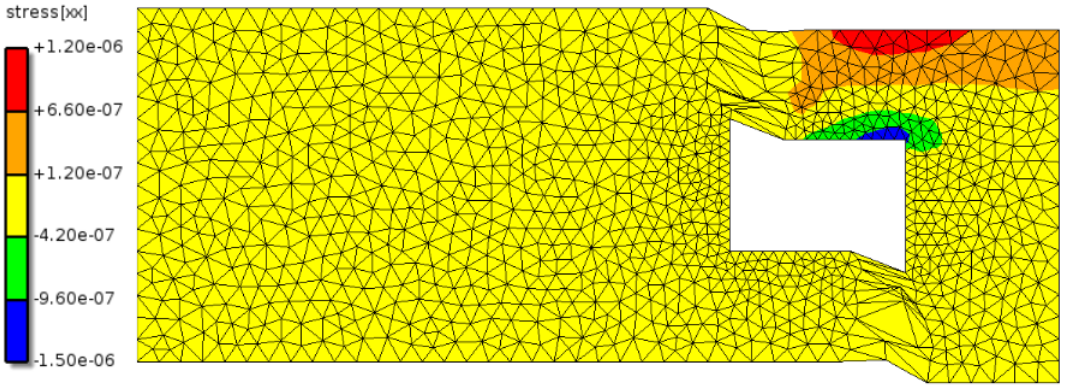

Figure 5.44: Deformed model with rectangular hole at the right

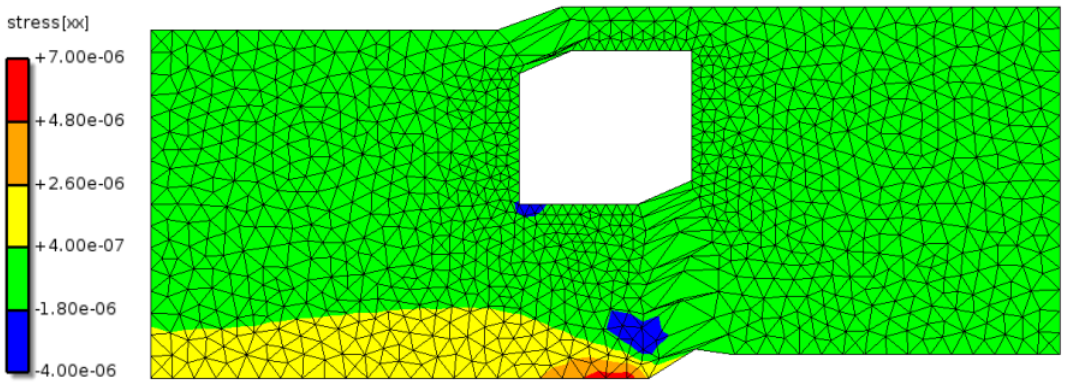

Figure 5.45: Deformed model with rectangular hole at the top

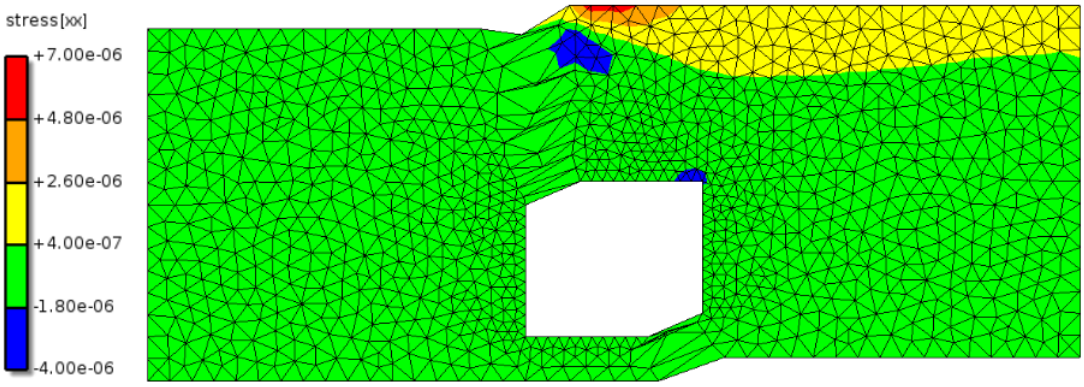

Figure 5.46: Deformed model with rectangular hole at the bottom

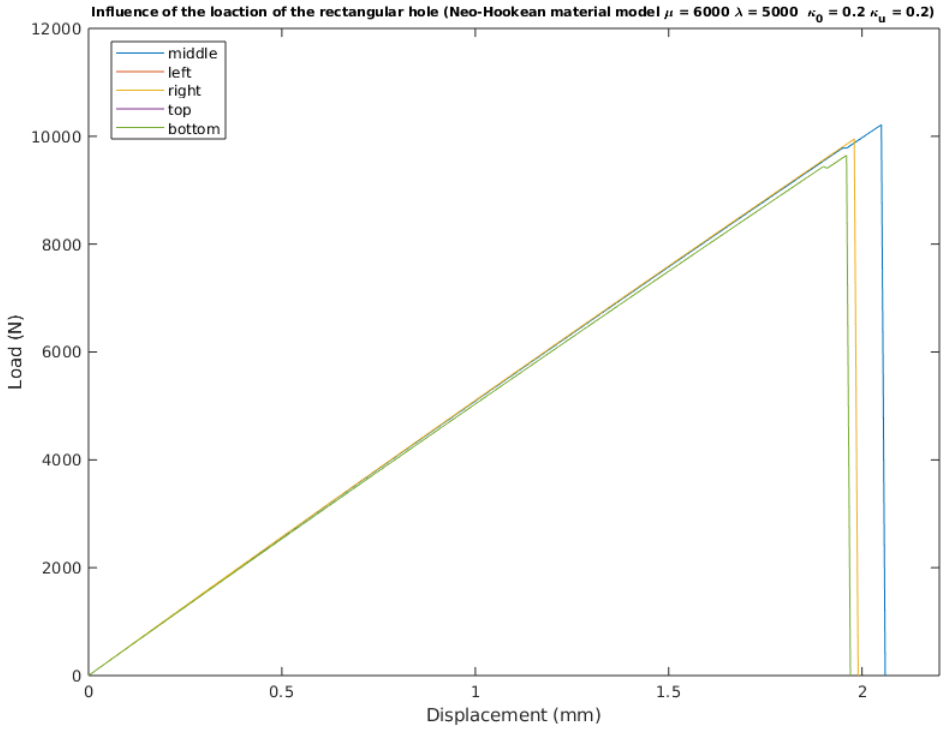

Figure 5.47: Load-displacement response curves for different rectangular hole sizes

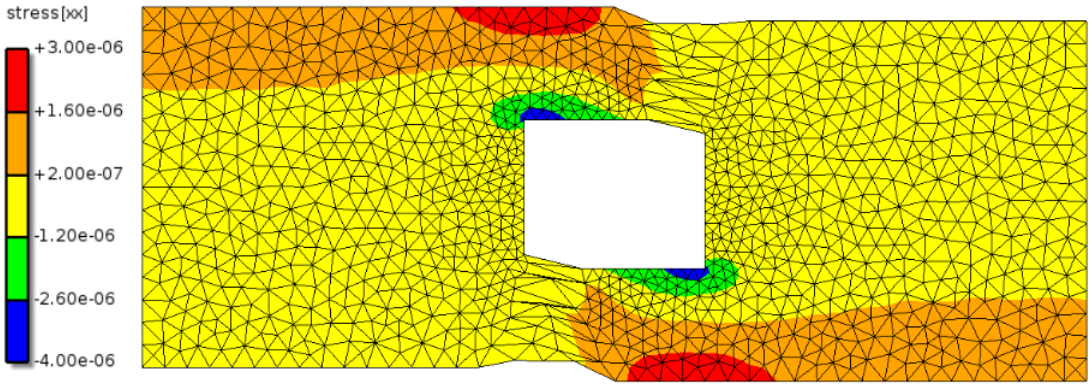

Figure 5.48: Deformed model with rectangular hole at the middle

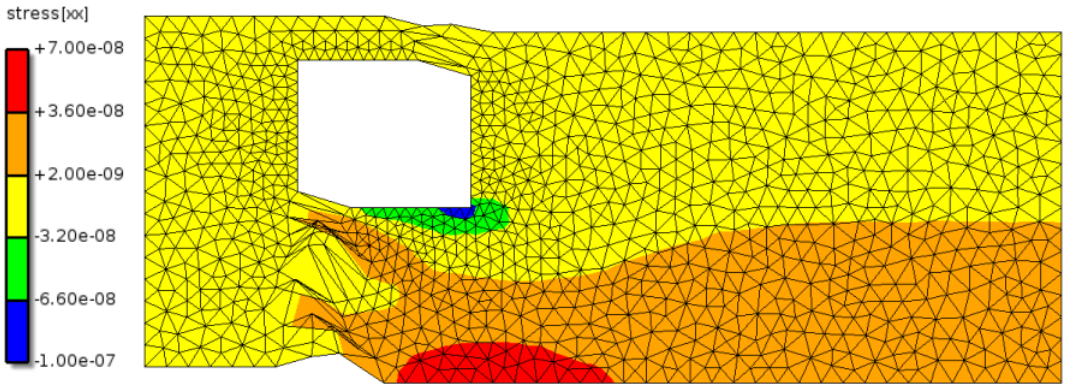

Figure 5.49: Deformed model with rectangular hole at the left-top

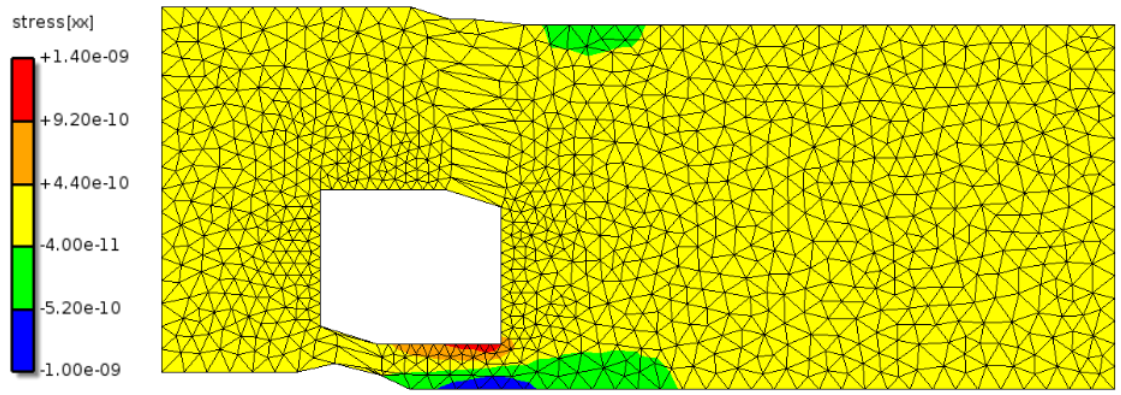

Figure 5.50: Deformed model with rectangular hole at the left-bottom

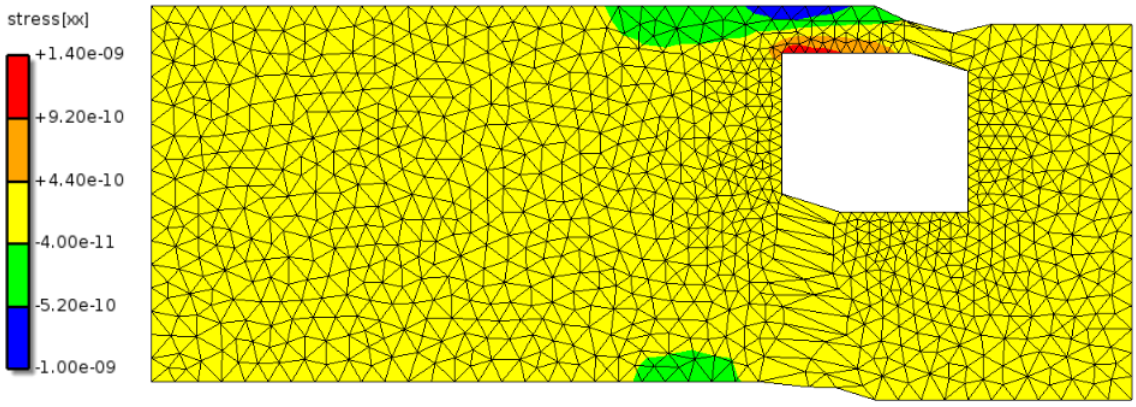

Figure 5.51: Deformed model with rectangular hole at the right-top

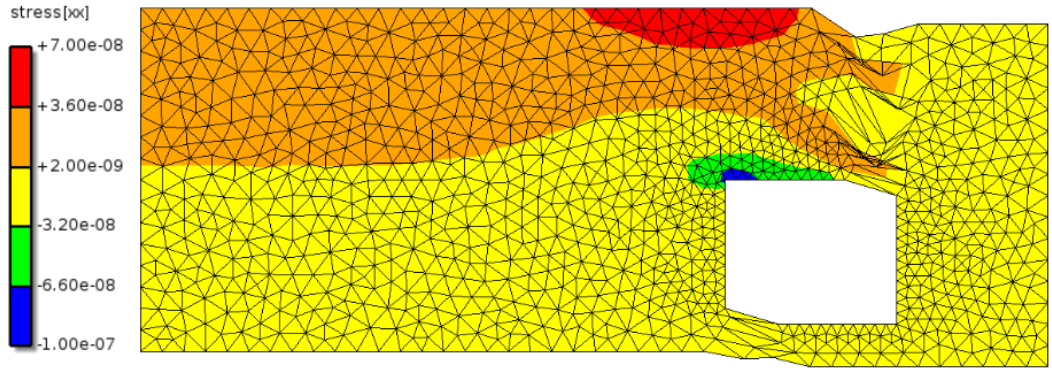

Figure 5.52: Deformed model with rectangular hole at the right-bottom

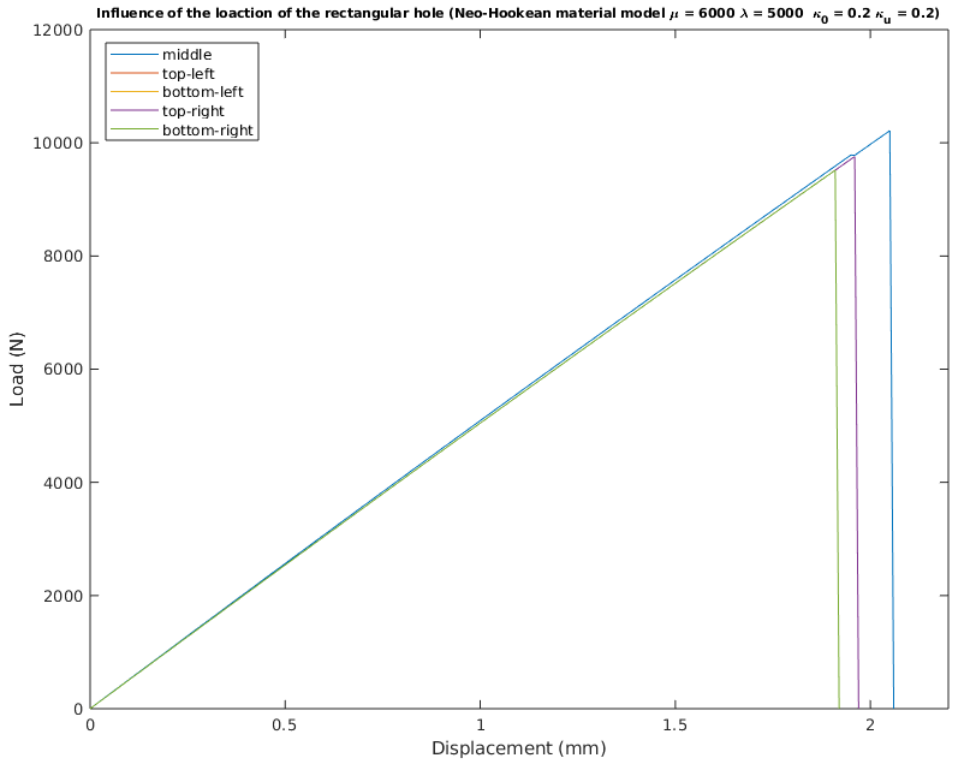

Figure 5.53: Load-displacement response curves for different rectangular hole sizes

6

Conclusion and recommendations

6.1. Conclusion

A constitutive model for failure in hyperelastic material has been obtained by combining the hyperelastic material model and the failure model. Three has been material models combined with a continuing damage model with linear softening. As a result, three constitutive models for failure in hyperelastic material are obtained. The constitutive model for failure in Neo-Hookean material model can be applied to represent the damage behaviour of the matrix in the arterial wall. Generally, there are two main components in the arterial wall, which are the matrix and collagen fibres. In order to represent the damage behaviour of the arterial wall, the constitutive model for failure in Holzapfel material model is set up. The constitutive model for failure in Gasser material model also includes the influence of the dispersion of the collagen fibres. Based on the results of the numerical analysis, they indicate that it is applicable to combine the material model and the failure model. The obtained constitutive models can be applied to represent the damage behaviour of the arterial wall.

Based on the failure analysis, it can be concluded that the constitutive models which are set up in this thesis can only be applied in simple models with a brittle damage behaviour. In the numerical analysis, the constitutive models are applied to a single element, and the obtained results are convincing. However, when it comes to some other simple models, problems appear. As for the model of a simple plane, only the constitutive model of the Neo-Hookean material model can have a ductile damage behaviour. As for the other two constitutive models, only brittle damage behaviour can be applied to the simple plane model. As for model of a plane with an imperfection and model of a plane with a rectangular hole in the middle, only the constitutive model of the Neo-Hookean material model can be applied with a brittle damage behaviour. The other two constitutive models cannot be applied to them even with brittle damage behaviour. It is concluded that the models are not yet in a shape that they allow for failure analysis in realistic geometries.

6.2. Recommendations

Five recommendations are given according to the problems which appear in the numerical analysis and failure analysis.

1. There is only one expression of the equivalent strain is applied in the thesis. However, there are several definitions of equivalent strain which can be found in the literature. The selection of the definition of the equivalent should dependence on the type of problem which is going to be analyzed. Some other definitions of the equivalent strain may be more suitable to be applied in the damage behaviour of the arterial wall.

2. In this thesis, only one linear damage model is combined with the material model. However, it is known that the damage behaviour of the arterial wall is not a linear damage behaviour. So, other non-linear damage models need to be combined with the material models.

3. In the failure analysis, only several simple models are analyzed. However, in order to set up sufficient simulation tools for the plaque rupture, models which are similar to the actual geometry of the plaque need to be set up. In this way, the damage behaviour of the plaque can be explored.

4. Mesh dependence analysis is performed in the thesis. Regularization can be applied to eliminate mesh dependence.

5. There are two main components in the artery wall tissue: matrix and fibres. In the thesis, the same equivalent strain measure is applied to them. The equivalent strain measures can be separated for the matrix and fibres.

Bibliography

[1] van Brummelen H. Miguel A. Gutiérrez Virmani .R van der Lugt .A van der Steen A.F. Wentzel J.J. Gijsen F.J. Akyildiz A.C., Speelman L. Effects of intima stiffness and plaque morphology on peak cap stress. *BioMedical Engineering OnLine*, 10, 2011. doi: 10.1186/1475-925X-10-25.

[2] Eliasson P. Pernilla E.and Thompson M.S. Bajuri M.N., Isaksson H. A hyperelastic fibre-reinforced continuum model of healing tendons with distributed collagen fibre orientations. *Biomechanics and Modeling in Mechanobiology*, 15(6):1457–1466, 2016. doi: 10.1007/s10237-016-0774-5.

[3] Dixon J.G. Boughner D. R. Canham P.B., Finlay H.M. and Chen A. Measurements from light and polarised light microscopy of human coronary arteries fixed at distending pressure. *Cardiovascular Research*, 23(11):973–982, 1989. doi: 10.1093/cvr/23.11.973.

[4] Patel D and Fry D. The elastic symmetry of arterial segments in dogs. *Circulation research*, 24: 1–8, 1969. doi: 10.1161/01.RES.24.1.1.

[5] de Borst R. and Sluys L.J. *Computational Methods in Non-Linear Solid Mechanics*. Delft University of Technology, Delft, the Netherlands, 2015.

[6] Ogden R.W. Gasser T.C. and Holzapfel G.A. Hyperelastic modelling of arterial layers with distributed collagen fibre orientations. *JOURNAL OF THE ROYAL SOCIETY INTERFACE*, 3(6): 15–35, 2006. doi: 10.1098/rsif.2005.0073.

[7] Thomas C.and Ogden R. W. Holzapfel G. A., Gasser. A new constitutive framework for arterial wall mechanics and a comparative study of material models. *Journal of elasticity and the physical science of solids*, 61(1):1–48, 2000. doi: 10.1023/A:1010835316564.

[8] Jay D. Humphrey. Mechanics of the arterial wall: Review and directions. *Critical Reviews and trade; in Biomedical Engineering*, 23(1-2):1–162, 1995.

[9] Lichtenstein O Lanir Y and Imanuel O. Optimal Design of Biaxial Tests for Structural Material Characterization of Flat Tissues. *Journal of Biomechanical Engineering*, 118(1):41–47, 1996. doi: 10.1115/1.2795944.

[10] Wickramasinghe K Bhatnagar P Leal J Luengo-Fernandez R Burns R Rayner M Townsend N Wilkins E, Wilson L. *European Cardiovascular Disease Statistics 2017*. European Heart Network, Belgium, 2017.